

A biomimetic artificial cervical disc
replacement: biomaterial and
biomechanical design
characterization

Celien Jacobs

Celien Antonia Maria Jacobs
Eindhoven University of Technology, The Netherlands

Copyright © 2023 by C.A.M. Jacobs
Cover design by Nick van Heugten
Printed by ADC Dereumaux

A catalogue record is available from the Eindhoven University of Technology Library
ISBN: 978-90-386-5711-0.

The research described in this thesis was supported by the research program AES Open Technology with project number 10025453 financed by the Dutch Research Council (NWO).

Financial support by Dutch Spine Society, Anna Fonds, the Netherlands Society for Biomaterials and Tissue Engineering (NBTE) and the department of Biomedical Engineering of Eindhoven University of Technology for the publication of this thesis is gratefully acknowledged.

A biomimetic artificial cervical disc replacement: biomaterial and biomechanical design characterization

PROEFSCHRIFT

Ter verkrijging van de graad van doctor aan de Technische Universiteit Eindhoven, op gezag van de rector magnificus prof.dr.ir. F.P.T. Baaijens, voor een commissie aangewezen door het College voor Promoties, in het openbaar te verdedigen op 19 april 2023 om 16:00 uur

door

Celien Antonia Maria Jacobs

geboren te Weert

Dit proefschrift is goedgekeurd door de promotoren en de samenstelling van de promotiecommissie is als volgt:

voorzitter:	prof. dr. M. Merkx
1e promotor:	prof. dr. K. Ito
copromotor:	dr. S. Hofmann
commissieleden:	prof. dr. ir. O. van der Sluis
	prof. dr. ir. G.J. Verkerke (Rijksuniversiteit Groningen)
	prof. dr. R.K. Wilcox (University of Leeds)
	prof. dr. B.P. Meij (Universiteit Utrecht)
	dr. S. Ghazanfari (Maastricht University)

Het onderzoek of ontwerp dat in dit proefschrift wordt beschreven is uitgevoerd in overeenstemming met de TU/e Gedragscode Wetenschapsbeoefening.

Table of contents

Summary	2
Samenvatting	4
Chapter 1	7
General introduction	
Chapter 2	25
Viscoelastic total disc replacement devices	
Chapter 3	51
Design optimization of the fiber jacket using warp-knitted fabric structure	
Chapter 4	69
Surface modifications to promote the osteoconductivity of UHMWPE fabrics	
Chapter 5	93
Biomechanical evaluation in canine cervical cadaveric spines	
Chapter 6	112
Mechanical characterization of the bioAID	
Chapter 7	135
General discussion	
Curriculum vitae	151
List of publications	152
Dankwoord (acknowledgements)	154

Summary

Neck pain is a musculoskeletal condition that is one of the leading causes commonly reported to restrict activities of daily living. Approximately 80% of the general population reports neck pain at some time in their life. Due to this high prevalence, neck pain is not only a health problem, but also results in a tremendous socioeconomic burden. Most neck pain is related to diseases of the intervertebral disc, that can result in herniation, protrusions, cervical spondylosis which can eventually deteriorate into cervical radiculopathy and/or myelopathy.

Initially, conservative treatments are used to relieve the pain, such as physiotherapy and pain medication. When these conservative treatments are insufficient, surgical treatments are considered. Cervical disc replacement has been proposed as an alternative treatment in which the diseased disc is replaced by a prosthesis that preserves the motion, thereby decreasing the risk of accelerating adjacent segment degeneration compared to disc excision and vertebral fusion. However, first generation prostheses were based on traditional synovial joint articulating arthroplasty designs, leading to a mismatch in the motion and kinematics of a natural cervical disc. Therefore, with the hypothesis that mimicking the natural structure of the disc would result in similar biomechanical properties, a biomimetic artificial intervertebral disc (bioAID) was developed based on a previous lumbar design by P. van den Broek et al., 2012. The design contains a hydroxyethyl methacrylate (HEMA) – sodium methacrylate (NaMA) hydrogel core representing the nucleus pulposus, an ultra-high-molecular-weight-polyethylene (UHMWPE) fiber jacket as annulus fibrosus, and titanium endplates with pins for primary mechanical fixation. To further develop the bioAID, this thesis describes both the mechanical and biological behavior of this novel device.

Chapter 1 provides background knowledge about the cervical spine, the composition of the intervertebral disc, disc degeneration and its treatment options. The main design related advantages and disadvantages of second-generation viscoelastic cervical disc replacement prostheses are extensively discussed in **Chapter 2**. This literature review shows that the advantage of including a viscoelastic component into the design is that it can replicate the shock-absorbing and variable center of rotation present in a natural disc.

To further develop the design of the bioAID, several different jacket design configurations were tested and compared, as described in **Chapter 3**. Results showed that 3 layers of a 2x1 lapping design was most promising to restrict the isotropic swelling of the hydrogel, conform with the complex shape of the hydrogel and ensures structural integrity.

One of the most important factors influencing clinical success of medical devices is osseointegration of the implant with the adjacent vertebrae. Therefore, **Chapter 4** investigated several surface modifications of UHMWPE fabrics to enhance the osteoconductive potential *in vitro*. It was seen that incorporating hydroxyapatite (HA) into UHMWPE fibers in combination with plasma treatment, resulted in an increased cell attachment and upregulated ALP activity, thus being the most promising fabric surface for facilitating osseointegration.

As previously mentioned, the main rationale of using a cervical disc replacement treatment is to preserve the motion. Therefore, in **Chapter 5** the initial biomechanical effect of the bioAID on the kinematic behavior of the cervical spine was assessed in an *ex vivo* biomechanical study in 6-degrees-of-freedom. Results showed that the bioAID retained the ROM at the treated and the adjacent levels, as well as the sigmoid, non-linear shape of the moment-rotation curves seen in the intact condition. This study indicated that the bioAID can not only replicate the ROM, but also the quality of motion.

Chapter 6 evaluates if the design of the bioAID can withstand physiological loads without functional failure or risk of migration. The bioAID remained intact up to 973 N under quasi-static axial compression and reported only 0.41 mm displacement under physiological shear load. In addition, after cyclic compression testing no subsidence was detected and the device expulsion load was almost 20 times higher than the physiological shear load. Together, these results indicate that the current design provides sufficient initial stability and is mechanically safe. Moreover, the bioAID design has the unique capability of replicating the swelling characteristics of a natural disc and could show similar diurnal creep behavior. In the final chapter, **Chapter 7**, the main findings, and overall implications of the thesis are discussed.

In conclusion, this thesis examined a novel biomimetic artificial disc replacement both mechanically and biologically and proposed multiple approaches for improving this concept. Although many steps are still needed to introduce it into the clinic, the insights obtained in this thesis show that this design could be a feasible and promising prosthesis for the treatment of severely degenerated discs.

Samenvatting

Nekpijn is een veel voorkomende klacht verantwoordelijk voor het beperken van patiënten in hun dagelijkse activiteiten. Ongeveer 80% van de bevolking ervaart nekpijn op een bepaald moment in hun leven. Aangezien dit zo vaak voorkomt is nekpijn niet alleen een gezondheidsprobleem, maar resulteert het ook in grote sociale en economische lasten. Meestal is nekpijn gerelateerd aan slijtage van de tussenwervelschijf, dat uiteindelijk kan leiden tot een hernia en in het ergste geval kan hierbij een zenuw bekneld raken die ernstige pijnklachten veroorzaakt.

In eerste instantie kunnen conservatieve therapieën, zoals fysiotherapie en pijnmedicatie, helpen om de pijn symptomen te verminderen. Als de conservatieve therapie niet of onvoldoende heeft gewerkt, worden operatieve behandelingen overwogen. Tot op heden werd vaak een fusie uitgevoerd, waarbij de versleten tussenwervelschijf wordt verwijderd en de aangrenzende wervels aan elkaar vast worden gezet. Het risico van deze behandeling is dat het verlies in bewegingsvrijheid in het geopereerde segment wordt gecompenseerd in de aangrenzende segmenten. Een alternatieve operatieve behandeling is het gebruik van een discus prothese. Tijdens deze operatie wordt de versleten tussenwervelschijf verwijderd en vervangen door een prothese die de bewegingsvrijheid van het behandelde segment behoudt. Dit heeft als voordeel dat de aangrenzende segmenten niet extra belast worden, zoals vaak het geval is bij een standaard fusie behandeling. Echter, de ontwerpen van de huidige discusprothesen zijn afgeleid van knie en heup implantaten, terwijl deze gewrichten een totaal andere anatomie en fysiologie hebben dan een natuurlijke tussenwervelschijf.

Op basis van de hypothese dat het nabootsen van de natuurlijke structuur van de tussenwervelschijf tot vergelijkbare biomechanische eigenschappen zou leiden, is een biomimetische synthetische tussenwervelschijf (bioAID) ontwikkeld. Het ontwerp bevat een hydroxyethyl methacrylaat (HEMA)-natrium methacrylaat (NaMA) hydrogelkern die de nucleus pulposus vertegenwoordigt, een ultrahoog-moleculair-gewicht-polyethyleen (UHMWPE)-textieljasje als annulus fibrosus en titanium-eindplaten met pinnen voor primaire mechanische fixatie. Om de bioAID verder te ontwikkelen, beschrijft dit proefschrift zowel het mechanische als biologische gedrag van deze nieuwe prothese.

Hoofdstuk 1 beschrijft de anatomie van de cervicale wervelkolom, de anatomie van de tussenwervelschijf, tussenwervelschijf slijtage en de behandelingen hiervan. De belangrijkste voor- en nadelen van de nieuwe generatie visco-elastische discusprothesen worden uitgebreid besproken via een literatuurstudie in **Hoofdstuk 2**. Deze literatuurstudie laat zien dat een

visco-elastische component in een discusprothese de schokdempende functie en variabele rotatie-as van een natuurlijke tussenwervelschijf kan nabootsen. Om de bioAID verder te ontwikkelen werden in **Hoofdstuk 3** verschillende ontwerpen van het textieljasje getest en vergeleken. De resultaten tonen aan dat 3 lagen van een 2x1 textielstructuur het meest veelbelovend is om de zwelling van de hydrogel te beperken en de structurele integriteit te waarborgen.

Een belangrijke factor die het klinisch succes van protheses beïnvloedt is de secundaire fixatie, een proces waarbij het implantaat vastgroeit aan het bot van de aangrenzende wervels. Daarom werden er in **Hoofdstuk 4** verschillende oppervlaktebehandelingen van het UHMWPE-textieljasje onderzocht die dit botgroeiproces zouden kunnen faciliteren/stimuleren. Uit de resultaten blijkt dat het toevoegen van het mineraal hydroxyapatiet (HA) in de UHMWPE-vezel, in combinatie met een plasmabehandeling, leidt tot een betere cel hechting en een verhoogde bot cel activiteit. Hieruit werd geconcludeerd dat deze oppervlaktebehandeling veelbelovend is om secundaire fixatie te faciliteren.

Het doel van een discusprothese is om de bewegingsvrijheid te behouden om zo overbelasting van de aangrenzende wervels te verminderen. Daarom werd in **Hoofdstuk 5** een biomechanisch onderzoek uitgevoerd om te testen of de bioAID het bewegingsmechanisme van een natuurlijke schijf kan reproduceren. De resultaten tonen aan dat de bioAID de bewegingsvrijheid van het behandelde segment kan behouden, maar ook van de aangrenzende segmenten. Daarnaast kan de bioAID de non-lineaire curves van de onbehandelde wervelkolommen imiteren. Dit onderzoek suggereert dat de bioAID niet alleen de bewegingsvrijheid kan reproduceren, maar ook het bewegingsmechanisme beter kan nabootsen.

In **Hoofdstuk 6** is het ontwerp van de bioAID mechanisch gekarakteriseerd onder fysiologische belastingen. De bioAID blijft intact tot een kracht van 973 N bij quasi-statische axiale compressie en vertoont enkel 0.41 mm verplaatsing onder fysiologische schuifkracht. Bovendien wordt na cyclische compressie geen verzakking van het implantaat in de aangrenzende wervels waargenomen en is er meer dan 20 keer de fysiologische schuifkracht nodig om de prothese te verschuiven tussen de wervels. Samen geven deze resultaten aan dat het huidige ontwerp voldoende primaire stabiliteit biedt en mechanisch veilig is. Bovendien heeft het ontwerp van de bioAID de unieke eigenschap om de vloeistofstroom van een natuurlijke schijf na te bootsen en kan het daardoor vergelijkbaar dagritme in kruipgedrag vertonen. In het laatste hoofdstuk, **Hoofdstuk 7**, worden de belangrijkste bevindingen en de algemene implicaties van dit proefschrift besproken.

Samenvatting

Dit proefschrift beschrijft een nieuwe biomimetische en synthetische discusprothese die zowel mechanisch als biologisch is onderzocht. Ondanks dat er nog veel onderzoek nodig is om deze prothese in de kliniek te introduceren, laten de resultaten in dit proefschrift zien dat dit concept een haalbaar en veelbelovende alternatieve prothese is voor de behandeling van patiënten met ernstig versleten tussenwervelschijven.

Chapter 1

General introduction

1.1 The cervical spine

The human spine can be divided in four different regions, starting with the cervical region in the neck, followed by the thoracic region, the lumbar region, and the sacral region (Figure 1.1). The cervical region consists of 7 vertebrae (C0-C7) and is the most mobile region being mainly responsible for protection of the spinal cord and mobile bearing of the head [1]. The vertebrae in this region increase in mass and volume in the caudal direction from C3 to C7, and have a saddle-like shape at both cranial and caudal sides, giving the cervical spine a lordotic curve (Figure 1.1) [1], [2]. Unlike the vertebrae in the other regions, the cervical vertebrae have unciniate processes and transverse processes that improve the overall range of motion. Moreover, the facet joints in the cervical region are positioned at an angle of 45° of the transversal plane, leading to specific biomechanical kinematics where axial rotation and lateral bending are coupled [1].

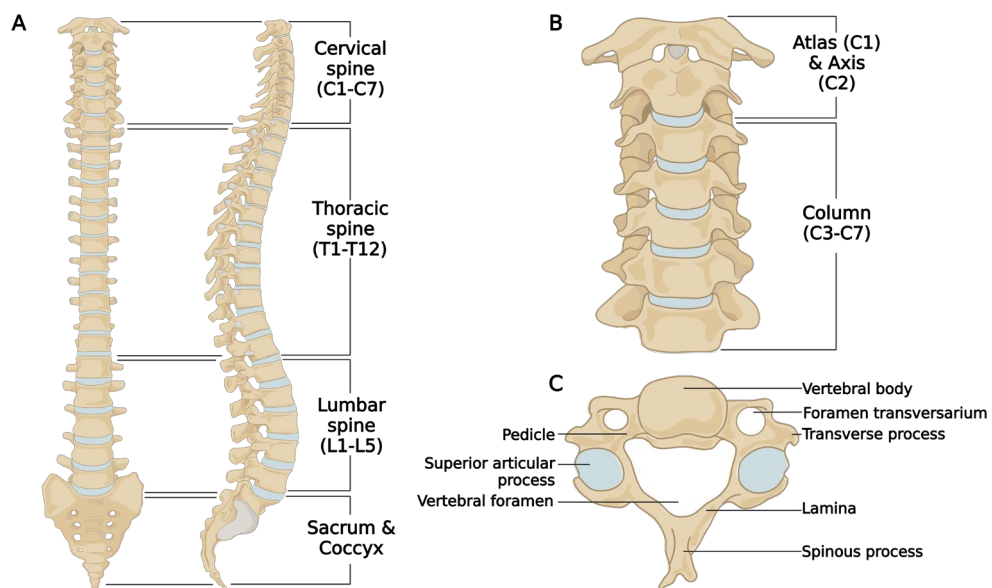


Figure 1.1: a) Different regions of the human spinal column b) cervical region divided in upper, middle, and lower region c) anatomy of vertebrae. Created with BioRender.com

1.2 The intervertebral disc

The vertebrae are separated by intervertebral discs, which have a load bearing and motion transfer function. The intervertebral disc is the largest avascular structure in the body, resulting in metabolite transport difficulties, small cell populations and thus low capacity for regeneration and repair. For this reason, the intervertebral disc is very vulnerable to injury and

to age-related changes in the composition of the intervertebral disc [3]. In general, the intervertebral disc consists of three integrated parts being a soft swelling core called the nucleus pulposus, which is surrounded by the collagen-rich annulus fibrosus and the cartilaginous endplates that connect the intervertebral disc to the adjacent vertebral bodies (Figure 1.2).

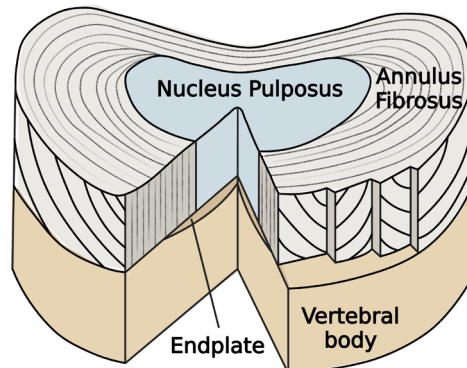


Figure 1.2: *Anatomy of intervertebral disc showing the alternating fiber alignment in lamellae of the annulus fibrosus. Created with BioRender.com and adapted from Guerin H.A., Elliot D.M. Spine Technology Handbook, Elsevier Academic Press: Amsterdam*

1.2.1 The nucleus pulposus

The nucleus pulposus is a gelatinous structure located in the center of the intervertebral disc. It consists mostly of proteoglycans (~65% of dry weight), which are held together by random orientated collagen type II fibers (~25% of dry weight) [4]–[7]. The proteoglycans contain sugar subunits called glycosaminoglycans (GAGs) that have negative charges which attract positive free ions which in turn attract water. This process is called Donnan Osmosis and results in a high-water content in the nucleus pulposus (70-90 %), and in a large osmotic intradiscal pressure (0.14 – 0.32 MPa) [8]–[10]. Loading causes the water content of the NP to change during the day, being maximum at night and lowest during day-time activities. As a result, the osmotic effects in the nucleus pulposus are dynamic and depend on the net fixed charged density and on the loading history [11]. Overall, the composition of the nucleus pulposus tissue provides the intervertebral disc its time-dependent behavior, acting as a shock absorber and cushioning of the spine during loading.

1.2.2 *The annulus fibrosus*

The nucleus is surrounded by the annulus fibrosis, forming the outer region of the intervertebral disc. The annulus fibrosis is mainly composed of collagen (66 % of dry weight), and proteoglycans (20% of dry weight), resulting in a water content of approximately 65% of the total weight [7]. Mainly collagen type I and II fibers are present which are oriented in concentric layers called lamellae (Figure 1.2) [4]–[7]. The composition of the lamellae shifts gradually to more collagen type I and a reduced proteoglycan content towards the outer part of the annulus. The orientation of the collagen fibers also changes from longitudinal in the outer layers to more cross-linked in the inner regions. Centrally, these collagen fibers connect to the cartilaginous endplate while at the periphery they are connected directly to the bone. The latter connections are called Sharpey's fibers and form a significantly stronger connection than those of the inner region. The annulus fibrosus also contains a small portion of elastin fibers (2% of dry weight), which are responsible for the elastic recoil, giving it its ability to recover to the initial shape when unloaded after deformation [12], [13]. The high content of collagen fibers within the annulus gives the intervertebral disc its superior tensile loading capacity [14]. Overall, the anisotropic structure of the annulus fibrosus due to the orientation of the collagen fibers inside the hydrated matrix of proteoglycans is crucial for the characteristic mechanical properties of the intervertebral disc.

1.2.3 *The cartilaginous endplate*

The last component of the intervertebral disc is the cartilaginous endplate, which is a thin layer of hyaline cartilage at the top and bottom of the nucleus pulposus and inner annulus. It consists of proteoglycans and a network of collagen fibrils that run parallel to the vertebral bony endplate [15]. The cartilaginous end plate is approximately 0.5-1 mm thick but changes within the region of the disc and is not present at the outer annulus [8], [15]. Its function is to act as an interface between the cortical bone shell of the vertebrae and the annulus and nucleus, by keeping the nucleus under pressure. Moreover, it is a semipermeable membrane that allows fluid exchange between the nucleus, annulus and the vertebral body for facilitating nutrient transport [4], [6], [16].

1.3 Biomechanical behavior of the cervical spine

1.3.1 *Intervertebral disc*

The function of the intervertebral disc is to provide flexibility and motion of the spine. It bears the load together with the facet joints, including dynamic, static, tensile, torsional and shear loads or a combination thereof. For the cervical region, providing mobility is the most important function, while load bearing capacity is slightly less due to the smaller cross-

sectional area of the disc compared to other regions of the spine [8]. As previously mentioned, the three components of the intervertebral disc are mainly composed of water, proteoglycans, and collagen. The relative amount of each component differs between the three tissues of the intervertebral disc, resulting in slightly different mechanical properties that combined give the disc its characteristic behavior. The interaction between the nucleus pulposus and annulus fibrosus enables the intervertebral disc to transmit loads while allowing constrained flexibility between the adjacent vertebral bodies [17]. This results in little resistance to motion at small deformations, due to the soft highly hydrated core, while at larger movements the collagen fibers in the annulus are stretched to resist motion.

Due to the composition of the intervertebral disc, it has both energy storing and energy absorbing properties giving it its time-dependent behavior. This time-dependent behavior arises from interactions between solid phase and fluid flow (poroelasticity) and from the viscoelastic nature of the solid phase. Due to the presence of proteoglycans, the intervertebral disc exhibits osmotic swelling and thus shows poroelastic time-dependent behavior. The resultant intradiscal pressure is crucial for the biomechanical behavior of the intervertebral disc. The intradiscal pressure prestresses the annulus fibers and supports the endplate, making it responsible for preserving the disc height, stiffness, and load distribution under axial compression (Figure 1.3). Due to the time-dependent properties, the intervertebral disc will behave stiffer with an increasing strain rate or when multiple loading modes are applied after each other [8]. Another effect of this time-dependency is that the disc loses height over time under continuous loading. *In vivo*, the intervertebral disc is subjected to a diurnal loading pattern that typically consists of 16 hours of loading followed by 8 hours of rest. As a result of this diurnal loading pattern, the disc height decreases during the day and regains height during the night, where both fluid flow (poroelasticity) and tissue deformation (viscoelasticity) play a role [18]–[21]. The rate of fluid flow is dependent on the difference in pressure between the intervertebral disc and the surrounding tissue. When the intervertebral disc is subjected to

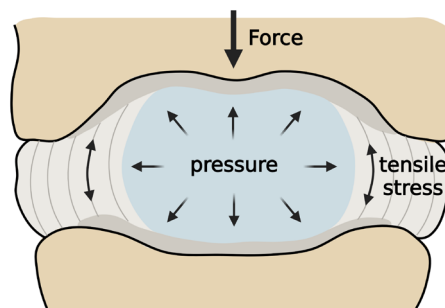


Figure 1.3: *The biomechanical relationship between the nucleus pulposus and annulus fibrosus to resist compressive forces. Created with BioRender.com*

load, the intradiscal pressure increases resulting in outflow of water from the intervertebral disc and thus a reduced disc height. When the intervertebral disc is unloaded, the swelling pressure generated by the negatively charged proteoglycans attract water into the disc, resulting in an increased disc height.

1.3.2 Spinal motion

As previously mentioned, the main function of the cervical spine is allowing movement that facilitates normal daily activities. The spinal motion segment, consisting of the intervertebral disc, adjacent vertebrae and attached ligaments, is the complex responsible for spinal motion [25]. It is a three-joint complex, and its motion is dependent on the geometry and behavior of the intervertebral disc and vertebrae, stiffness and geometry of the ligaments, and the orientation and shape of the facet joints [12]. Moreover, spinal motions are very complex since there are translations and angulations along all three axes. As a consequence, the spinal motion segment has 6 degrees of freedom of motion, being flexion, extension, lateral bending (left or right), axial rotation (left and right), lateral translation, vertical translation, and anterior-posterior translation (Figure 1.4). These spinal movements are almost always coupled angular motions over more than one axis and are combined with translations along the axis. Due to this complex three-dimensional loading *in vivo*, mechanical spine testers are developed which can apply combinations of compression, bending and torsion motions on spinal motion segments *ex vivo* [25]. Results of these mechanical spine testers give the characteristic moment-rotation graphs that show the nonlinearity and hysteresis behavior of the spinal motion segment (Figure 1.5). The most frequently used parameters that are captured in these load-displacement curves are the neutral zone (NZ), the elastic zone (EZ), the range of motion (ROM), and information about the flexibility and stiffness of the motion segment. The neutral zone is the part where there is little resistance to motion, whereas the elastic zone describes the part of the curve where the resistance to motion increases as the load increases. Another parameter describing the motion of the cervical spine is the center of rotation (COR). The COR gives information about the rotational as well as the translational functioning of the vertebrae

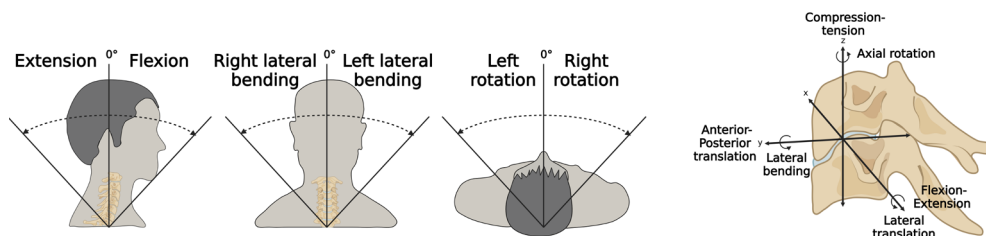


Figure 1.4: Left: The different ROM of the cervical spine, being flexion-extension, lateral bending, and axial rotation. Right: the 6-DOF of a spinal motion segment. Created with BioRender.com

and intervertebral disc of a spinal motion segment. The location of the COR is stable over time for the vertebrae, but varies over time for the intervertebral disc. The variable COR of the intervertebral disc assures that surrounding anatomical structures, such as the facet joints, are not overloaded during normal movements.

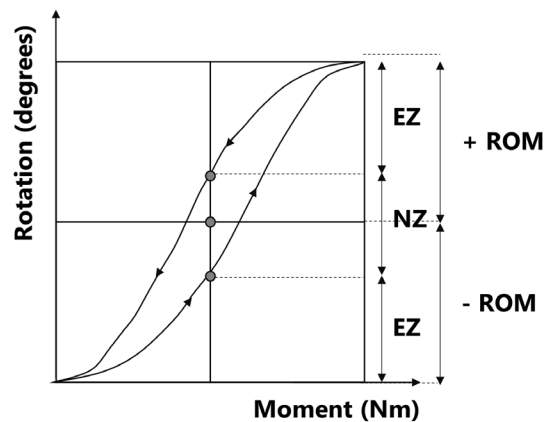


Figure 1.5: *Moment (Nm) – Rotation curve typical for spinal motion segment showing non-linear behavior with a neutral zone and elastic zone.*

1.4 Neck pain, disc degeneration and treatments

Neck pain is a musculoskeletal condition that is one of the leading causes commonly reported to restrict activities of daily living [22]. Approximately 80% of the population report neck pain for an unspecified period at some time in their life [23]. Due to this high prevalence, neck pain is not only a health problem, but also results in an enormous socioeconomic burden. Neck pain is most frequently related to the degeneration of the intervertebral disc [24]. Intervertebral disc degeneration can result in a decrease of disc height, bulging of the disc and a reduced shock absorbance capacity. These degenerative alterations can progress into herniation, protrusion, osteophyte formation or cervical spondylosis that can deteriorate and result in cervical radiculopathy and/or myelopathy [25]. In cervical radiculopathy and/or myelopathy, a cervical spinal nerve or its roots are compressed, inflamed or damaged resulting in a change in neurological function, and often in neck pain and/or shoulder and arm pain [26]. Initially, patients are treated with conservative treatments such as pain medication and physiotherapy [27]. When conservative treatments become insufficient to relieve the pain for the patient, surgical interventions are considered.

1.4.1 Fusion

Currently, the gold standard to treat pain related myelopathy and/or radiculopathy is anterior cervical discectomy and fusion (ACDF) [28]. ACDF aims to reduce compression of neural tissue and restore the disc height by stabilizing the spinal column. This is done by dissecting the diseased intervertebral disc, replacing it with a cage (autograft or allograft) and fusing the vertebrae of the treated segment [29]. Despite good clinical results, there are several limitations of fusing the vertebrae. It is hypothesized that due to the loss of motion, which may be aggravated by sagittal malalignment, adjacent segments compensate leading to a higher risk of degeneration and pain, i.e. adjacent segment disease. Previous research has shown an occurrence of radiographic degeneration of the adjacent segments in 92 % of the patients 5 years after the fusion surgery [30]. Hilibrand et al. (1999) also observed that 25.6 % of the patients suffered from symptomatic adjacent segment disease 10 years post-surgery [31]. Biomechanical data also confirms that fusion leads to elevated intradiscal pressures at the adjacent levels and altered motion compared to an intact motion segment [32]. Another commonly reported complication is subsidence, where the device sinks into the adjacent vertebral bodies. This can result in loss of disc height, change in the lordotic shape and eventually this can hamper spine kinematics and cause recurrent neck pain [33].

1.4.2 Cervical disc replacement

Cervical disc replacement (CDR) has been proposed as an alternative surgical treatment, in which the diseased intervertebral disc is replaced by a prosthesis. The rationale of CDR is to maintain cervical mobility while relieving pain, thereby reducing the risk of adjacent segment disease. CDR was first introduced in the 1960s by Ulf Fernstrom, who developed a stainless steel ball bearing device [34]. Unfortunately, due to high complication rates this device became unpopular. A new generation of disc replacement devices were developed in the 1980s, resulting in stainless-steel ball-and-socket designs derived from large synovial articulating joint arthroplasties such as the knee and hip [35]. Initial clinical results were unsatisfactory, but after some design iterations, promising results were achieved [36], [37]. Hereafter, a range of articulating ball-and-socket designs using metal-on-metal or metal-on-polymer bearing surfaces were developed. Clinical patient outcomes of these articulating prosthesis have shown equivalent or even superior results compared to ACDF [38]–[41]. Like ACDF, subsidence is a frequently reported complication that is mainly associated with a mismatch in the footprint and a poor compressive strength of the neighboring vertebral bone [42]. However, the main reason why these CDR devices do not always show significantly superior outcomes to ACDF is mainly related to the implant design. These articulating ball-and-socket prostheses provide motion based on sliding whereas the natural disc allows motion based on deformation, and thus are a highly simplified version of the complex anatomy and kinematics of a natural

intervertebral disc [43], [44]. The lack of shock absorbance in the design of these implants can lead to an unstable environment where soft spinal structures and facet-joints are overloaded to compensate [45], [46]. As previously mentioned, the smallest complex responsible for facilitating motion in the spine is the spinal motion segment (SMS). The SMS does not only include the intervertebral disc, but also the adjacent vertebrae and all adjoining ligaments. Each of these components play a role in enabling motion and thus its kinematic behavior. Replacing one of the elements of the SMS, such as the IVD during CDR procedure, can result in an overall change in kinematics [47]. Previous research has shown a high incidence of facet joint degeneration at the treated level using both unconstrained and constrained devices [48]. It is hypothesized that a more constrained design has a fixed center of rotation that can result in facet overloading. On the other hand, a less constrained design is unable to resist sufficient shear, which can in turn lead to increased facet loading [49]. These results indicate the importance of not only replicating the quantity of motion, but also the quality of motion to avoid subsequent pathologies on surrounding anatomical structures.

This has driven the development of deformable viscoelastic total disc replacement prosthesis to better replicate the anatomy and kinematics of a natural intervertebral disc. One of those deformable poro- and viscoelastic total discs replacement prosthesis is the biomimetic artificial intervertebral disc (bioAID), which will be further introduced and investigated in the current thesis.

1.5 Design of the biomimetic artificial intervertebral disc

The biomimetic artificial intervertebral disc (bioAID) is based on the hypothesis that mimicking the natural structure of the intervertebral disc will lead to mimicking the biomechanical properties, thereby improving clinical outcome and reducing the risk of adjacent segment disease [50]. The bioAID design contains a hydrogel core, representing the soft swelling nucleus pulposus, a polymer fiber jacket mimicking the tensile strong annulus fibrosus and metal endplates with pins to connect the prosthesis with the vertebrae as the cartilaginous endplates do (Figure 1.6).

The main goal of CDR devices is to restore biomechanical functions of the spinal motion segment. This includes preserving the range of motion, as well as the motion patterns and center of rotation. In contrast to first-generation articulating devices, the bioAID provides motion based on deformation as seen in a natural motion segment. Due to the symbiotic relationship between the hydrogel and the fiber jacket, it can provide semi-constrained motion, where the soft swelling hydrogel provides little resistance to small deformations while larger deformations are resisted by the tensile strong fibers of the jacket. It is hypothesized

that by replicating this mechanism of motion, it will also result in replicating a variable center of rotation.

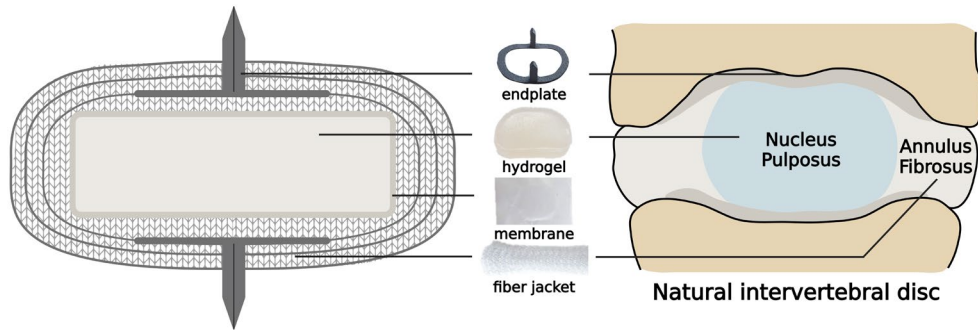


Figure 1.6: Schematic representation of the bioAID design and its mimicry to a natural intervertebral disc. Created with BioRender.com

Besides preserving motion, due to the restricted swelling of the hydrogel by the fiber jacket, the bioAID can generate a high intradiscal pressure and act as a shock absorber to avoid overloading, which is one of the primary functions of a natural disc. This swelling of the hydrogel will also allow the bioAID to replicate the diurnal rhythm, which helps in dissipating stress and releasing tension in surrounding tissues. Moreover, the materials used in this design are softer compared to fully metal-on-metal designs, or metal-on-hard-polymer designs, resulting in a reduced risk of stress-shielding and abnormal loading on adjacent structures.

Primary stability is mainly achieved by the pins of the endplate that sink into the adjacent vertebrae as anchorage. This stability is further improved by the swelling of the hydrogel, since this is not only restricted by the fiber jacket but also by the available disc space, thereby maximizing the contact surface between the implant and the adjacent vertebrae. However, previous results have shown that functional biomimicry of the bioAID is dependent on the interconnection of the jacket fibers to the adjacent vertebrae, especially during rotational movements [50]. It is therefore critical to create a suitable surface for osseointegration at the cranial and caudal sides of the implant. It is hypothesized that the fibrous jacket structure replicates how the collagen fibers in the natural disc form the connection between the disc and adjacent vertebrae [14]. In this way, loads can be transferred and distributed in a similar fashion as in a natural disc. Overall, it is hypothesized that these unique design features of the bioAID lead to an improved functionality compared to existing articulating devices.

1.5.1 Hydrogel

Hydrogels are hydrophilic three-dimensional polymer networks that are capable of absorbing large amounts of water while retaining their structure. Hydrogels have been developed for

several applications in the biomedical industry and became especially popular because of their tunable mechanical properties and swelling characteristics that match many highly hydrated tissues found in the human body. For the bioAID, the hydrogel mainly replicates the function of the nucleus pulposus and consists of two different monomers, 2-hydroxyethyl methacrylate (HEMA) and sodium methacrylate (NaMA) reinforced with a polyurethane foam. HEMA is a well-known hydrogel in the biomedical field gaining popularity already in the early sixties as soft contact lenses, mainly because of its biocompatibility, high permeability and high hydrophilicity [51]. To enhance the mechanical properties, a polyurethane foam is integrated to inhibit crack propagation, thereby increasing the toughness and reducing the risk of mechanical failure. The HEMA-NaMA hydrogel can attract water by Donnan osmosis due to the negative charges of the sodium (of NaMA) present inside the hydrogel. This results in an isotropic swelling capacity similar to how the proteoglycans function in the nucleus pulposus. The water inside the hydrogel behaves as a cushion to absorb and dissipate the loads acting on the intervertebral disc. The viscoelastic and poro-elastic nature of the hydrogel gives the bioAID similar time dependent behavior as a native disc, leading to a constant exchange of fluid between the hydrogel and the surrounding environment. As a result, the hydrogel is mainly responsible for the implant's compressive strength, viscoelastic behavior, and shock absorbance capacity. To avoid any hydrogel particles to enter the surrounding tissues, the hydrogel is wrapped in an UHMWPE membrane. This membrane is very thin (38 μm thick) and has pores of 0.9 μm to allow exchange of fluid flow while retaining small hydrogel particles.

1.5.2 *Fiber jacket*

The usage of textiles as a biomaterial started already in the 1960s [52], mainly because textiles match the mechanical properties of human tissues better compared to the hard materials used previously. Within the bioAID design, the fiber jacket is a tubular textile that aims to mimic the fibrous collagen-rich annulus fibrosus of a native disc. It is produced from a multifilament UHMWPE yarn, known for its low friction, high abrasion resistance, high toughness, ease of fabrication, biocompatibility and biostability [52]. The UHMWPE yarn is produced through a gel spinning process, in which the fibers are drawn, heated, elongated, and cooled resulting in molecular alignment, high crystallinity, and low density [53], [54]. In the first prototype designed by Peter van den Broek et al. (2012), the fiber jacket was a weft-knitted stocking fabricated from a single UHMWPE yarn. Results showed that the jacket within the bioAID remained intact after 10 million cycles of axial compression [55]. Nevertheless, the integrity of the fiber jacket using a single yarn weft-knitted textile structure is at risk during the implantation procedure where it is often exposed to sharp bony protrusions and sharp surgical tools. Unlike weft-knitting, warp-knitted structures are made from multiple yarns, making them less susceptible to failure upon damage. In addition, warp-knitted textiles are usually

flatter and have a lower elasticity which can help in restricting the swelling of the hydrogel core while still able to follow the complex shape of the hydrogel. Therefore, the fiber jacket described in this thesis was produced using warp-knitting textile technology.

As already mentioned, the fiber jacket surrounds the hydrogel and endplates, such that it behaves as one integrated unit similar to a natural intervertebral disc. Similar to the annulus fibrosus, the fiber jacket is mainly responsible for the tensile strength of the implant due to the high tensile stiffness of the UHMWPE yarn. In addition, it inhibits the swelling of the hydrogel, leading to a high internal pressure and pre-stressing of the jacket fibers. The combination of hydrogel surrounded by the fiber jackets gives the bioAID its load bearing capacity, and semi-constrained motion behavior similar to a native disc. The fiber jacket is also in direct contact with the adjacent vertebrae, and thus responsible for providing a suitable surface that allows osseointegration of the implant with the bony endplates of the adjacent vertebrae. To achieve this, the fabric structure should have an optimal pore size for facilitating osseointegration, shown to be in the range of 300-600 μm [49]–[54]. The fiber jacket surface should, however, only facilitate osseointegration on the cranial and caudal sides of the device, while bone formation needs to be inhibited on the lateral sides to avoid a fusion. Therefore, besides porosity, the cranial and caudal surfaces should have physical and chemical properties that enable osseointegration [55].

1.5.3 Endplate

The risk of migration or device expulsion should be reduced as much as possible since this can greatly affect the patient clinical outcome and prevent revision surgeries [56], [57]. In the bioAID, titanium ring endplates, having similar contours as the hydrogel, with either spikes or keels that sink into the adjacent vertebrae to provide stability. Besides avoiding instabilities, the endplate should not interfere with the biomimetic function of the hydrogel and fiber jacket. In addition, it should not alter the stress profiles in the vertebrae and work together with the jacket. Lastly, it should be visible with fluoroscopy and positioned in the midline to guide the implantation. Throughout the thesis, the design of the endplate has gone through several iterations to allow for a reproducible and controlled implantation procedure while providing good fixation.

1.6 Aim and thesis outline

The aim of this thesis is to further develop the bioAID for the treatment of severely degenerated discs that require a total disc replacement. Overall, the most important considerations for the design of an artificial cervical disc are mimicking the mechanical behavior of a natural intervertebral disc, preserving the physiological range of motion and securing long-term stability. Therefore, each of the chapters in this thesis cover one of those aspects.

In the current chapter (**Chapter 1**) an introduction was given about the anatomy and physiology of the spine and intervertebral disc, whereafter the clinical problem and current treatments were described.

Chapter 2 gives an overview of design related advantages and disadvantages of deformable viscoelastic CDR devices that are currently on the market or are under development. The aim of this review was to get more insight into design characteristics of this relatively new group of CDR devices, and use this to avoid previously reported design related complications. Based on this literature review, it was seen that most viscoelastic CDR devices can provide motion in all six-degrees-of-freedom and have a variable center of rotation. However, some of the viscoelastic materials have short history in orthopedics, so long-term behavior of these materials *in vivo* is still unknown.

Several parameters need to be taken into consideration for the design of the knitted jacket, such as surface coverage, fabric extensibility, and drapability to conform with the complex shape of the hydrogel core. In addition, to restrict the swelling of the hydrogel, the jacket needs to have a certain density and limited elasticity. Therefore, in **Chapter 3**, several different jacket design configurations were tested that can ensure structural integrity and allow for isotropic swelling constrain of the hydrogel core.

One of the most important factors influencing clinical success of load bearing prosthesis is osseointegration to achieve long-term stability. Although the bioAID has titanium endplates with pins that provide initial fixation, osseointegration of the UHMWPE fibers to the adjacent vertebrae is required to provide long-term fixation and allow for proper biomimetic behavior. UHMWPE is known for its good mechanical properties, but it is also inert and hydrophobic, being a poor surface for facilitating osseointegration. Therefore, in **Chapter 4** several different surface modifications of UHMWPE fabrics were assessed in an *in vitro* cell culture model to assess the osteoconductive potential of these different surfaces.

Chapter 1

The main rationale of performing a cervical total disc replacement is to preserve the natural range of motion of the spinal segment. Hence, in **Chapter 5**, the bioAID's capability to restore the physiological kinematics of the cervical spine were assessed. Especially since this biomimetic design is hypothesized to be able to replicate the non-linear kinematics of the native disc better compared to first-generation ball-and-socket designs. This was assessed using an *ex vivo* cervical canine spine model in a six-degrees-of-freedom tester.

Chapter 6 evaluates the design of the bioAID for withstanding physiological loads without functional failure or risk of migration. Although different loading modes act on the motion of a spinal segment, in normal daily life the loads that are being transferred through the intervertebral disc are mainly compressive. As a results, the bioAID was assessed for its compressive strength and shear-compressive strength. To verify if the titanium rings with pins can provide good initial fixation, tests were performed to assess the risk of subsidence and device expulsion. Lastly, one of the unique characteristics of the bioAID is that it can replicate the creep behavior seen in a natural intervertebral disc. Therefore, the creep behavior of the bioAID was characterized during a diurnal loading regime.

In the final **Chapter 7**, the main findings and implications of the complete thesis are discussed, concluding with the remaining challenges and future perspectives.

References

- [1] R. Jonas and H. Wilke, "Chapter 2 - The Cervical Spine," in *Biomechanics of the Spine*, Elsevier Ltd., 2018, pp. 11–34.
- [2] A. White and M. Panjabi, *Clinical Biomechanics of the Spine*, 2nd ed. London: Lipincott Company, 1990.
- [3] D. Skrzypiec, M. Tarala, P. Pollintine, P. Dolan, and M. A. Adams, "When are intervertebral discs stronger than their adjacent vertebrae?," *Spine (Phila. Pa. 1976)*, vol. 32, no. 22, pp. 2455–2461, 2007.
- [4] F. Galbusera, M. Van Rijsbergen, K. Ito, J. M. Huyghe, M. Brayda-Bruno, and H. J. Wilke, "Ageing and degenerative changes of the intervertebral disc and their impact on spinal flexibility," *Eur. Spine J.*, vol. 23, no. SUPPL. 3, pp. S324–S332, 2014.
- [5] M. A. Adams, "Intervertebral Disc Tissues," in *Mechanical properties of aging soft tissues*, Springer International Publishing Switzerland, 2015, pp. 7–35.
- [6] N. Newell, J. Little, A. Christou, M. Adams, C. Adam, and S. Masouros, "Biomechanics of the human intervertebral disc: A review of testing techniques and results," *J. Mech. Behav. Biomed. Mater.*, vol. 69, pp. 420–434, May 2017.
- [7] D. R. Eyre, "Biochemistry of the intervertebral disc," *Int. Rev. Connect. Tissue Res.*, vol. VOL. 8, pp. 227–291, Jan. 1979.
- [8] B. Frost, S. Camarero-Espinosa, and E. Foster, "Materials for the spine: anatomy, problems, and solutions," *Materials (Basel)*, vol. 12, no. 2, p. 253, Jan. 2019.
- [9] K. Wang, Z. Deng, H. Wang, Z. Li, H. Zhan, and W. Niu, "influence of variations in stiffness of cervical ligaments on C5-C6 segment," *J. Mech. Behav. Biomed. Mater.*, vol. 72, no. 1, pp. 129–137, 2017.
- [10] J. Pospiech, D. Stolke, H. J. Wilke, and L. E. Claes, "Intradiscal pressure recordings in the cervical spine," *Neurosurgery*, vol. 44, no. 2, pp. 379–385, 1999.
- [11] A. Malandrino, A. R. Jackson, J. M. Huyghe, and J. Noailly, "Poroelastic modeling of the intervertebral disc: A path toward integrated studies of tissue biophysics and organ degeneration," *MRS Bull.*, vol. 40, no. 4, pp. 324–332, Apr. 2015.
- [12] M. L. Schollum, P. A. Robertson, and N. D. Broom, "ISSLS prize winner: microstructure and mechanical disruption of the lumbar disc annulus: part I: a microscopic investigation of the translamellar bridging network," *Spine (Phila. Pa. 1976)*, vol. 33, no. 25, pp. 2702–2710, 2008.
- [13] J. M. Cloyd and D. M. Elliott, "Elastin content correlates with human disc degeneration in the anulus fibrosus and nucleus pulposus," *Spine (Phila. Pa. 1976)*, vol. 32, no. 17, pp. 1826–1831, 2007.
- [14] M. Sharabi, K. Wade, and R. Haj-ali, Chapter 7 - The Mechanical Role of Collagen Fibers in the Intervertebral Disc. Elsevier Ltd., 2018.
- [15] K. Wade, Chapter 8 - Vertebral Endplates. Elsevier Ltd., 2018.
- [16] M. B. Panzer, "Numerical Modelling of the Human Cervical Spine in Frontal Impact," University of Waterloo, 2006.
- [17] S. Kirnaz et al., "Fundamentals of Intervertebral Disc Degeneration," *World Neurosurg.*, vol. 157, pp. 264–273, Jan. 2022.
- [18] P. P. A. Vergroesen, A. J. Van Der Veen, B. J. Van Royen, I. Kingma, and T. H. Smit, "Intradiscal pressure depends on recent loading and correlates with disc height and compressive stiffness," *Eur. Spine J.*, vol. 23, no. 11, pp. 2359–2368, 2014.
- [19] P. P. A. Vergroesen, A. J. van der Veen, K. S. Emanuel, J. H. van Dieën, and T. H. Smit, "The poroelastic behaviour of the intervertebral disc: A new perspective on diurnal fluid flow," *J. Biomech.*, vol. 49, no. 6, pp. 857–863, Apr. 2016.
- [20] P. P. A. Vergroesen, K. S. Emanuel, M. Peeters, I. Kingma, and T. H. Smit, "Are axial intervertebral disc biomechanics determined by osmosis?," *J. Biomech.*, vol. 70, pp. 4–9, Mar. 2018.

- [21] A. J. Van der Veen, A. Bisschop, M. G. Mullender, and J. H. van Dieën, "Modelling creep behaviour of the human intervertebral disc," *J. Biomech.*, vol. 46, no. 12, pp. 2101–2103, Aug. 2013.
- [22] C. C. Scarabottolo, R. Z. Pinto, C. B. Oliveira, E. F. Zanuto, J. R. Cardoso, and D. G. D. D. Christofaro, "Back and neck pain prevalence and their association with physical inactivity domains in adolescents," *Eur. Spine J.*, vol. 26, no. 9, pp. 2274–2280, Sep. 2017.
- [23] V. F. Ferrario, C. Sforza, G. Serrao, G. P. Grassi, and E. Mossi, "Active range of motion of the head and cervical spine: A three-dimensional investigation in healthy young adults," *J. Orthop. Res.*, vol. 20, no. 1, pp. 122–129, 2002.
- [24] A. S. Przybyla, D. Skrzypiec, P. Pollintine, P. Dolan, and M. A. Adams, "Strength of the Cervical Spine in Compression and Bending," *Spine (Phila. Pa. 1976)*, vol. 32, no. 15, pp. 1612–1620, Jul. 2007.
- [25] B. I. Woods and A. S. Hilibrand, "Cervical Radiculopathy," *J. Spinal Disord. Tech.*, vol. 28, no. 5, pp. E251–E259, Jun. 2015.
- [26] N. Bogduk, "The Anatomy and Pathophysiology of Neck Pain," *Physical Medicine and Rehabilitation Clinics of North America*, vol. 22, no. 3. *Phys Med Rehabil Clin N Am*, pp. 367–382, Aug-2011.
- [27] A. P. Verhagen, "Physiotherapy management of neck pain," *J. Physiother.*, vol. 67, no. 1, pp. 5–11, Jan. 2021.
- [28] I. Zechmeister, R. Winkler, and P. Mad, "Artificial total disc replacement versus fusion for the cervical spine: a systematic review," *Eur. Spine J.*, vol. 20, no. 2, pp. 177–184, Feb. 2011.
- [29] G. W. Smith and R. A. Robinson, "The Treatment of Certain Cervical-Spine Disorders by Anterior," *J. Bone Jt. Surg.*, vol. 40, no. 3, pp. 607–624, 1958.
- [30] J. Goffin et al., "Long-term follow-up after interbody fusion of the cervical spine," *J. Spinal Disord.*, vol. 17, no. 2, pp. 79–85, Apr. 2004.
- [31] A. S. Hilibrand, G. D. Carlson, M. A. Palumbo, P. K. Jones, and H. H. Bohlman, "Radiculopathy and myelopathy at segments adjacent to the site of a previous anterior cervical arthrodesis," *J. Bone Jt. Surg. - Ser. A*, vol. 81, no. 4, pp. 519–528, Apr. 1999.
- [32] A. E. Dmitriev, B. W. Cunningham, N. Hu, G. Sell, F. Vigna, and P. C. McAfee, "Adjacent level intradiscal pressure and segmental kinematics following a cervical total disc arthroplasty: An *in vitro* human cadaveric model," *Spine (Phila. Pa. 1976)*, vol. 30, no. 10, pp. 1165–1172, May 2005.
- [33] A. Parisien, E. K. Wai, M. S. A. Elsayed, and H. Frei, "Subsidence of Spinal Fusion Cages: A Systematic Review," *Int. J. spine Surg.*, vol. 16, no. 6, pp. 1103–1118, Dec. 2022.
- [34] U. Fernström, "Arthroplasty with intercorporeal endoprosthesis in herniated disc and in painful disc," *Acta Chir. Scand. Suppl.*, vol. 357, pp. 154–159, 1966.
- [35] P. B. Derman and J. E. Zigler, "Cervical disc arthroplasty: Rationale and history," *Int. J. Spine Surg.*, vol. 14, no. s2, pp. S5–S13, Aug. 2020.
- [36] B. H. Cummins, J. T. Robertson, and S. S. Gill, "Surgical experience with an implanted artificial cervical joint," *J. Neurosurg.*, vol. 88, no. 6, pp. 943–948, Jun. 1998.
- [37] C. C. Wigfield, S. S. Gill, R. J. Nelson, N. H. Metcalf, and J. T. Robertson, "The new Frenchay artificial cervical joint: Results from a two-year pilot study," *Spine (Phila. Pa. 1976)*, vol. 27, no. 22, pp. 2446–2452, 2002.
- [38] D. Ohnmeiss, R. Guyer, Y. Samocha, J. Zigler, and S. Blumenthal, "Cervical Total Disc Replacement Versus Anterior Cervical Fusion: Data from Four Prospective, Randomized, Multicenter Trials," in *The Spine Journal*, 2011, vol. 11, no. 10, pp. S150–S151.
- [39] R. J. Davis et al., "Cervical total disc replacement with the Mobi-C cervical artificial disc compared with anterior discectomy and fusion for treatment of 2-level symptomatic degenerative disc disease: a prospective, randomized, controlled multicenter clinical trial," *J. Neurosurg. Spine*, vol. 19, no. 5, pp. 532–545, 2013.
- [40] M. E. Janssen, J. E. Zigler, J. M. Spivak, R. B. Delamarter, B. V. Darden, and B. Kopjar, "ProDisc-C total disc replacement versus anterior cervical discectomy and fusion for single-level

- symptomatic cervical disc disease," *J. Bone Jt. Surg. - Am. Vol.*, vol. 97, no. 21, pp. 1738–1747, 2014.
- [41] P. V. Mummaneni, J. K. Burkus, R. W. Haid, V. C. Traynelis, and T. A. Zdeblick, "Clinical and radiographic analysis of cervical disc arthroplasty compared with allograft fusion: A randomized controlled clinical trial," *J. Neurosurg. Spine*, vol. 6, no. 3, pp. 198–209, Mar. 2007.
- [42] C. K. Lee, "Osteopenia and Total Disc Prosthesis Subsidence: Inclusion/Exclusion Criteria for Total Disc Replacement," *SAS J.*, vol. 1, no. 2, pp. 82–84, 2007.
- [43] J. J. Costi, I. A. Stokes, M. G. Gardner-Morse, and J. C. Iatridis, "Frequency-Dependent Behavior of the Intervertebral Disc in Response to Each of Six Degree of Freedom Dynamic Loading," *Spine (Phila. Pa. 1976)*, vol. 33, no. 16, pp. 1731–1738, Jul. 2008.
- [44] H. A. L. Guerin and D. M. Elliott, "Structure and Properties of Soft Tissues in the Spine," in *Spine Technology Handbook*, Amsterdam: Elsevier Academic Press, 2006, pp. 35–62.
- [45] F. Galbusera, C. M. Bellini, M. Brayda-Bruno, and M. Fornari, "Biomechanical studies on cervical total disc arthroplasty: A literature review," *Clin. Biomech.*, vol. 23, no. 9, pp. 1095–1104, Nov. 2008.
- [46] V. V. Patel et al., "Cervical facet force analysis after disc replacement versus fusion," *Clin. Biomech.*, vol. 44, pp. 52–58, May 2017.
- [47] T. Zander, A. Rohlmann, and G. Bergmann, "Influence of different artificial disc kinematics on spine biomechanics," *Clin. Biomech.*, vol. 24, no. 2, pp. 135–142, Feb. 2009.
- [48] C. S. Shim et al., "CHARITI versus ProDisc: A comparative study of a minimum 3-year follow-up," *Spine (Phila. Pa. 1976)*, vol. 32, no. 9, pp. 1012–1018, 2007.
- [49] M. A. Rousseau, D. S. Bradford, R. Bertagnoli, S. S. Hu, and J. C. Lotz, "Disc arthroplasty design influences intervertebral kinematics and facet forces," *Spine J.*, vol. 6, pp. 258–266, 2006.
- [50] P. R. Van Den Broek, "Development of a biomimetic artificial intervertebral disc," Eindhoven University of Technology, 2012.
- [51] L. Ambrosio, R. De Santis, and L. Nicolais, "Composite hydrogels for implants," *Proc. Inst. Mech. Eng. Part H J. Eng. Med.*, vol. 212, no. 2, pp. 93–99, Feb. 1998.
- [52] R. Vaishya, A. K. Agarwal, M. Tiwari, A. Vaish, V. Vijay, and Y. Nigam, "Medical textiles in orthopedics: An overview," *J. Clin. Orthop. Trauma*, vol. 9S, pp. S26–S33, Mar. 2018.
- [53] B. Sanborn, A. M. DiLeonardi, and T. Weerasooriya, "Tensile Properties of Dyneema SK76 Single Fibers at Multiple Loading Rates Using a Direct Gripping Method," *J. Dyn. Behav. Mater.*, vol. 1, no. 1, pp. 4–14, Mar. 2015.
- [54] R. Siskey, H. Smelt, K. Boon-Ceelen, and M. Persson, "UHMWPE Homocomposites and Fibers," in *UHMWPE Biomaterials Handbook: Ultra High Molecular Weight Polyethylene in Total Joint Replacement and Medical Devices*, Elsevier Inc., 2015, pp. 398–411.
- [55] P. R. Van Den Broek, J. M. Huyghe, and K. Ito, "Biomechanical behavior of a biomimetic artificial intervertebral disc," *Spine (Phila. Pa. 1976)*, vol. 37, no. 6, pp. 367–373, 2012.
- [56] C. K. Lee and V. K. Goel, "Artificial disc prosthesis: design concepts and criteria," *Spine J.*, vol. 4, no. 6, Supplement, pp. S209–S218, Nov. 2004.
- [57] M. F. Eijkelkamp, J. M. Huyghe, C. C. van Donkelaar, J. R. van Horn, A. G. Veldhuizen, and G. J. Verkerke, "Requirements for an artificial intervertebral disc," *Int. J. Artif. Organs*, vol. 24, no. 5, pp. 311–321, 2001.



Chapter 2

Viscoelastic cervical total disc replacements

The contents of this chapter are based on:

C.A.M. Jacobs, C.J. Siepe, K. Ito. Viscoelastic cervical total disc replacement devices: design concepts. *The Spine Journal*, vol. 20, no. 12, p. 1911-1924, Dec. 2020

DOI: [10.1016/j.spinee.2020.08.007](https://doi.org/10.1016/j.spinee.2020.08.007)

Abstract

Cervical disc replacement (CDR) is a motion-preserving surgical procedure for treating patients with degenerative disorders. Numerous reports of first-generation CDR “ball-and-socket” articulating devices have shown satisfactory clinical results. As a result, CDR devices have been safely implemented in the surgeon’s armamentarium on a global scale. However, only minor design improvements have been made over the last few years, as first generation CDRs devices were based on traditional synovial joint arthroplasty designs. As a consequence, these articulating designs have limited resemblance to the complex kinematic behavior of a natural disc. This has driven the development of deformable viscoelastic CDR devices to better mimic the biomechanical behavior of a natural disc. As a result, several viscoelastic CDR devices have been developed in recent years that vary in terms of materials, design and clinical outcomes. Since these viscoelastic CDR devices are fairly new, their weaknesses and strengths, which are related to their design characteristics, have not been well described. Therefore, this literature review discusses design related advantages and disadvantages of deformable viscoelastic CDR devices. As such, this paper can provide insight for surgeons and engineers on specific design characteristics of several viscoelastic devices and could potentially help to develop and design future implants. Eleven viscoelastic CDR devices were identified. An extensive database search on the devices’ tradenames in Medline and PubMed was performed next. The devices were categorized based on common design characteristics to give an overview of both category and device specific complications and advantages. Overall, literature shows that most of these viscoelastic CDR devices can provide motion in all six degrees-of-freedom and have a variable center of rotation. Nevertheless, the viscoelastic materials used do not have an extensive history in orthopedics, so the long-term material behavior *in vivo* is still unknown. Although the viscoelastic devices have common benefits and risks, each specific design and category also has its own design related advantages and drawbacks that are described in this review. Altogether, viscoelastic total disc replacements seem to be a promising option for the future of cervical arthroplasty, but long-term clinical outcome is needed to confirm the advantages of mimicking the viscoelasticity of a natural disc.

2.1 Introduction

Currently, the gold standard to treat myelopathy and/or radiculopathy is anterior cervical discectomy and fusion (ACDF) [1]. Despite good clinical results, there are several limitations of fusing the vertebrae. It is hypothesized that due to the loss of motion, which may be aggravated by sagittal malalignment, adjacent segments compensate leading to a higher risk of degeneration and pain, i.e. adjacent segment disease. Previous research has shown an occurrence of radiographic degeneration of the adjacent segments in 92% of the patients 5 years after fusion surgery [2]. Biomechanical data also confirms that fusion leads to elevated intradiscal pressures at the adjacent levels and altered motion compared to an intact motion segment [3].

Therefore, cervical disc replacement (CDR) has been proposed as an alternative treatment, in which the affected intervertebral disc is replaced by a prosthesis. The rationale of CDR is to maintain cervical mobility while relieving pain, thereby reducing the risk of adjacent segment disease. Multiple *in vitro* studies have shown reduced intradiscal pressures in the adjacent level discs when using motion-preserving implants [3]–[7].

First generation prostheses were derived from knee and hip implants, resulting in articulating ball-and-socket designs using metal-on-metal or metal-on-polymer bearing surfaces. Clinical patient outcomes of these first-generation prostheses have shown equivalent or even superior results compared to ACDF [8]. However, first generation implants were based on sliding motions, providing little dampening and energy storage. As a consequence, these first-generation devices are a highly simplified version of the complex anatomy, motion, and kinematics of a natural cervical disc [9], [10]. This can create an unstable environment where the ligaments, muscles, uncovertebral joints and facet-joints are placed under abnormal loading patterns that could lead to progressive facet and uncovertebral joint degeneration at the treated and adjacent segments [11]–[17].

New generation total disc replacements that can mimic the viscoelastic behavior of a native disc may offer distinct advantages when compared to first-generation devices. These devices provide motion arising from deformable components, therefore being able to provide all six degrees of freedom and combined motions.

Several different viscoelastic disc replacement devices have been developed in recent years that vary in terms of materials, design, and clinical outcomes. The present manuscript provides an overview of all design related advantages and disadvantages of compressible, viscoelastic total disc replacements that are currently available, which will provide insight for surgeons and

engineers on each of these specific designs and which may help to develop new viscoelastic total disc replacements.

Overall, eleven viscoelastic cervical disc replacements were identified, which are either already commercially available or still under development, for which literature was collected through an extensive database search in PubMed and Medline using the device's tradename and the snowball method. As a next step, the devices were divided into groups based on their design structure: either endplate sandwiched viscoelastic devices or devices without endplates. Those with endplates can be further categorized into either a monoblock design, where all the components are firmly bonded to each other, or mobile bumpers where the different components are not bonded. An overview of the eleven viscoelastic devices, organized based on their design category, are shown in Table 2.1.

2.2 Endplate sandwiched

Endplate sandwiched devices all have the common design principle of an elastomeric core sandwiched between two endplates. This group can be further subdivided in either a monoblock or mobile bumper design. In the monoblock design, the elastomeric core is firmly bonded to the adjacent endplates. In the mobile bumper design, a polymer core is also sandwiched between two metal endplates, but the metal endplates are not attached to the elastomeric core. As a result, the core can move and articulate freely to provide motion. In the majority of these endplate sandwiched designs, the endplates are made out of titanium alloy, which is known to allow osseous integration [18]. To increase bone growth on the endplates even more, they are often coated with hydroxyapatite, or its structure is modified to provide a porous bone in growth structure by e.g. titanium plasma deposition [19], [20]. As a consequence, all these designs show good osseous integration. Nevertheless, the use of metal also has its downsides since it can hamper follow-up imaging due to metal artefacts [21], [22], particularly in the cervical spine.

2.2.1 Monoblock

The advantage of the monoblock design is that this one-piece structure enables motion only by deformation, thereby leading to a reduced risk of wear particles compared to implants using sliding surfaces. However, a potential weakness in these designs is the bond between the polymer and metal endplates. The material properties of these two materials are substantially different and therefore bear the risk to delaminate at the interface [23]. Another potential weakness, based on experience in large joint arthroplasty, is that using a monoblock constrained design can transfer shear stress to the interface between vertebrae and implant, leading to the risk of implant migration and loosening [24]. Another potential pitfall is the risk

of applying damaging tensile loads on the core during extension movements [19]. Multiple monoblock viscoelastic devices are currently available, such as the Freedom[®], CP-ESP[®], Rhine[™], D-flex Carbon, NeoPhytos and UFO, which are discussed in the following paragraphs.

2.2.1.1 Freedom

The Freedom[®] Cervical Disc (FCD, Axiomed LLC) has gone through several design iterations before it became commercially available in the EU. The first version, a precursor of the Freedom[®] disc named Acroflex (Depuy, Acromed Inc. Raynham Mass.), was an unconstrained lumbar design consisting of porous coated titanium endplates with a polyolefin rubber core [25]. Although the rubber was extensively tested for its fatigue life and wear properties [26], the results of this study demonstrated rubber tears in 36% of the patients [27]. After gaining knowledge from these initial studies, Acroflex was reintroduced with a modified design as Freedom[®]. The major difference between the Acroflex and Freedom[®] is the material of the viscoelastic core, where instead of rubber a thermoplastic silicone polycarbonate urethane (CarboSil[™], The Polymer Technology Group, Berkely, CA) was used. The bond between the rubber core and titanium endplates is very unique to the design and achieved in two ways. The first mechanism is through chemical bonding using a custom-made primer and adhesive. The second bond is achieved mechanically by using titanium beads that mechanically interlock with the elastomeric core [27]. Moreover, a raised ridge and wedged titanium endplates were incorporated to relieve the bond from strain at high stresses during movement and to distribute the loads equally. Although it has been thought that the rubber-titanium-bond would be the inherent weakness of the design, no failure has been reported whilst being in clinical use up until now [24], [25], [27]–[31]. The design was extensively tested for its mechanical performance, the results were not completely similar to a natural disc but showed similar mechanical behavior and good durability [28]. There is only one study that describes the clinical outcomes of the cervical version of the Freedom[®] disc [31]. Unfortunately, only patient outcomes were described, which demonstrated similar pain relief and lower disability for both 1 and 2-level treatment compared to other total disc replacements (Table 2.2). No device related adverse events and no range of motion (ROM) data were reported.

2.2.1.2 CPESP

The Cervical Prosthesis Elastic Spine Pad (CP ESP[®], FH Orthopedics) is a one-piece viscoelastic design, inspired by a silent block bush [32]. The implant consists of a polycarbonate urethane (PCU) core that is securely bonded through adhesion molding to the two titanium endplates. The PCU core has a distinct shape which has been optimized to achieve similar mobility as natural discs, and to control shear and translation loads during motion. Moreover, the PCU component is reinforced with male and female inner pegs, positioned at the inferior surfaces

of the titanium endplates. The shape and location of these pegs are designed to control compression and translation while their contactless fit is intended to reduce shear during anteroposterior and medio-lateral translations. Primary fixation is provided by anchoring pegs, while secondary fixation is achieved by osseous integration onto a textured T40 titanium and hydroxyapatite layer [32]. It is suggested that the CP ESP[®] can provide 6 degrees of freedom and has an inherent resistance to motion which increases with an increased amplitude of movement. Biomechanical analysis showed similar stiffness for compression and similar moments for extension, flexion, lateral bending, and rotation when compared to a natural disc [32], [33]. Moreover, it demonstrated fatigue and wear results that were within an acceptable range (Table 2.3). Only one clinical study with 2-year follow-up of 62 patients for the cervical version of the ESP[®] was found which reported satisfactory pain relief and improved function (Table 2.2) [32]. No device related complications were reported and the ROM at the treated level increased from $6.8^{\circ} \pm 4.1^{\circ}$ at three months follow up to $10.7^{\circ} \pm 4.2$ at 24 months. Pre-op and post-op ROM were only reported for one patient, being 4° pre-op to 14° post-op. In studies of both the lumbar and cervical versions of the ESP[®], the authors point out how the center of rotation (COR) varies within the physiological range during different follow-up periods [32]–[35]. This is a significant difference compared to first generation ball-and-socket devices, which often have a fixed COR and therefore are more sensitive for correct implant positioning. Moreover, a physiological COR is believed to be related to a reduced risk of facet and ligament overloading [36], [37]. In addition, with only limited axial rotation and with translational movements with an elastic return, the facet joints may potentially be protected from overloading. A 5-year follow-up study from the lumbar version did, in fact, not reveal any incidences of facet joint pain, which endorses this theory [35]. However, long-term results with larger cohorts are needed to confirm this hypothesis.

2.2.1.3 *Rhine*

The Rhine[™] (Rhine[™], K2m Inc., Leesburg, Virginia) is a non-articulating, monoblock prosthesis with an elastomeric polyurethane core sandwiched between two titanium alloy endplates [20]. The endplates have a central keel to provide initial fixation and are coated with plasma sprayed titanium to promote bone ingrowth [20]. An *in vitro* biomechanical study showed that the Rhine[™] disc was able to provide physiological motion in flexion/extension compared to an intact cervical spine cadaver [20]. However, the Rhine[™] was not able to recreate the segmental load-displacement curves in lateral bending and axial rotation, indicating that the device has different kinematics compared to a natural disc. Restoration of segmental height and changed lordosis could also be partially responsible, since it may create tension in the surrounding soft tissues compared to the pre-operative situation. Nevertheless, it could also indicate that this implant is more susceptible for risk of facet degeneration due to the altered loading patterns

after implantation. With the lumbar precursor of the Rhine, the Physio-L, radiological signs of facet degeneration after 7 years follow up in 7 out of 15 patients were observed [38]. It should be noted that only one out of 7 was symptomatic and that the design of the cervical Rhine and the anatomy of the cervical spine is somewhat different, which could possibly affect the outcome. Secondly, larger cohorts are required in order to verify whether this increased risk of facet joint degeneration is design specific. Nevertheless, the study also revealed that a more lateral placement of the device did not have any influence on the segmental load-displacement curves compared to a more central placement [20]. This is also seen for other viscoelastic prostheses, being less susceptible for device placement in order to obtain the intended ROM due to a variable COR [39], [40]. However, a preload and more anterior placement did show a significant increase in flexion/extension ROM [20]. Nevertheless, it seems logical that these viscoelastic devices are more susceptible to a change in ROM under preload due to the presence of the compressible core.

2.2.1.4 *Others*

Other viscoelastic designs are also available but do not yet have published data on their performance, such as D-flex carbon (Norm Medical) and NeoPhytos (Art World Medical). D-flex carbon features a compressible silicone core between peek carbon endplates to reduce imaging artefacts (Table 2.1). NeoPhytos (Art World Medical) is also a one-piece design with a silicone core between hydroxyapatite coated titanium endplates with small fins for immediate fixation (Table 2.1).

2.2.2 *Mobile bumper*

In the mobile bumper design, the core and endplate can move freely since these are not firmly bonded to each other. This has the benefit that there is no stress peak at the interface between the core and endplates since stresses can be distributed between multiple elements of the prosthesis. Nevertheless, it does pose a higher risk of generating wear particles in comparison to the monoblock design. To prevent wear particles from entering the surrounding environment, these mobile bumper designs often have an envelope or cover surrounding the core. To date, two implants are reported that have a mobile bumper design, being the M6-C™ and Bryan Disc®. Both implants do not provide a physiological height which is due to the manufacturing procedure [24]. The smallest height for the M6-C™ is 6 mm and the Bryan Disc® is only available with 8.5 mm height [24], [41], while the height of a natural disc may vary between 3.5-6.1 mm in height [42], [43]. Therefore, these designs have the risk to over distract the disc space, thereby limiting the natural ROM and also exerting additional forces on the facet joints and joint capsules. In the following paragraph, both M6-C™ and Bryan Disc® are discussed in more detail.

Table 2.1: comparison of viscoelastic total disc replacement devices per design category.




device	company	articulation	materials	sizes	primary fixation	secondary fixation
Endplate sandwiched						
<i>Monoblock</i>						
Freedom®	Axiomed	non-articulating monoblock metal-elastomer-metal	silicone polycarbonate urethane titanium alloy endplates	superior endplate: 13 x 16 mm inferior plates: 12 x 15 mm 16 x 19 mm	rail slots	porous beads
						
CP-ESP®	FH Orthopedics	non-articulating monoblock metal-polymer-metal	polycarbonate urethane core titanium alloy endplates	endplate: 13 x 15 mm 14 x 17 mm 15 x 22 mm heights: 5 mm 6 mm 7 mm	anchoring pegs	textured T40 titanium and hydroxyapatite layer
						
Rhine™	K2M	non-articulating monoblock metal-polymer-metal	polyurethane core titanium alloy endplates	-	central keel	titanium plasma spray
						

Table 2.1 continued: comparison of viscoelastic TDR devices per design category.




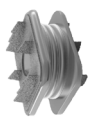




device	company	articulation	materials	sizes	primary fixation	secondary fixation
D-flex Carbon 	Norm Medical Devices	non-articulating monoblock peek-silicon-peek	silicone core peek carbon endplates	-	anchoring teeth	-
neoPhytos 	Art World Medical	non-articulating monoblock metal-silicon-metal	silicon core titanium alloy endplates	-	anchoring teeth	hydroxyapatite layer
<i>Mobile Bumper</i>						
Bryan disc® 	Medtronic	bi-articulating metal-polymer-metal	polyurethane core titanium alloy endplates	diameter: 14 mm 15 mm 16 mm 17 mm 18 mm height: 8.5 mm	convex shape of endplates matches precisely milled intervertebr al disc space	porous titanium coating
M6-C™ 	Spinal Kinetics	non-articulating metal-polymer-metal	polycarbonate urethane core titanium alloy endplates polymer sheath ultra-high-molecular-weight polyethylene fiber	baseplate: 12.5 x 15 mm 15 x 15 mm 14 x 17 mm 16 x 17 mm heights: 6 mm 7 mm	3 low profile keels	titanium plasma spray

Table 2.1 continued: comparison of viscoelastic TDR devices per design category.

device	company	articulation	materials	sizes	primary fixation	secondary fixation
	No endplates					
NeoDisc™ 	NuVasive	non-articulating	solid silicone elastomer core polyester fiber	-	flanges fixed with titanium screws to adjacent vertebrae	polyester material stimulates soft tissue ingrowth
3D-F 	Takiron	non-articulating monoblock	ultra-high-molecular-weight polyethylene fibers coated with polyethylene	surface area: 18 x 15 mm height: 7 mm	no fixation bioresorbable pins anterior plate	hydroxyapatite layer apatite wollastonite glass ceramics
cadisc™-C 	Ranier Technology	non-articulating monoblock	polycarbonate-polyurethane with a changing modulus	-	low-profile fixation	calcium phosphate coating
UFO 	Paonian Biotech	non-articulating monoblock	hard silicone outer part titanium alloy core	surface area: 15 x 14 mm heights: 5 mm 6 mm 7 mm 8 mm	micro- spikes	porous surface

2.2.2.1 *Bryan Disc*

The Bryan disc[®] (Medtronic Sofamor Danek, Inc, Memphis, TN) was first described by Goffin et al. (2002) with a design that features two convex titanium alloy endplates with a polyurethane core and cavity in between, surrounded by a polyurethane sheath [44]. The sheath surrounding the polyurethane core is attached with a retaining wire, connecting the two endplates. The goal of the sheath is to contain polymeric wear debris and prevent soft tissue ingrowth [45], [41]. Primary fixation is achieved by the convex shaped endplates that precisely match the milled space during surgery. Moreover, the endplates are coated with porous titanium to allow osseous integration, while also creating a high-friction environment to inhibit non-physiological torsion. Flanges at the anterior side of the implant are added to use as a posterior stop and to attach a guiding arm for implant insertion during surgery. Motion is limited by the maximum allowed movement of the shell post and endplates.

As for the other prosthesis, it is suggested that the benefit of the Bryan disc is having a mobile center of rotation that allows physiological kinematics at multiple implant locations [46], [47]. As a result, it is thought that due to the preservation of the mobile center of rotation, the facets and ligaments are not subjected to abnormal loading and thus there is a reduced risk of facet degeneration [36], [37]. There is only limited data available which has investigated this hypothesis. There are two finite element modelling (FEM) studies that showed no significant difference during extension in facet forces when compared to untreated segments while another FEM study of Gandhi et al. (2019) revealed an increase in facet loading [48]–[50]. A FEM study of Kang et al. (2010) also found similar facet forces in all ROM compared to intact segments, but found an increased loading at the uncovertebral joints, mainly during lateral bending [51]. One clinical study found that one out of 61 patients showed signs of facet degeneration at mean follow-up of 6-months [52]. Therefore, more research is needed to elucidate the actual risk of facet degeneration using the Bryan disc.

Although the Bryan disc[®] shows good patient outcome for both 1 and 2-level procedures, as illustrated in Table 2.2, a number of complications have been reported which can be attributed to the design and implant specific surgical procedure of the Bryan disc[®]. Kyphosis after implantation has been reported by several studies [52]–[59]. There are several reasons that could contribute to the increase in kyphosis, such as the complex implantation procedure or pre-operative presence of kyphosis [52]. Potential solutions suggested to avoid kyphosis from occurring are a small adjustment in the milling angle and prevention of asymmetric endplate milling or over-milling [41]. Another commonly reported complication is the occurrence of heterotopic ossifications (HO), which was found in approximately 6–29 % of the cases [55], [60]–[64]. Severity of HO ranged from barely detectable bony spurs to complete segmental

fusions and was found to be higher in patients that underwent two-level arthroplasty [57], [65]. The incidence of HO has been attributed to the excessive endplate milling needed to fix and match the concave endplates of the device [54], [63], [66]. As a solution, patients were given nonsteroidal anti-inflammatory drugs in the early post-operative period to avoid excessive HO formation [54], [60], [62]–[64], [67], [68]. Another potential risk of the excessive milling is the risk of the spheres touching with multi-level treatments [62].

Hybrid surgery has been increasingly applied in multilevel treatments to reduce costs while also aiming at reducing the impact on the adjacent segments compared to 2-level fusion procedures. The biomechanical influence on the spine for the Bryan disc in hybrid surgery has been investigated by a FEM study. This study showed increased intradiscal pressure in the adjacent segments, highest loading at bone-implant interface, but lowest stress in the facet joints compared to ball-and-socket prosthesis [69]. Two clinical studies showed similar complications as single level surgeries, indicating good short-term outcomes for the Bryan disc in hybrid surgery [70], [71].

2.2.2.2 M6-C

The M6-C™ (Spinal Kinetics, Sunnyvale, CA) design is based on the anatomical structures of a native disc. The core is made of a compressible polycarbonate urethane polymer that intends to mimic the native nucleus. The annulus is mimicked by a woven-fiber construct from ultra-high-molecular-weight-polyethylene (UHMWPE) fibers and is responsible for facilitating the semi-constrained 6-degrees of freedom [72], [73]. The artificial annulus is laser-welded to a superior and inferior titanium endplate. Both endplates contain 3 keels to provide immediate fixation and are coated with porous titanium to promote bone ingrowth [39]. An additional design feature is the polymer sheath that surrounds the core and woven-fiber construct to limit tissue ingrowth and contain possible wear debris [72], [73]. An *in vitro* study with M6-C™ demonstrated that the design led to a more physiological motion quality compared to Mobi-C®, which resembles a ball-and-socket type of implant [74]. The moment versus angular displacement curves of Mobi-C® showed an increased laxity around the neutral posture of the spine. It is hypothesized by Panjabi (1992) that increased laxity can lead to compensation by spinal muscles and ligaments to provide spine stability in daily life [75]. This suggests that using a viscoelastic component compared to a ball-and-socket design could be advantageous for diminishing the risk of adjacent segment disease and facet joint overloading. However, the results are only short-term effects and will have to be confirmed with longer follow-up data.

The M6-C™ was subjected to several bench tests, and results indicated that the mechanical properties of M6-C™ were well within the defined safety requirements (Table 2.3). As a next

step, several clinical studies were performed on both 1 and 2 levels which have been summarized in Table 2.2 [72], [73], [76], [77]. Clinical outcomes have shown contradictory results when comparing 1 and 2 level procedures. Laurysen et al. only found a significant improvement in neck pain in the 2-level treatment, while Reyes-Sanchez et al. found significant improvement in NDI and pain severity for the 1-level patients compared to 2-level patients. However, it should be noted that the cohort and follow-up time of 24 months in both studies are insufficient to draw conclusions. Patwardhan et al (2012), showed that M6-C™ has a variable COR as also seen for other viscoelastic devices making them less susceptible for malpositioning [39]. Although *in vitro* and *in vivo* results showed very promising results of the M6-C™, there were also some device related complications reported. One case study showed a posterior height reduction of the prosthesis due to extrusion of the fibers, which also led to a revision surgery [78]. In another case study, herniation of the core was observed based on radiographic results [21]. Initially, a posterior displacement of the inferior titanium endplate was suspected based on radiography and MRI. However, due to metal artifacts caused by the titanium, the authors found it difficult to interpret. Therefore, the use of metal in the design of artificial cervical disc replacement should be limited since it can hamper follow-up assessments. The first reason suggested by the authors is the fatigue life, although this was extensively tested in the lab [79]. However, it could be that the local microenvironment *in vivo* caused the rupture, which was not simulated in the lab tests. Another explanation given is that the grooves created to slide the keels of the implant into the adjacent vertebrae were made too far posteriorly, leading to abnormal loading on the fibers of the artificial annulus. Eventually the fibers could have ruptured leading to the core herniation [21].

2.3 No endplates

The advantage of not using (metal) endplates in the design is that these implants do not create imaging artefacts, making this category more compatible with follow-up imaging methods such as MRI. A disadvantage of these devices is the risk of reduced osseous integration between the vertebrae and the implant. In the 'no endplates' designs, polymers, in bulk or fiber form, are often in contact with the adjacent vertebrae. Many polymers have a surface chemistry that is not osteoconductive, e.g. hydrophobic. As a result, surface treatments are often needed to achieve a more stable osseous integration, such as plasma etching or hydroxyapatite coating. In addition, these softer materials might need some settling and can experience creep with subsequent risk of migration. An additional advantage of not using endplates is that endplates could limit ROM by impinging at a certain flexion/extension or lateral bending angle. Without having endplates, the ROM is only constrained by the viscoelasticity of the device and the surrounding ligaments, muscles and soft tissue which more closely resembles the situation of a natural disc. On the contrary, this might create an

instability or even the risk of potential kyphotic deformity in the mid- to long term. Moreover, there might be a risk of damaging the material of the implant during insertion with, for example, the surgical tools or sharp bony ends formed by milling of the intervertebral disc. Also, after implantation, there is a risk of damaging the implant at the bone-implant interface due to abrasion between the bone and the implant. There are several implants that fall within the no endplates category, namely the NeoDisc™, CaDisc™-C and the 3D-F, which are described in the following paragraphs.

2.3.1 *NeoDisc*

The NeoDisc™ (NuVasive, Inc., San Diego, CA) is an elastomeric total disc replacement consisting of a solid silicone elastomer core surrounded by an embroidered polyester fiber jacket. The jacket contains two flanges which are fixed to the two adjacent vertebrae by four titanium bone screws. Long-term fixation is achieved by using a polyester fiber for the jacket, known to stimulate soft tissue ingrowth [19]. The jacket is a complex piece of fabric produced by a computer-controlled embroidery process, allowing for control on position and thread size of each individual fiber within the construct. Two flanges of the jacket are interconnected in a way that the superior flange passes through the inferior flange. As a result, during extension/flexion movement, the flanges are pulled in opposing directions thereby transferring a compressive load through the silicon core. An advantage of the NeoDisc™ is its low amount of metal, allowing for detailed follow-up MRI and CT imaging. This could be even further improved by replacing the titanium screws with nonmetallic ones. The device was mechanically evaluated, and results demonstrated that the defined safety requirements were fulfilled (Table 2.3) [19]. As a next step, an animal study was performed in sheep to assess *in vivo* performance. In this study, fibrous tissue ingrowth onto the jacket was observed [19]. According to the authors, this is a desirable outcome since this connection prevents the fibers to slide, and thereby wear along each other. It seems counterintuitive to stimulate soft tissue compared to bone ingrowth onto the jacket, since bone ingrowth mimics more the natural connection between the annulus and vertebral endplates. However, the endplates were resected without causing them to bleed, which is normally done to stimulate bone growth, which could explain the low amount of bone ingrowth. There were also signs of an inflammatory response, potentially as a reaction to the polyester/silicon material. After the animal study in sheep, smaller clinical trials have been performed using the NeoDisc™. The clinical patient outcomes are summarized in Table 2.2. No adverse clinical or device related events were reported. The flexion/extension segmental motion was reported to be 6° after 1-year compared to 8° pre-op [19]. After 2 years, the flexion/extension motion was 10°, 9° and 6° for three patients. For unreported/unknown reasons, NuVasive have aborted their FDA IDE trials for the NeoDisc™ [24].

2.3.2 3D-F

The 3D-F (Takiron, Inc., Osaka, Japan) is a 3D woven fabric made out of one continuous long fiber of ultra-high molecular weight polyethylene (UHMWPE) [80], [81]. To promote osseous integration, the fibers on the 3D fabric are coated with hydroxyapatite or apatite-wollastonite glass ceramics to a depth of 3 mm from the surface of the implant. An advantage of the 3D-F design is that it does not contain a composite interface that is often a weak spot in the design. Moreover, the stress can be distributed within the single fiber, thereby reducing the stress concentration [80]. Even though the 3D-F does not contain a viscoelastic component, due to its structural organization, it showed viscoelastic behavior based on creep recovery tests and hysteresis curves [80]. However, a disadvantage of the 3D-F is its very complex production procedure.

Initially, no primary fixation was incorporated into the design. This lack of fixation seemed to be the most critical issue in the design of the 3D-F. Three different methods of fixation have been explored in several animal studies, being no fixation, temporary fixation with a Kaneda SR (KSR) one rod system (DePuy Acromed, Inc., Raynham, MA) and also a bioresorbable system of two titanium screws with a bioabsorbable rod [80], [82]–[84]. The designs without any primary fixation resulted in some migration cases and reports of reduced ROM or even spontaneous fusion (2.5–3°) after 6 months [80], [82], [84]. The KSR one rod system led to proper fixation and physiological ROM results [80], [82], [84]. However, using a temporary fixation system is very undesirable in a clinical setting since it would require a second surgery.

Therefore, the bioresorbable rod was examined which demonstrated adequate initial fixation, however the rod eventually cracked [83], [84]. In general, it would be more beneficial to have an incorporated fixation method within the design, then having an additional external component. Therefore, the next generation of the implant contained bioactive bioresorbable central pins as a primary fixation and included bioactive resorbable porous perforated sheets cranial and caudal as a scaffold for bone ingrowth [85]. Results showed good osseous integration after six months, but ROM values were lower compared to intact discs [85], [86]. These results furthermore demonstrate the importance of primary stability and controlling of bone ingrowth.

Only one study, by Shikinami et al. (2010), focusing solely on the cervical version, was performed on human cadaveric spines [87]. ROM of the 3D-F discs compared to intact controls showed similar results for axial rotation and lateral bending, but an increase of approximately 45% in flexion/extension compared to the intact group. However, the absolute angle was 14°, being within a physiological range [88]–[90]. Also, neutral zone ROMs were not significantly different compared to the intact group.

Table 2.2: Clinical outcome measurements of several viscoelastic TDR devices.* statistically significant difference ($p > 0.05$) compared to ACDF control group.† statistically significant difference ($p > 0.05$) compared to baseline.

ref	device	study design	LOE	levels	control group	patients	patients available at terminal f/u	follow-up (mo)
[31]	Freedom®	post-market clinical study	IV	1 & 2	-	39	35	24
[32]	CP-ESP®	feasibility study	IV	1 & 2	-	62	62	24
[59]	Bryan disc®	prospective randomized controlled multicenter clinical trial	I	1	TDR	242	242	24
					ACDF	221	221	24
[86]	Bryan disc®	prospective randomized controlled study	II	2	TDR	31	30	24
					ACDF	34	32	24
[87]	Bryan disc®	prospective randomized controlled single site clinical trial	I	1	TDR	21	18	48
					ACDF	26	20	48
[88]	Bryan disc®	prospective randomized controlled multicenter clinical trial	I	1	TDR	60	60	24
					ACDF	60	60	24
[89]	Bryan disc®	prospective randomized controlled multicenter clinical trial	II	1	TDR	242	128	120
					ACDF	221	104	120
[48]	Bryan disc®	Prospective single center study	IV	1 & 2	-	20	18	180
[64]	M6-C™	feasibility study	IV	1 & 2	-	36	25	24
[63]	M6-C™	multicenter FDA10 regulated feasibility study	IV	1 & 2	-	30	28	24
[67]	M6-C™	retrospective study	III	1 & 2	-	33	24	17.1
[69]	M6-C™	multicenter clinical trial	IV	1	-	112	112	36
[18]	NeoDisc™	two site European study	IV	1	-	14	14	12
[90]	NeoDisc™	prospective randomized FDA IDE clinical trial	I	1	TDR	31	25	24
					ACDF	30	28	24

Table 2.2 continued: Clinical outcome measurements of several viscoelastic TDR devices.* statistically significant difference ($p > 0.05$) compared to ACDF control group.† statistically significant difference ($p > 0.05$) compared to baseline

NDI improvement (%)	VAS arm improvement (%)	VAS neck improvement (%)	SF-36 improvement (%)		ROM index level pre-op (°)	ROM index level (°)	overall success (%)
			PCS	MCS			
92	78	76	-	-	-	-	-
66†	75†	52†	107†	115†	-	10.7 ± 4.2	-
68†*	73†	70†	47†	22†	6.5 ± 3.4*	-	82.6*
62†	70†	59†	46†	16†	8.4 ± 4.5	-	72.7
78†*	80†*	79†*	43*	-	-	-	-
63†	63†	63†	32	-	-	-	-
80	86	82	49	24	-	-	-
69	73	67	47	13	-	-	-
72†	77†	72†	-	-	8.00 ± 1.40	8.79 ± 0.89*	-
71†	76†	69†	-	-	7.93 ± 1.18	0.79 ± 0.63	-
75*	80	72	48*	-	6.5 ± 3.4	8.69†	81.3*
66	73	67	42	-	8.4 ± 4.5	0.6†	66.3
63†	69†	53†	24†	14†	-	9 ± 3.9	-
46†	43†	51†	26†	14†	12.2	11.1	-
69†	70†	69†	57†	16	8.8	6.3	89
-	-	-	-	-	-	-	87.5
73†	81†	82†	-	-	6.4 ± 2.5	8.8 ± 2.6	95.6
58	85	66	-	-	8	6	-
65*	64*	-	-	10.7	8.2	-	-
38	50	-	-	-	-	-	-

2.3.3 *Cadisc-C*

Cadisc™'s design is made out of solely polycarbonate-polyurethane with a graduated modulus throughout the implant. In this way, the Cadisc™ tries to resemble the nucleus with a lower modulus region and the annulus with a higher modulus region as well as hard endplates [40]. As a result, there are no articulating surfaces or bonding regions, thereby leading to a low risk of wear debris. To date, data has only been published on the lumbar version of the implant [40], [91]. Results showed that in comparison with intact cadaveric specimens, the implantation of the Cadisc™ led to a 50 ± 11 % reduction in compressive stiffness [40]. Even more interesting was that the compressive stiffness was even lower compared to single Cadisc™ samples, indicating a large contribution of the vertebrae to the stiffness. Moreover, posterior height was 27 ± 13 % higher compared to intact samples [40]. Although the design aimed to mimic the structure of a native intervertebral disc, the design did not exhibit a large neutral zone similar to a natural intervertebral disc [40]. As also seen for the other viscoelastic implants, the Cadisc™ showed a mobile instantaneous axis of rotation, although not similar to a natural intervertebral disc [40]. It is hypothesized that biomechanical changes might contribute to a higher risk of degeneration of surrounding spinal structures [36], [37]. However, to date there are no studies that have investigated this for the Cadisc™.

2.3.4 *UFO*

The UFO design is a mix between a cage and disc replacement, having a titanium cage-like core with micro-spikes at the surface to provide implant stability and bone ingrowth, while the outer part is made from hard silicone to provide motion. This design is counterintuitive compared to the structure of a natural disc, since in a natural disc the soft part is in the center and it becomes stiffer towards the outside. Unfortunately, there are no studies to date that have published data on the performance of the device which would allow to discuss any design related outcomes.

2.4 Discussion

First generation disc replacement implants have shown equivalent or even superior results to the ACDF gold standard treatment and have therefore been globally implemented in the surgeon's armamentarium [8]. Nonetheless, these first-generation devices are too simplistic to replicate the complex motion characteristics of a natural disc. As a result, incorporating a viscoelastic component could be a promising next step in an attempt to better replicate the complex kinematics of a natural motion segment more closely. As a result of the viscoelastic component, adjacent anatomical structures may also have to compensate less for an aberrant

Table 2.3: Mechanical characterization outcomes of several viscoelastic TDRs.

ref	device	wear test		axial compression		shear-compression		expulsion test		torsion	
		medium	wear	static	dynamic	static	dynamic	static	dynamic	static	dynamic
<i>Monoblock</i>											
[31]	CP-ESP®	-	0.8 mg/MC ¹	733 N/m	0.02 – 0.12 mm no functional failure	-	-	-	-	-	-
<i>Mobile Bumper</i>											
SSED M6-C™	bovine calf serum	0.03 mg/MC ¹ (ASTM F2346)	> 24694 ± 460 N	873 ± 168 N/mm 047 ± 0.05 mm height loss no mechanical failure after 20 MC ¹	6714 ± 113 N	no mechanical failure after 10 MC ¹	no mechanical or functional failure after 10 MC ¹	-	10.4 ± 1.4 Nm	no mechanical or functional failure after 10 MC ¹ at ±0.35 Nm	-
<i>No endplates</i>											
[18]	NeoDisc™	saline	0.69 mg/MC ¹	4728 – 6975 N	0.16 mm height loss no functional failure after 10 MC ¹	574 – 829 N	0.14 mm no functional failure after 10 MC ¹	238 N to dislodge 293 N to expel from disc space	-	-	-

biomechanical behavior as seen for current ball-and-socket designs. In this respect, the design alterations could potentially serve to lower the risk of accelerated degeneration of surrounding spinal structures such as the ligaments, uncovertebral joints and facet joints. However, clinical proof of this hypothesis is still absent, and long-term studies of viscoelastic total disc replacements are needed. Altogether, it can be stated that viscoelastic devices may have a number of benefits but also distinct drawbacks, with each of the different designs having its own pros and cons. One of the benefits of viscoelastic devices is that these devices have a variable COR, therefore being less susceptible for errors in device malpositioning. Moreover, viscoelastic devices provide motion characteristics which are based on deformation rather than sliding movements as seen in ball-and-socket designs, thereby allowing all the 6-DOF in a way that may resemble the motion of a natural disc more closely in comparison to first-generation implants. A closer resemblance of the COR and of the physiological motion patterns with these second-generation implants could serve to reduce excessive strains on the facet joints and surrounding ligaments as frequently observed with first generation type of implants, and thus may aid to reduce the risk of postoperative complaints from these structures. However, to date the effect on facet and ligament kinematics of these viscoelastic devices has not been investigated in sufficient detail and further studies in this field are needed. Nevertheless, there are also some potential risks for using viscoelastic devices. Since most of the devices use high strength materials in combination with viscoelastic materials, there is a potential weak spot at the interface. Moreover, most of the elastomeric materials used do not have an extensive history in orthopedics. Thus, the long-term material behavior *in vivo* is still unknown; it will be important to get further insight on issues such as the wear profile. Potential wear particles could elicit a host response which may result in implant loosening. Moreover, subsidence where the implant sinks into the adjacent vertebral bodies remains a recurrent problem. Most subsidence is related to a mismatch in footprint, poor bone quality and amount of loading applied to the spine. To date, the available data on this topic is still limited and the precise motion characteristics of viscoelastic devices and their resemblance to that of a native disc is still unknown. Initial data on these viscoelastic devices seem to be promising and have reported satisfactory results for the treatment of myelopathy and/or radiculopathy. However, further insight into this topic and prospective long-term studies are needed to provide the final answer.

Acknowledgements

This work was supported by the TTW research program with project number TTW 10025453, financed by the Netherlands Organization for Scientific Research (NWO). Conflict of interest: K. Ito has received in-kind research support from Meliora Medical BV and in-kind and financial research support from DSM Biomedical.

References

- [1] I. Zechmeister, R. Winkler, and P. Mad, "Artificial total disc replacement versus fusion for the cervical spine: a systematic review," *Eur. Spine J.*, vol. 20, no. 2, pp. 177–184, Feb. 2011.
- [2] J. Goffin et al., "Long-term follow-up after interbody fusion of the cervical spine," *J. Spinal Disord.*, vol. 17, no. 2, pp. 79–85, Apr. 2004.
- [3] A. E. Dmitriev, B. W. Cunningham, N. Hu, G. Sell, F. Vigna, and P. C. McAfee, "Adjacent level intradiscal pressure and segmental kinematics following a cervical total disc arthroplasty: An *in vitro* human cadaveric model," *Spine (Phila. Pa. 1976.)*, vol. 30, no. 10, pp. 1165–1172, May 2005.
- [4] C. Barrey, S. Campana, S. Persohn, G. Perrin, and W. Skalli, "Cervical disc prosthesis versus arthrodesis using one-level, hybrid and two-level constructs: an *in vitro* investigation," *Eur. Spine J.*, vol. 21, no. 3, pp. 432–442, Mar. 2012.
- [5] W. Womack, P. D. Leahy, V. V. Patel, and C. M. Puttlitz, "Finite element modeling of kinematic and load transmission alterations due to cervical intervertebral disc replacement," *Spine (Phila. Pa. 1976.)*, vol. 36, no. 17, pp. E1126–E1133, Aug. 2011.
- [6] C. C. Wigfield, D. Skrzypiec, A. Jackowski, and M. A. Adams, "Internal stress distribution in cervical intervertebral discs," *J. Spinal Disord. Tech.*, vol. 16, no. 5, pp. 441–449, Oct. 2003.
- [7] A. Faizan, V. K. Goel, A. Biyani, S. R. Garfin, and C. M. Bono, "Adjacent level effects of bi level disc replacement, bi level fusion and disc replacement plus fusion in cervical spine- a finite element based study," *Clin. Biomech.*, vol. 27, no. 3, pp. 226–233, Mar. 2012.
- [8] D. Ohnmeiss, R. Guyer, Y. Samocha, J. Zigler, and S. Blumenthal, "Cervical Total Disc Replacement Versus Anterior Cervical Fusion: Data from Four Prospective, Randomized, Multicenter Trials," *Spine J.*, vol. 11, no. 10, pp. S150–S151, Oct. 2011.
- [9] J. J. Costi, I. A. Stokes, M. G. Gardner-Morse, and J. C. Iatridis, "Frequency-Dependent Behavior of the Intervertebral Disc in Response to Each of Six Degree of Freedom Dynamic Loading," *Spine (Phila. Pa. 1976.)*, vol. 33, no. 16, pp. 1731–1738, Jul. 2008.
- [10] H. A. L. Guerin and D. M. Elliott, "Structure and Properties of Soft Tissues in the Spine," in *Spine Technology Handbook*, Amsterdam: Elsevier Academic Press, 2006, pp. 35–62.
- [11] F. Galbusera, C. M. Bellini, M. Brayda-Bruno, and M. Fornari, "Biomechanical studies on cervical total disc arthroplasty: A literature review," *Clin. Biomech.*, vol. 23, no. 9, pp. 1095–1104, Nov. 2008.
- [12] V. V. Patel et al., "Cervical facet force analysis after disc replacement versus fusion," *Clin. Biomech.*, vol. 44, pp. 52–58, May 2017.
- [13] C. J. Siepe et al., "The fate of facet joint and adjacent level disc degeneration following total lumbar disc replacement: A prospective clinical, X-ray, and magnetic resonance imaging investigation," *Spine (Phila. Pa. 1976.)*, vol. 35, no. 22, pp. 1991–2003, 2010.
- [14] C. K. Park, K. S. Ryu, and W. H. Jee, "Degenerative changes of discs and facet joints in lumbar total disc replacement using ProDisc II: Minimum two-year follow-up," *Spine (Phila. Pa. 1976.)*, vol. 33, no. 16, pp. 1755–1761, 2008.
- [15] S. Botolin et al., "Facet joint biomechanics at the treated and adjacent levels after total disc replacement," *Spine (Phila. Pa. 1976.)*, vol. 36, no. 1, pp. 27–32, 2010.
- [16] C. S. Shim et al., "CHARITE versus ProDisc: A comparative study of a minimum 3-year follow-up," *Spine (Phila. Pa. 1976.)*, vol. 32, no. 9, pp. 1012–1018, 2007.
- [17] A. van Ooij, F. C. Oner, and A. J. Verbout, "Complications of cervical artificial disc replacement: A report of 27 patients with the SB Charité Disc," *J. Spinal Disord. Tech.*, vol. 16, no. 4, pp. 369–383, 2003.
- [18] H. Kienapfel, C. Sprey, A. Wilke, and P. Griss, "Implant fixation by bone ingrowth," *J. Arthroplasty*, vol. 14, no. 3, pp. 355–368, Apr. 1999.
- [19] J. J. Yue, R. Bertagnoli, P. C. McAfee, and H. S. An, "Motion Preservation Surgery of the Spine: Advanced Techniques and Controversies," *Am. J. Neuroradiol.*, vol. 30, no. 9, pp. E134–E134, Oct.

- 2008.
- [20] R. D. Guyer et al., "Kinematic assessment of an elastic-core cervical disc prosthesis in one and two-level constructs," *JOR Spine*, vol. 1, no. 4, p. e1040, Dec. 2018.
- [21] C. Brenke, K. Schmieder, and M. Barth, "Core herniation after implantation of a cervical artificial disc: case report," *Eur. Spine J.*, vol. 24, no. S4, pp. S536–S539, May 2015.
- [22] J. Sundseth, E. A. Jacobsen, F. Kolstad, O. P. Nygaard, J. A. Zwart, and P. K. Hol, "Magnetic resonance imaging evaluation after implantation of a titanium cervical disc prosthesis: a comparison of 1.5 and 3 Tesla magnet strength," *Eur. Spine J.*, vol. 22, no. 10, pp. 2296–2302, Oct. 2013.
- [23] AxioMed, "Freedom Lumbar Disc Polymer-Metal Bond Integrity," 2010.
- [24] M. D. Staudt, K. Das, and N. Duggal, "Does design matter? Cervical disc replacements under review," *Neurosurg. Rev.*, vol. 41, no. 2, pp. 399–407, Apr. 2018.
- [25] B. W. Cunningham et al., "Total disc replacement arthroplasty using the AcroFlex lumbar disc: a non-human primate model," *Eur. Spine J.*, vol. 11, no. S2, pp. S115–S123, Oct. 2002.
- [26] R. J. Moore et al., "The Biologic Response to Particles From a Lumbar Disc Prosthesis," *Spine (Phila. Pa. 1976)*, vol. 27, no. 19, pp. 2088–2094, Oct. 2002.
- [27] R. D. Fraser, E. R. Ross, G. L. Lowery, B. J. Freeman, and M. Dolan, "AcroFlex design and results," *Spine J.*, vol. 4, no. 6, pp. S245–S251, Nov. 2004.
- [28] E. C. Benzel, I. H. Lieberman, E. R. Ross, R. J. Linovitz, J. Kuras, and K. Zimmers, "Mechanical Characterization of a Viscoelastic Disc for Lumbar Total Disc Replacement," *J. Med. Device.*, vol. 5, no. 1, pp. 011005-1-011005-7, Mar. 2011.
- [29] B. Rischke, R. S. Ross, B. A. Jollenbeck, K. B. Zimmers, and N. D. Defibaugh, "Preclinical and clinical experience with a viscoelastic total disc replacement," *SAS J.*, vol. 5, no. 4, pp. 97–107, Dec. 2011.
- [30] B. Rischke, K. B. Zimmers, and E. Smith, "Viscoelastic Disc Arthroplasty Provides Superior Back and Leg Pain Relief in Patients with Lumbar Disc Degeneration Compared to Anterior Lumbar Interbody Fusion," *Int. J. Spine Surg.*, vol. 9, no. 26, pp. 1–8, 2015.
- [31] K. R. Chin, J. R. Lubinski, K. B. Zimmers, B. E. Sands, and F. Pencle, "Clinical experience and two-year follow-up with a one-piece viscoelastic cervical total disc replacement," *J. Spine Surg.*, vol. 3, no. 4, pp. 630–640, Dec. 2017.
- [32] J. Lazennec, A. Aaron, O. Ricart, and J. P. Rakover, "The innovative viscoelastic CP ESP cervical disk prosthesis with six degrees of freedom: biomechanical concepts, development program and preliminary clinical experience," *Eur. J. Orthop. Surg. Traumatol.*, vol. 26, no. 1, pp. 9–19, Jan. 2016.
- [33] J.-Y. Lazennec, A. Aaron, A. Brusson, J.-P. Rakover, and M.-A. Rousseau, "The LP-ESP® lumbar disc prosthesis with 6 degrees of freedom: development and 7 years of clinical experience," *Eur. J. Orthop. Surg. Traumatol.*, vol. 23, no. 2, pp. 131–143, Feb. 2013.
- [34] J.-Y. Lazennec, J. Even, W. Skalli, J.-P. Rakover, A. Brusson, and M.-A. Rousseau, "Clinical outcomes, radiologic kinematics, and effects on sagittal balance of the 6 df LP-ESP lumbar disc prosthesis," *Spine J.*, vol. 14, no. 9, pp. 1914–1920, Sep. 2014.
- [35] J.-Y. Lazennec, J.-P. Rakover, and M.-A. Rousseau, "Five-year follow-up of clinical and radiological outcomes of LP-ESP elastomeric lumbar total disc replacement in active patients," *Spine J.*, vol. 19, no. 2, pp. 218–224, Feb. 2019.
- [36] M. A. Rousseau, D. S. Bradford, T. M. Hadi, K. L. Pedersen, and J. C. Lotz, "The instant axis of rotation influences facet forces at L5/S1 during flexion/extension and lateral bending," *Eur. Spine J.*, vol. 15, no. 3, pp. 299–307, Mar. 2006.
- [37] H. Koller, O. Meier, J. Zenner, M. Mayer, and W. Hitzl, "*In vivo* analysis of cervical kinematics after implantation of a minimally constrained cervical artificial disc replacement," *Eur. Spine J.*, vol. 22, no. 4, pp. 747–758, 2013.
- [38] L. Pimenta, L. Marchi, L. Oliveira, J. Nogueiraneto, E. Coutinho, and R. Amaral, "Elastomeric lumbar total disc replacement: Clinical and radiological results with minimum 84 months follow-up," *Int. J. Spine Surg.*, vol. 12, no. 1, pp. 49–57, 2018.

- [39] A. G. Patwardhan et al., "Primary and coupled motions after cervical total disc replacement using a compressible six-degree-of-freedom prosthesis," *Eur. Spine J.*, vol. 21, no. S5, pp. S618–S629, Jun. 2012.
- [40] D. McNally, J. Naylor, and S. Johnson, "An *in vitro* biomechanical comparison of Cadisc™-L with natural lumbar discs in axial compression and sagittal flexion," *Eur. Spine J.*, vol. 21, no. S5, pp. S612–S617, Jun. 2012.
- [41] M. Wenger and T.-M. Markwalder, "Bryan total disc arthroplasty: a replacement disc for cervical disc disease," *Med. Devices Evid. Res.*, vol. 3, pp. 11–24, Jul. 2010.
- [42] I. Busscher, J. J. W. Ploegmakers, G. J. Verkerke, and A. G. Veldhuizen, "Comparative anatomical dimensions of the complete human and porcine spine," *Eur. Spine J.*, vol. 19, no. 7, pp. 1104–1114, Jul. 2010.
- [43] B. Frost, S. Camarero-Espinosa, and E. Foster, "Materials for the spine: anatomy, problems, and solutions," *Materials (Basel)*, vol. 12, no. 2, p. 253, Jan. 2019.
- [44] J. Goffin et al., "Preliminary Clinical Experience with the Bryan Cervical Disc Prosthesis," *Neurosurgery*, vol. 51, no. 3, pp. 840–847, Sep. 2002.
- [45] P. A. Anderson, J. P. Rouleau, V. E. Bryan, and C. S. Carlson, "Wear Analysis of the Bryan Cervical Disc Prosthesis," *Spine (Phila. Pa. 1976)*, vol. 28, no. 20S, pp. S186–S194, Oct. 2003.
- [46] B. C. R. Lazaro et al., "Effect of arthroplasty design on cervical spine kinematics: Analysis of the Bryan disc, ProDisc-C, and Synergy disc," *Neurosurg. Focus*, vol. 28, no. 6, pp. 1–8, 2010.
- [47] G. E. Pickett, J. P. Rouleau, and N. Duggal, "Kinematic analysis of the cervical spine following implantation of an artificial cervical disc," *Spine (Phila. Pa. 1976)*, vol. 30, no. 17, pp. 1949–1954, 2005.
- [48] F. Galbusera, C. M. Bellini, M. T. Raimondi, M. Fornari, and R. Assietti, "Cervical spine biomechanics following implantation of a disc prosthesis," *Med. Eng. Phys.*, vol. 30, no. 9, pp. 1127–1133, 2008.
- [49] Z. Mo, Y. Zhao, C. Du, Y. Sun, M. Zhang, and Y. Fan, "Does Location of Rotation Center in Artificial Disc Affect Cervical Biomechanics?," *Spine (Phila. Pa. 1976)*, vol. 40, no. 8, pp. E469–E475, 2015.
- [50] A. A. Gandhi, N. M. Grosland, N. A. Kallemeyn, S. Kode, D. C. Fredericks, and J. D. Smucker, "Biomechanical analysis of the cervical spine following disc degeneration, disc fusion, and disc replacement: A finite element study," *Int. J. Spine Surg.*, vol. 13, no. 6, pp. 491–500, Dec. 2019.
- [51] H. Kang, P. Park, F. La Marca, S. J. Hollister, and C. Y. Lin, "Analysis of load sharing on uncovertebral and facet joints at the C5-6 level with implantation of the Bryan, Prestige LP, or ProDisc-C cervical disc prosthesis: An *in vivo* image-based finite element study," *Neurosurgical Focus*, vol. 28, no. 6, pp. 1–8, 2010.
- [52] C. S. Shim, S.-H. Lee, H.-J. Park, H.-S. Kang, and J.-H. Hwang, "Early Clinical and Radiologic Outcomes of Cervical Arthroplasty with Bryan Cervical Disc Prosthesis," *J. Spinal Disord. Tech.*, vol. 19, no. 7, pp. 465–470, Oct. 2006.
- [53] D. H. Yoon, S. Yi, H. C. Shin, K. N. Kim, and S. H. Kim, "Clinical and radiological results following cervical arthroplasty," *Acta Neurochir. (Wien)*, vol. 148, no. 9, pp. 943–950, Sep. 2006.
- [54] Y. C. Yang, L. Nie, L. Cheng, and Y. Hou, "Clinical and radiographic reports following cervical arthroplasty: a 24-month follow-up," *Int. Orthop.*, vol. 33, no. 4, pp. 1037–1042, Aug. 2009.
- [55] V. Heidecke, W. Burkert, M. Brucke, and N. G. Rainov, "Intervertebral disc replacement for cervical degenerative disease – clinical results and functional outcome at two years in patients implanted with the Bryan® cervical disc prosthesis," *Acta Neurochir. (Wien)*, vol. 150, no. 5, pp. 453–459, May 2008.
- [56] S. Y. Fong, S. J. DuPlessis, S. Casha, and R. J. Hurlbert, "Design limitations of Bryan disc arthroplasty," *Spine J.*, vol. 6, no. 3, pp. 233–241, May 2006.
- [57] V. Pointillart, J.-E. Castelain, P. Coudert, D. T. Cawley, O. Gille, and J.-M. Vital, "Outcomes of the Bryan cervical disc replacement: fifteen year follow-up," *Int. Orthop.*, vol. 42, no. 4, pp. 851–857, Apr. 2018.
- [58] S. W. Kim, J. H. Shin, J. J. Arbatin, M. S. Park, Y. K. Chung, and P. C. McAfee, "Effects of a cervical

- disc prosthesis on maintaining sagittal alignment of the functional spinal unit and overall sagittal balance of the cervical spine," *Eur. Spine J.*, vol. 17, no. 1, pp. 20–29, Jan. 2008.
- [59] R. C. Sasso, N. H. Metcalf, J. A. Hipp, N. D. Wharton, and P. A. Anderson, "Sagittal Alignment After Bryan Cervical Arthroplasty," *Spine (Phila. Pa. 1976)*, vol. 36, no. 13, pp. 991–996, Jun. 2011.
- [60] J. Goffin et al., "Intermediate Follow-up After Treatment of Degenerative Disc Disease With the Bryan Cervical Disc Prosthesis: Single-Level and Bi-Level," *Spine (Phila. Pa. 1976)*, vol. 28, no. 24, pp. 2673–2678, Dec. 2003.
- [61] M. Wenger, P. van Hoonacker, B. Zachee, R. Lange, and T.-M. Markwalder, "Bryan cervical disc prostheses: preservation of function over time," *J. Clin. Neurosci.*, vol. 16, no. 2, pp. 220–225, Feb. 2009.
- [62] G. E. Pickett, L. H. S. Sekhon, W. R. Sears, and N. Duggal, "Complications with cervical arthroplasty," *J. Neurosurg. Spine*, vol. 4, no. 2, pp. 98–105, Feb. 2006.
- [63] C. Leung et al., "Clinical Significance of Heterotopic Ossification in Cervical Disc Replacement: A Prospective Multicenter Clinical Trial," *Neurosurgery*, vol. 57, no. 4, pp. 759–763, Oct. 2005.
- [64] J. F. Parkinson and L. H. S. Sekhon, "Cervical arthroplasty complicated by delayed spontaneous fusion," *J. Neurosurg. Spine*, vol. 2, no. 3, pp. 377–380, Mar. 2005.
- [65] J. C. Wu et al., "Differences between 1- and 2-level cervical arthroplasty: More heterotopic ossification in 2-level disc replacement. Clinical article," *J. Neurosurg. Spine*, vol. 16, no. 6, pp. 594–600, Jun. 2012.
- [66] P. C. McAfee, B. W. Cunningham, J. Devine, E. Williams, and J. Yu-Yahiro, "Classification of Heterotopic Ossification (HO) in Artificial Disk Replacement," *J. Spinal Disord. Tech.*, vol. 16, no. 4, pp. 384–389, Aug. 2003.
- [67] V. E. Bryan, "Cervical motion segment replacement," *Eur. Spine J.*, vol. 11, no. S2, pp. S92–S97, Oct. 2002.
- [68] J. G. Heller et al., "Comparison of BRYAN Cervical Disc Arthroplasty With Anterior Cervical Decompression and Fusion," *Spine (Phila. Pa. 1976)*, vol. 34, no. 2, pp. 101–107, Jan. 2009.
- [69] Z. Mo, Q. Li, Z. Jia, J. Yang, D. W. C. Wong, and Y. Fan, "Biomechanical consideration of prosthesis selection in hybrid surgery for bi-level cervical disc degenerative diseases," *Eur. Spine J.*, vol. 26, no. 4, pp. 1181–1190, 2017.
- [70] J. Chen et al., "Cervical anterior hybrid technique with bi-level Bryan artificial disc replacement and adjacent segment fusion for cervical myelopathy over three consecutive segments," *J. Clin. Neurosci.*, vol. 27, pp. 59–62, May 2016.
- [71] G. M. V. Barbagallo et al., "Early results and review of the literature of a novel hybrid surgical technique combining cervical arthrodesis and disc arthroplasty for treating multilevel degenerative disc disease: Opposite or complementary techniques?," *Eur. Spine J.*, vol. 18, no. SUPPL. 1, pp. 29–39, Jun. 2009.
- [72] A. Reyes-Sanchez, V. Miramontes, L. M. R. Olivarez, A. A. Aquirre, A. O. Quiroz, and B. Zarate-Kalfopulos, "Initial clinical experience with a next-generation artificial disc for the treatment of symptomatic degenerative cervical radiculopathy," *SAS J.*, vol. 4, no. 1, pp. 9–15, Mar. 2010.
- [73] C. Laurusssen, D. Coric, T. Dimmig, D. Musante, D. D. Ohnmeiss, and H. A. Stubbs, "Cervical total disc replacement using a novel compressible prosthesis: Results from a prospective Food and Drug Administration–regulated feasibility study with 24-month follow-up," *Int. J. Spine Surg.*, vol. 6, no. 1, pp. 71–77, Dec. 2012.
- [74] A. G. Patwardhan and R. M. Havey, "Prosthesis design influences segmental contribution to total cervical motion after cervical disc arthroplasty," *Eur. Spine J.*, Jul. 2019.
- [75] M. M. Panjabi, "The stabilizing system of the spine. Part II. Neutral zone and instability hypothesis," *J. Spinal Disord.*, vol. 5, no. 4, pp. 390–397, Dec. 1992.
- [76] S. Thomas, K. Willems, L. Van den Daelen, P. Linden, M.-C. Ciocci, and P. Bocher, "The M6-C Cervical Disk Prosthesis," *Clin. Spine Surg.*, vol. 29, no. 4, pp. E182–E187, May 2016.
- [77] V. A. Byval'tsev, A. A. Kalinin, I. A. Stepanov, Y. Y. Pestryakov, and V. V. Shepelev, "Analysis of the

- results of total cervical disc arthroplasty using a M6-C prosthesis: a multicenter study," Burdenko's J. Neurosurg., vol. 81, no. 5, pp. 46–55, 2017.
- [78] C. Baltus, E. Costa, G. Vaz, and C. Raftopoulos, "Granulomatous Reaction on a Double-Level Cervical Total Disc Arthroplasty," World Neurosurg., vol. 122, pp. 360–363, Feb. 2019.
- [79] I. Spinal Kinetics, "Mechanical Characterization of M6-C artificial cervical disc."
- [80] K. Kadoya et al., "Biomechanical and Morphologic Evaluation of a Three-Dimensional Fabric Sheep Artificial Intervertebral Disc," Spine (Phila. Pa. 1976)., vol. 26, no. 14, pp. 1562–1569, Jul. 2001.
- [81] Y. Shikinami and H. Kawarada, "Potential application of a triaxial three-dimensional fabric (3-DF) as an implant," Biomaterials, vol. 19, no. 7–9, pp. 617–635, Apr. 1998.
- [82] M. Takahata et al., "Bone Ingrowth Fixation of Artificial Intervertebral Disc Consisting of Bioceramic-Coated Three-dimensional Fabric," Spine (Phila. Pa. 1976)., vol. 28, no. 7, pp. 637–644, Apr. 2003.
- [83] Y. Kotani et al., "Artificial Intervertebral Disc Replacement Using Bioactive Three-Dimensional Fabric," Spine (Phila. Pa. 1976)., vol. 27, no. 9, pp. 929–935, May 2002.
- [84] Y. Kotani et al., "Two-year observation of artificial intervertebral disc replacement: results after supplemental ultra—high strength bioresorbable spinal stabilization," J. Neurosurg. Spine, vol. 100, no. 4, pp. 337–342, Apr. 2004.
- [85] Y. Shikinami, Y. Kotani, B. W. Cunningham, K. Abumi, and K. Kaneda, "A Biomimetic Artificial Disc with Improved Mechanical Properties Compared to Biological Intervertebral Discs," Adv. Funct. Mater., vol. 14, no. 11, pp. 1039–1046, Nov. 2004.
- [86] Y. Shikinami, Y. Kawabe, K. Yasukawa, K. Tsuta, Y. Kotani, and K. Abumi, "A biomimetic artificial intervertebral disc system composed of a cubic three-dimensional fabric," Spine J., vol. 10, no. 2, pp. 141–152, Feb. 2010.
- [87] Y. Kotani et al., "Multidirectional flexibility analysis of cervical artificial disc reconstruction: *in vitro* human cadaveric spine model," J. Neurosurg. Spine, vol. 2, no. 2, pp. 188–194, Feb. 2005.
- [88] A. White and M. Panjabi, Clinical Biomechanics of the Spine, 2nd ed. London: Lip pincott Company, 1990.
- [89] J. Dvorak, D. Froehlich, L. Penning, H. Baumgartner, and M. M. Panjabi, "Functional Radiographic Diagnosis of the Cervical Spine: Flexion/Extension," Spine (Phila. Pa. 1976)., vol. 13, no. 7, pp. 748–755, Jul. 1988.
- [90] J. Dvorak, J. Hayek, and R. Zehnder, "CT - Functional Diagnostics of the Rotatory Instability of the Upper Cervical Spine," Spine (Phila. Pa. 1976)., vol. 12, no. 8, pp. 726–731, Oct. 1987.
- [91] A. Mahomed, P. M. Moghadas, D. E. T. Shepherd, D. W. L. Hukins, A. Roome, and S. Johnson, "Effect of Axial Load on the Flexural Properties of an Elastomeric Total Disc Replacement," Spine (Phila. Pa. 1976)., vol. 37, no. 15, pp. E908–E912, Jul. 2012.
- [92] A. Kienle, N. Graf, T. Villa, and L. La Barbera, "Standard testing," in Biomechanics of the spine: Basic concepts, spinal disorders and treatments, First edit., London: Academic Press, 2018, pp. 223–238.



Chapter 3

Design optimization of the fiber jacket using warp-knitted fabric structures

The contents of this chapter are based on:

C.A.M. Jacobs, A.M. Abdelgawad, S. Ghazanfari, S. Jockenhoevel, K. Ito. Warp-knitted fabric structures for a novel biomimetic artificial intervertebral disc for the cervical spine.

Submitted to the Journal of Materials Science.

Abstract

To replicate the complex kinematics of a natural disc, a biomimetic artificial intervertebral disc replacement (bioAID) has been developed containing a swelling hydrogel core as nucleus pulposus, a fiber jacket as annulus fibrosus and metal endplates to connect the device to the adjacent vertebrae. The first prototype consisted of a weft-knitted fiber jacket, in which only a single fiber was used to create the jacket structure. This can endanger the structural integrity of the complete device upon yarn damage. Therefore, several warp-knitted textile structures were assessed and optimized to ensure structural integrity, allowing for swelling constraint of the hydrogel core, and behaving as one integrated unit similar to a natural IVD.

In this study, 4 different stitch patterns, including 2x1 and 1x1 lapping with and without a pillar stitch, were produced. The effect of the stitch pattern and stitch density on the fabric mechanical properties and device swelling and compressive strength was assessed. As a next step, the effect of using multiple layers of fabrics, mimicking the layered structure of annulus fibrosus, on the functional capacity of the bioAID was characterized.

All textile structures were capable of limiting the swelling of the hydrogel while withstanding its internal pressure and showing sufficient wear resistance. However, only the 2x1 and 2x1 with pillar stitch had a pore size range that was suitable for cell infiltration to facilitate osseointegration as well as having the highest strength of the complete device to ensure safety under compression loading. Incorporating different number of jacket layers of these two stitch patterns did not show any clear effect. When also taking the structural parameters into consideration, the 2x1 lapping design with 4 layers was able to constrain hydrogel swelling, provide a high compressive strength, could facilitate cell infiltration, and had dimensions within the range of a natural intervertebral disc.

3.1 Introduction

Neck pain is a persistent problem that affects millions of people nowadays, mainly caused by spinal disorders affecting intervertebral discs (IVD) [1]. The most common surgical practice to treat severely diseased IVDs is anterior cervical discectomy and fusion (ACDF), where after removal of the dysfunctional IVD, the vertebrae are fused with new bone growth to resolve the pain by restoring the disc height and blocking the motion. However, occurrence of adjacent segment diseases due to the loss of motion drove the development of cervical total disc replacements (CDRs) where the diseased natural disc is replaced with a motion preserving prosthesis. First-generation designs were based on the ball-and-socket principle, which consists of the superposition of solid plates and a core to provide motion based on articulation. The axial properties of such devices are rigid, providing little compression absorption while the natural IVD is an osmotic, viscoelastic body, showing hysteresis and time-dependent deformation [2]. Several clinical trials showed that the implantation of such CDR devices altered the natural motion pattern, caused facet joints overload, and increased the risk of adjacent segment disease [3],[4].

Therefore, second-generation artificial intervertebral discs (AIDs) that can mimic the viscoelastic behavior of a natural discs have been developed in recent years. These devices provide motion from deformable components, allowing motion in all six degrees of freedom and combined motions [5],[6]. One of those devices is the biomimetic artificial intervertebral disc (bioAID) introduced by Peter van den Broek et al. (2012) [6]. The bioAID device contains a hydrogel core mimicking the natural swelling nucleus pulposus, a textile fiber jacket as the tensile load-bearing annulus fibrosis, and a titanium endplate to secure the device to the adjacent vertebrae (Figure 3.1).

One of the key components in the fiber jacket is the medical-grade ultra-high-molecular-weight-polyethylene (UHMWPE) fiber, tradename Dyneema Purity® (DSM Biomedical, Geleen, the Netherlands), that encloses the hydrogel core to imitate the non-linear viscoelastic behavior and osmotic pre-stress of the natural IVD. Dyneema Purity® fiber has exceptionally long and oriented molecular chains that can withstand and distribute high loads effectively. In addition, the fiber exhibits high abrasion and cut resistance and inert chemical properties [7]. Therefore, the bioAID possesses the required, strength, stability and shock absorbance capacity while allowing a semi-constrained motion based on deformation.

The first design of Peter van den Broek et al. (2012) was developed for the lumbar region of the spine [6]. However, clinical need, market size, interest of industry and clinicians revealed more opportunities for the cervical spine. Moreover, the fiber jacket of this first prototype was

a weft-knitted stocking fabricated from a single Dyneema Purity® yarn [8]. The jacket showed no failure up to 15kN (30-35% strain) static compression and remained intact after 10 million cycles of axial loading between 600 – 6000 N; however, the structure safety and integrity are of concern as the yarn could be cut or damaged e.g. during device implantation.

Unlike weft-knitting, warp-knitted structures are made from several yarns, which makes them more resistant to failure [9]. In comparison with weft-knitted structures, warp-knitted ones are typically less elastic which leads to a better swelling and range of motion constraint function of the fiber jacket. Therefore, in this study, several warp-knitted textile patterns were mechanically and structurally assessed and optimized to fit the cervical intervertebral space. More specifically, the biomechanical objectives of the fiber jacket are 1) ensuring structural integrity, 2) while allowing for swelling constrain of the hydrogel and 3) behaving as one integrated unit similar to natural IVD. Moreover, the fiber jacket should 4) act as a scaffold that allows bone ingrowth to ensure long-term stability and 5) have a good durability, 6) be wear resistant and 7) have good manufacturing feasibility with good quality control.

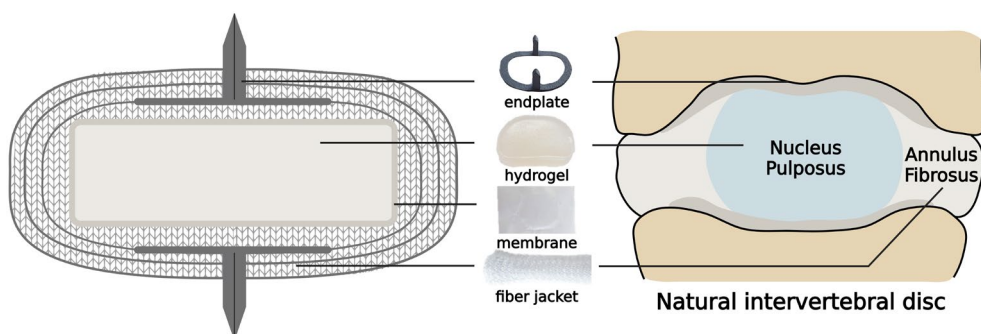


Figure 3.1: Schematic representation of the bioAID and its biomimicry compared to a natural disc. Created with BioRender.com

3.2 Materials & Methods

3.2.1 Hydrogel preparation

The hydrogel was produced by dissolving sodium methacrylate (monomer, 0.02 mol ratio), 2-hydroxyethyl methacrylate (monomer, 0.18 mol ratio), poly (ethylene glycol) dimethacrylate (cross-linker, 0.00001 mol ratio), 2x2' azobis (2-methylpropionamide) dihydrochloride (initiator, 0.001 mol ratio) in distilled water (all analytical grade, Sigma Aldrich, Zwijndrecht, the Netherlands). This hydrogel solution was then poured onto a disc of polyurethane foam (diameter 10 x height 0.2 cm, MCF.03, Corpura B.V., Etten-Leur, The Netherlands) that soaked up the solution, after which it was exposed to UV light (UVP XX15L, 365 nm, Analytik Jena,

Upland, CA USA) for two hours at room temperature in ambient air. To complete the polymerization, it was submerged in a 45°C water bath for 14 hours. Next, the hydrogels were punched out in kidney shape of 21 x 14.5 x 2 mm or 14 x 13 x 2 mm, being the human and canine dimensions respectively.

3.2.2 Fiber jacket fabrication

The production of the tubular warp-knitted jackets was performed on a double-face Raschel machine with Jacquard unit of type DJ 6/2 EL (Karl Mayer Textilmaschinenfabrik GmbH, Obertshausen, Germany) with a machine gauge of E32 at a speed of 60 rpm. First, the UHMWPE yarn was rewound from the parent bobbin to suitable bobbins for the creel of the warp-knitting machine. Next, to identify optimal design properties of the fiber jacket and achieve a stable manufacturing process, several experiments were executed (Table 3.1). In the first experiment, the effect of 4 different fabric structures ((Figure 3.2), lapping design being 2x1, 1x1, 2x1+ open pillar stitch, and 1x1+ open pillar stitch) of 10 stitch/cm, on the biomechanical properties and assembly of the device was studied. In the second knitting experiment a stitch density of 8 stitch/cm was used to facilitate usage of more commonly available textile machines (double needle bed Rachel machine with gauge E20, Mini-tronic 800, Rius comatex, Barcelona, Spain). Based on the ease of assembly, structural characteristics, swelling and compression strength of experiment 1, only the 2x1 and 2x1 + pillar stitch lapping designs were used to determine the effect of the stitch density and amount of layers for optimal functioning of the bioAID (6, 5 or 4 layers for the 2x1 lapping design and 5, 4 or 3 layers for the 2x1 lapping with pillar stitch design) to replicate the layered structure of the annulus fibrosus [10]. The diameter of the tubular fiber jackets was calculated to tightly fit

Table 3.1: Experimental design to determine the optimal fiber jacket configuration.

	Experiment 1: effect of stitch patterns	Experiment 2: effect of stitch density and layers
<i>density</i>	10 stitch/cm	8 stitch/cm
<i>stitch pattern</i>	1x1 1x1 + pillar stitch 2x1 2x1 + pillar stitch	2x1 2x1 + pillar stitch
<i>read outs</i>	human device mechanical characterization	canine device mechanical characterization
	fabric mechanical and structural properties	fabric mechanical and structural properties

around the hydrogel core and restrict swelling, resulting in a theoretical diameter of 18 mm. However, this diameter had to be adjusted for fabrics with different course stitch densities and lapping designs since this affects the elasticity of the fabric. Both fabric structures and complete assembled devices were mechanically assessed.

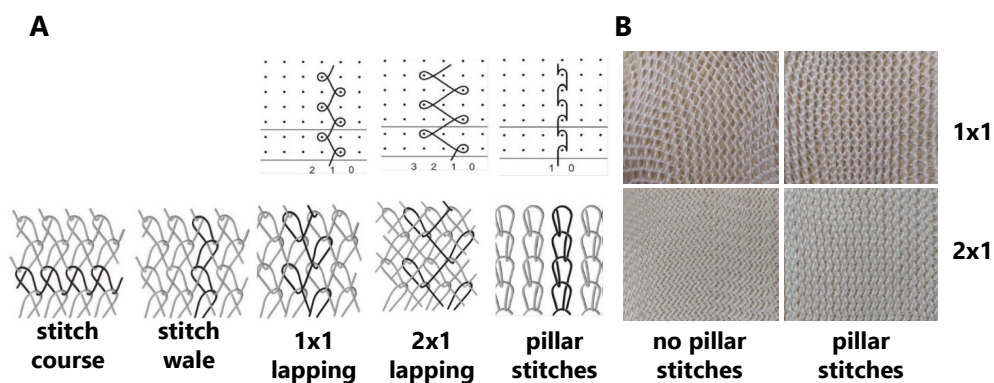


Figure 3.2: A) Schematic drawings of the lapping diagram indicating how the guide bar is switching from one needle to another needle (top) and the corresponding loop structure (bottom) of the different stitch designs; B) knitted tubes with different lapping designs (1x1, 1x1+pillar stitches, 2x1, and 2x1+pillar stitches).

3.2.3 Device assembly

The device is composed of three parts, a hydrogel core, a fiber jacket and two end plates (Figure 3.1) which are assembled to create human and canine prototypes [6]. Canine prototypes were evaluated as preparation for the planned animal trials. First of all, the hydrogel was wrapped in an UHMWPE membrane (38 μm thick, 5 g/m^2 , 0.9 μm pore, membrane, DSM Biomedical, Geleen, the Netherlands) and heat sealed using a thermal cutter (HSG-0, HSGM, Walluf, Germany) to contain the hydrogel and prevent leaching of hydrogel particles. The hydrogel sealed in the membrane was then inserted inside the tubular warp-knitted fiber jacket made of multifilament UHMWPE yarn (Dyneema Purity[®] SGX, dtex110, TS 100, DSM Biomedical, Geleen, Netherlands). After the core was positioned at the bottom of the jacket such that it laid in the transverse plane of the tube, the open end was twisted tight, and the jacket was pulled backwards, inside out, over the core again, closing the open side with a 180° twist, resulting in the first two jacket layers. The wrapping process was repeated until the number of desired layers was reached. At the innermost layer of the jacket layers, two wire-eroded titanium endplate rings (10 x 9 x 0.3 mm) with 2 mm pins, on either flat surface of the implant, was inserted before closing the jacket, such that the pins protruded out of the jacket. The open end of the jacket was closed by manually stitching using UHMWPE yarn (Dyneema Purity[®] SGX, dtex110, TS 100, DSM Biomedical, Geleen, Netherlands).

3.2.4 Fabric Structural and Mechanical Evaluation

The fabric structures (1x1 (10 stitch/cm), 1x1 with pillar (10 stitch/cm), 2x1 (8 and 10 stitch/cm) and 2x1 with pillar stitch (8 and 10 stitch/cm) were characterized in terms of the fabric weight, thickness, porosity, bursting strength and abrasion resistance. Fabric weight (g/m^2) was determined based on ASTM D3776, where the areal density (mass/unit area) was obtained by weighing $2 \times 10 \text{ cm}^2$ samples and dividing it by the area ($n=3$). Thickness (mm) measurements were executed following ASTM D1777-96. An automatic thickness gauge was used, where a specimen was placed on the base of a thickness gauge and a weighted presser foot applied a pressure of 0.41 Bar ($n=3$). The porosity of the fabric ($n=3$) was analyzed by microscopy using a magnification of 100x (Keyence Microscope VHX S550t, the USA). Next, the images were binarized using ImageJ (NIH, the USA) and used to calculate the pore size (50 pores per image measured, $n=3$, μm). Bursting strength was assessed as described in ASTM D3786/D3786M. Briefly, a compressive force was applied at a constant rate of 300 mm/min on the sample (12x12mm) using a polished, hardened steel ball until rupture occurred (Autoburst SDL-Atlas M229, SDL Atlas Textile Testing Solutions, Rock Hill, USA). Displacement and load were continuously recorded and used to calculate the average failure load ($n=5$). Lastly, abrasion resistance was measured, as reported in ASTM D4966-12, to assess the risk of wear debris. Three samples (circular, diameter = 38 mm) were preconditioned at 20 °C at relative humidity of 65% and rubbed against standard wool felt under 12 kPa pressure until two or more yarns were broken, or when a hole appeared (Martindale Wear and Abrasion Tester M235, SDL Atlas Textile Testing Solutions, Rock Hill, USA). The average number of rubs required to rupture two or more yarns or develop a hole in a knitted fabric was reported ($n=4$). Mean and standard deviation were calculated using Microsoft Excel and reported for each group.

3.2.5 Device evaluation: swelling and mechanical integrity

To assess what textile structure and number of jacket layers is optimal for the complete implant, in terms of swelling restriction and compressive mechanical strength, the swelling properties and compressive mechanical strength of the implants were evaluated. It was assumed that the incorporation of the endplate would not have a large effect on the swelling and compressive strength of the device and was therefore not included in the tested prototypes. Swelling capacity of the produced bioAID prototypes was tested in PBS (Dulbecco's Phosphate Buffered Saline, Sigma Aldrich) at 37 °C under a 50 N load to mimic the passive compressive load of a cervical spine [11],[12]. The mass was determined before the experiment and after reaching swelling equilibrium (duration was determined based on previous swelling experiments) and used to calculate the swelling mass ratio (Q) by equation (3.1), where M_s is the mass in the swollen state and M_d is the mass in the dry state.

$$Q = \frac{M_s - M_d}{M_d} \quad (3.1)$$

Compressive strength and mechanical integrity were determined by a static axial compression test. Samples were subjected to compressive load at 3 mm/min until failure or limit of the load cell (MTS; criterion model 42, MTS Systems corporation, Eden Prairie, MN USA, load cell of 5 kN). Failure was defined as a force drop at constant displacement. The strength was defined as the highest load before failure, or "higher than 5 kN" (limit of load cell) and stiffness was determined as the slope of the linear region of the curve. After testing, damage of fiber jacket was macroscopically inspected. Mean and standard deviation were calculated using Microsoft Excel and reported for each group.

3.3 Results

3.3.1 Fabric structural properties

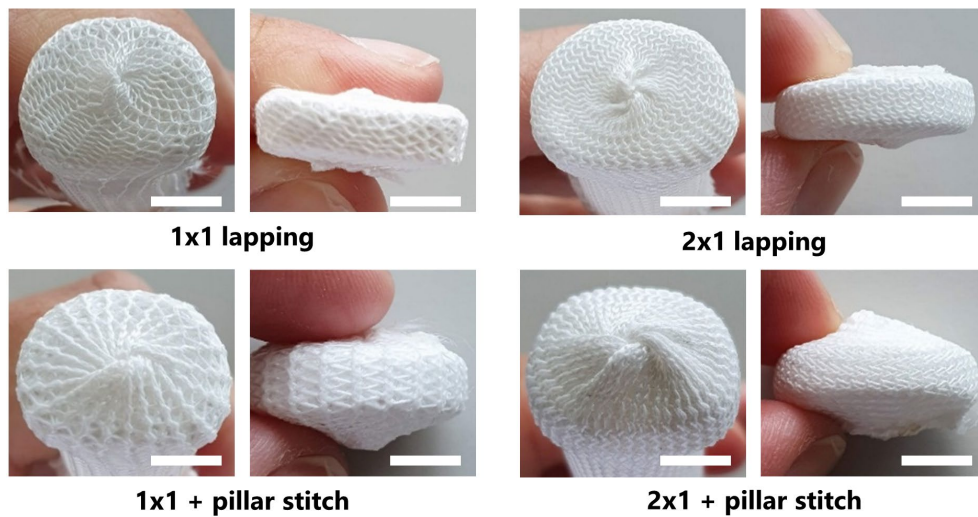


Figure 3.3: Images during the production procedure for each textile structures, showing the formation of the knot at the central cranial and caudal sides of the implant. Scale: 5 mm.

As expected, fabric thickness and fabric weight were lower for the 1x1 lapping design compared to the 2x1 lapping design and decreased with decreasing fabric density. The introduction of a pillar stitch resulted in an increased fabric thickness and weight compared to the same fabric without pillar stitch (Table 3.2). The twists in the jacket resulted in a disc with slightly thicker central areas on both cranial and caudal surfaces. As a result, both jackets with pillar stitch fabrics had a significant thicker knot of approximately 0.2 mm at cranial and caudal sides of the device and overall disc height caused by the twisting assembly method (Figure 3.3).

To assess which textile structure is more suitable to facilitate osseointegration by cell infiltration, the pore sizes of the different textile structures were measured (Table 3.2). The pore sizes were mostly influenced by the lapping design, being highest for 1x1 lapping, followed by 1x1 with pillar stitch, 2x1 and 2x1 with pillar stitch. The reduction in fabric density also gave rise to larger pore sizes for the same textile structure.

3.3.2 Fabric mechanical properties

Abrasion resistance (number of rubs needed until loop damage) was only influenced by the introduction of a pillar stitch, and not by the lapping design or change in fabric density (Table 3.2). On the other hand, bursting strength (force required for loop rupture) increased for the 2x1 lapping design compared to 1x1 and when introducing a pillar stitch (Table 3.2). Overall, the effect of the pillar stitch on the bursting strength was larger compared to the effect of the lapping design.

3.3.3 Device evaluation: swelling and mechanical integrity

3.3.3.1 Effect of knitting lapping design

Only the combination of the 2x1 lapping design with pillar stitch decreased the swelling capacity compared to the other stitch patterns (Figure 3.4). Restricting the swelling results in an osmotic internal pressure required to withstand compressive forces. When looking at the

Table 3.2: Fabric properties for the 4 different textile structures with either fabric density of 10 stitch/cm or 8 stitch/cm

	Fabric thickness (mm)	Fabric weight (g/m ²)	Fabric pore size (μm)	Abrasion resistance (cycles)	Burst strength (MPa)
<i>density of 10 stitch/cm</i>					
1x1	0.35 ± 0.005	91 ± 0.88	1150 ± 25	50 000 ± 2000	1.25 ± 0.07
1x1 +pillar stitch	0.47 ± 0.004	154 ± 0.57	940 ± 50	55 000 ± 2000	1.68 ± 0.10
2x1	0.53 ± 0.004	128 ± 0.72	730 ± 35	50 000 ± 2000	1.46 ± 0.10
2x1 +pillar stitch	0.80 ± 0.005	176 ± 1.2	400 ± 50	60 000 ± 3000	1.84 ± 0.11
<i>density of 8 stitch/cm</i>					
2x1	0.48 ± 0.006	110 ± 0.83	860 ± 25	50 000 ± 2000	1.14 ± 0.05
2x1 +pillar stitch	0.61 ± 0.005	158 ± 0.93	540 ± 40	60 000 ± 3000	1.60 ± 0.09

compressive properties, it can be seen that all textile structures were able to withstand more than the physiological load of 75 N (Figure 3.4) [11],[12]. However, using the 2x1 lapping, either with or without pillar stitch, increased both the ultimate load as well as the stiffness of the bioAID above peak and impact loads reported to range between 100 – 1200 N and physiological stiffness of 500 N/mm [11], [13]–[15]. No macroscopical damage of the fiber jacket was observed after the test, bioAIDs failed due to cracking of the hydrogel.

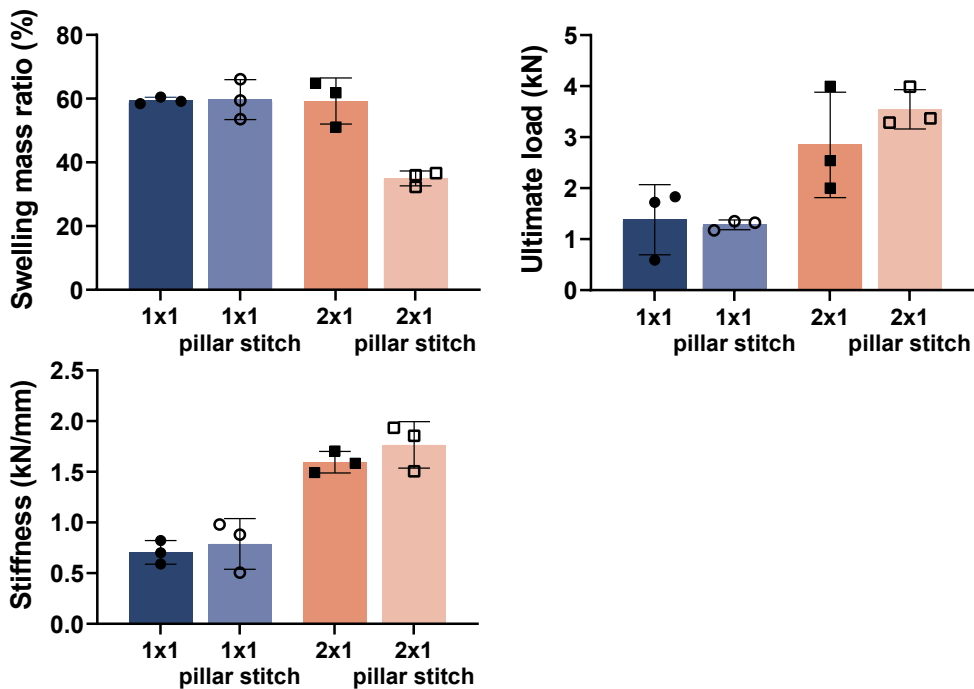


Figure 3.4: Swelling mass ratio, compressive ultimate load, and compressive stiffness (mean \pm SD) of each fiber jacket design in human prototypes.

3.3.3.2 Effect of the number of jacket layers

Based on the results of the different textile structures, it was concluded that both 2x1 lapping with and without pillar stitch seemed to be the best for ensuring safety under physiological compressive loads of the bioAID. Therefore, these two textile structures were assessed to determine the number of layers for optimal functioning of the full device. No clear effect could be observed between the different knits and number of layers used and all groups were able to withstand the physiological load of 75 N (Figure 3.5) [11],[12]. No macroscopical damage of the jacket was observed after the test.

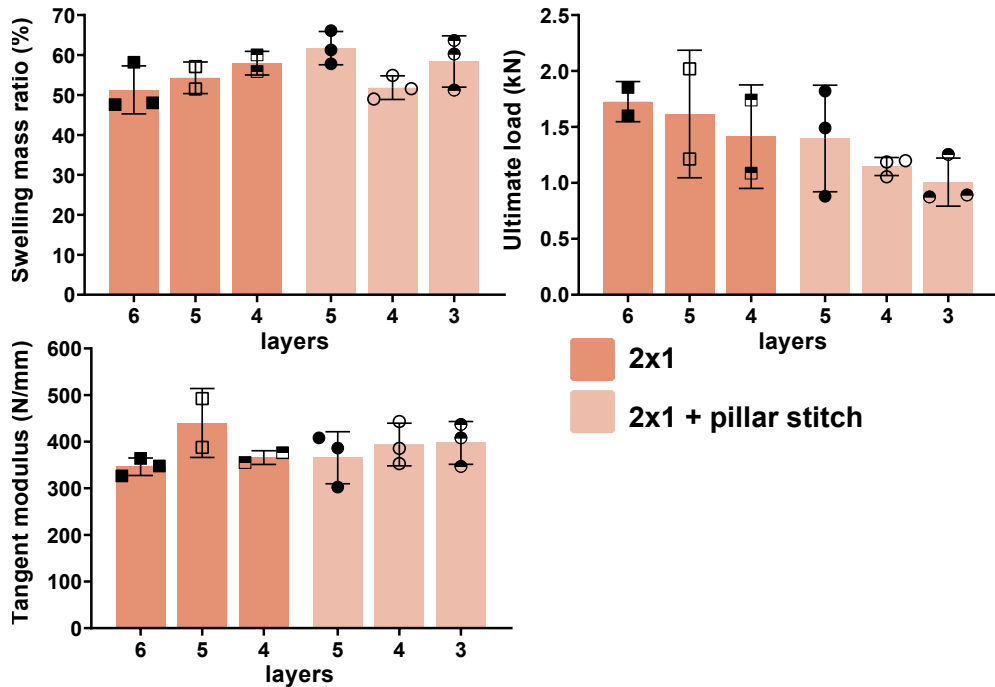


Figure 3.5: Swelling mass ratio, compressive ultimate load, and compressive stiffness (mean \pm SD) of each fiber jacket design and corresponding number of layers of 2x1 and 2x1 + pillar stitch structures in canine prototypes.

3.4 Discussion

In the previous design, the integrity of the fiber jacket using single yarn weft-knitting technique was not full proof and could have become compromised, especially since it is often exposed to sharp bony protrusions and sharp surgical tools during implantation [6]. Using warp-knitting as a textile structure reduces the risk of disintegration upon yarn damage since it is produced from multiple yarns. Therefore, the objective of this study was to investigate several warp-knitted textile patterns for the fabrication of a novel biomimetic disc replacement device.

One of the most important requirements of the fiber jacket is limiting the swelling of the hydrogel to replicate the semi-constrained motion characteristics seen in a natural disc [16]. The semi-constrained motion, where small deformations are easily allowed by the soft hydrogel, while larger deformations are resisted by the tensile stiff jacket, have been assessed in another study [17]. In this research, all devices had a swelling capacity of 60% or less compared to the mass immediately after preparation. Previous results (data not shown) have

shown that the isolated hydrogel can swell up to double its initial weight when swollen unconstrained [18]. This indicates that all the different textile groups are capable of restricting the swelling of the hydrogel to create an internal pressure that can withstand physiological compressive forces. Only the combination of 2x1 lapping design with a pillar stitch resulted in a lower swelling. This might be related to the pillar stitch, resulting in a reduced stretchability. When reducing the density to 8 stitch/cm, this effect becomes non apparent.

This difference in swelling capacity did not affect the ultimate compressive load and stiffness of the complete device, which was most influenced by the lapping design. The 2x1 lapping design showed a higher stiffness and ultimate load, and no effect of the pillar stitch was visible. This can be explained by the fact that the underlap is longer and has a flatter course, making it less elastic in the transverse direction compared to the 1x1 lapping structure [19]. The lack of influence of introducing a pillar stitch can be explained by the fact that there is no lateral connection but only a connection with the other binding elements of the lapping design, increasing the stability only in the longitudinal (and radial) direction [20]. Although loads in normal daily life that are being transferred through the intervertebral disc all have a compressive component, these findings cannot be extrapolated to all different loading modes that act on a spinal segment. Therefore, additional studies that assess multiple loading modes and investigate the effect on the kinematics of the spine are required.

Although the function of UHMWPE membrane is to contain the hydrogel, it is loose and does not limit it from swelling. Thus, it was relevant to assess if the fiber jacket could withstand the hydrogel's swelling pressure without yarn rupture. As can be seen for the bursting strength data, all textile patterns only failed above the previously measured hydrogel swelling pressure tested in a rigidly confined compression set-up of 1 MPa [18]. Also being above the physiological internal pressures measured for natural nucleus pulposus that ranges between 0.3-1 MPa [12], [21]–[23]. This is also consistent with the results of the swelling and compression test of the full device, where no macroscopical damage of the fiber jacket was observed.

To ensure longevity of the device, the fiber jacket should be wear resistant as the layers of the fiber jacket are not restricted from moving relative to each other. To assess the wear performance of the different textile patterns, an abrasion test was performed to give insight into the number of cycles needed before a loop is damaged, which could potentially weaken the fiber jacket. The differences in abrasion resistance between the different textile structures were small, and only the introduction of a pillar stitch in the 2x1 lapping design resulted in an increased abrasion resistance. This indicates that the yarn its mechanical properties play the

largest role in the jacket's wear performance. It is known that UHMWPE yarns have an extremely high wear resistance, represented by its high abrasion resistance and flexlife (> 100 000 cycles) [7], [24]. This indicates that the risk of yarn rupture causing weakening of the complete fiber jacket is assumed to be minimal for all the textile structures that were investigated. This study did not include assessment of wear debris, which can trigger an inflammatory response that could lead to aseptic loosening and prosthesis failure [24]. Therefore, further work is needed to establish this risk of wear debris, especially since in the current design multiple layers of UHMWPE textile are used that can rub against each other, increasing the risk of creating wear particles. However, as no yarn rupture occurred one could assume that this is not of considerable volume. The risk is even further reduced after bone has grown into multiple layers of the fiber jacket, limiting motions that could cause wear. In addition, the durability, fatigue and creep properties of the jacket and full device should also be assessed to get a more complete picture of the bioAIDs longevity.

Another important aspect that should be considered when designing the fiber jacket is that the surface directly interfacing the vertebral bodies should facilitate osseointegration, known to be one of the most critical parameters influencing clinical success [25]–[27]. In this study, based on the structural properties, it was assessed if the pore size of each textile structure would allow cell infiltration. For both stitch densities, only the 2x1 with pillar stitch design was within the optimal range of 100 – 600 μm [28]–[33]. It should however be noted that by introducing multiple layers, the total porosity of the jacket is affected and likely reduced. It was therefore assumed that also the 2x1 lapping design could be a suitable surface for cell infiltration. Besides structural properties, chemical and physical characteristics will also influence the osseointegration of the device. UHMWPE is known to be inert and hydrophobic, and thus unsuitable for cells to adhere to [34]. Hence, to improve the osseointegration potential of the bioAID, surface modifications, such as plasma treatment or hydroxyapatite coatings, that improve bioactivity were assessed in another study [35].

The fiber jacket should behave as a homogeneous structure that covers the hydrogel and endplate such that it behaves as one integrated unit similar to a natural IVD. This can be either achieved by increasing the stitch density or by wrapping the hydrogel and endplate in multiple layers. Based on the mechanical properties, especially the 2x1 and 2x1 with pillar stitch of both the 8 stitch/cm and 10 stitch/cm samples demonstrated to be suitable for functioning of the bioAID. However, an advantage of the 8 stitch/cm fabrics is that it can be produced on more commonly available textile machines, improving the manufacturing capabilities and quality control. It was expected that decreasing the stitch density from 10 stitch/cm to 8 stitch/cm would lead to a reduced compressive strength of the complete device. Thus, although the 10

stitch/cm 1x1 lapping prototypes resembled the natural stiffness better, it was decided to continue with the 2x1 and 2x1 with pillar stitch and prioritize a higher failure load to ensure structural integrity under reported impact loads of 100 – 1200 N [11], [13]–[15]. Therefore, the effect of layers on functioning of the bioAID for the 2x1 and 2x1 with pillar stitch textile structures was investigated with 8 stich/cm density structures.

No clear differences in swelling and mechanical characteristics were found between samples with different layers or stich densities, making the structural parameters of the bioAID after assembly an important consideration for choosing the most optimal jacket configuration. By introducing a pillar stitch, the textile construct becomes denser and heavier because of the higher yarn consumption in the underlap. As a result, the twists in the 2x1 with pillar stitch jacket resulted in a disc with a significant thicker center part on both cranial and caudal sides compared to the 2x1 samples. This was considered to be a disadvantage for the implantation of the device, increasing the risk of over distracting the disc space. Moreover, the 2x1 textile structure with pillar stitch has a fabric thickness that with only 3 layers already results in a final thickness of approximately 4 mm when unswollen. The optimal height of the device should be within the physiological height range of the IVD of the cervical spine, being between 4-6 mm [36]–[38]. Therefore, the 2x1 lapping design was considered to be most optimal based on all discussed parameters. To reduce the need of vertebral distraction during implantation, four layers was hypothesized to be most optimal.

This study was focused on the effect of fabric properties within a novel cervical disc replacement device. Whilst this study varied in testing human and canine prototypes (as preparation for animal trials), complicating mutual comparisons, it was still useful for determining the optimal fiber jacket configuration. It would, however, be valuable to investigate the complex interplay of the textile structure, geometry and yarn properties in future studies with a larger sample size. In addition, it should be noted that the current device is still a prototype, requiring multiple manual assembly steps that can give rise to variabilities and suboptimal characteristics such as the knot formation due to the jacket twisting. In the future, it would be desirable to set-up a more automated assembly procedure to rule out these effects. Taken together, these findings suggest that using 4 layers of the 2x1 lapping structure is the most optimal configuration for functioning of the bioAID and future studies.

Acknowledgements

This publication is part of the project BioAID with project number 10025453 of the research program AES Open Technology Program, partly financed by the Dutch Research Council (NWO). The authors are grateful to DSM Biomedical for providing the UHMWPE fibers used in this publication.

References

- [1] R. Webb, T. Brammah, M. Lunt, M. Urwin, T. Allison, and D. Symmons, "Prevalence and Predictors of Intense, Chronic, and Disabling Neck and Back Pain in the Uk General Population," *Spine (Phila. Pa. 1976)*, vol. 28, no. 11, pp. 1195–1202, Jun. 2003.
- [2] J. E. Smeathers and D. N. Joanes, "Lumbar Intervertebral Joints: a Comparison Between Fresh and Thawed Specimens," *J. Biomech.*, vol. 21, no. 5, pp. 425–433, 1988.
- [3] C. S. Shim et al., "CHARITI versus ProDisc: A comparative study of a minimum 3-year follow-up," *Spine (Phila. Pa. 1976)*, vol. 32, no. 9, pp. 1012–1018, 2007.
- [4] M. A. Rousseau, D. S. Bradford, R. Bertagnoli, S. S. Hu, and J. C. Lotz, "Disc arthroplasty design influences intervertebral kinematics and facet forces," *Spine J.*, vol. 6, pp. 258–266, 2006.
- [5] C. A. M. Jacobs, C. J. Siepe, and K. Ito, "Viscoelastic cervical total disc replacement devices: Design concepts," *Spine Journal*, vol. 20, no. 12. Elsevier, pp. 1911–1924, Aug-2020.
- [6] P. R. Van Den Broek, "Development of a biomimetic artificial intervertebral disc," Eindhoven University of Technology, 2012.
- [7] R. Kirschbaum and J. L. J. van Dingenen, "Advances in gel-spinning technology and Dyneema fiber applications," in *Integration of Fundamental Polymer Science and Technology—3*, Springer, Dordrecht, 1989, pp. 178–198.
- [8] P. R. van den Broek, J. M. Huyghe, W. Wilson, and K. Ito, "Design of next generation total disk replacements," *J. Biomech.*, vol. 45, no. 1, pp. 134–140, 2012.
- [9] Y. E. Elmogahzy, *Engineering textiles: Integrating the design and manufacture of textile products*. Elsevier, 2019.
- [10] S. Ghazanfari, A. Werner, S. Ghazanfari, J. C. Weaver, and T. H. Smit, "Morphogenesis of aligned collagen fibers in the annulus fibrosus: Mammals versus avians," *Biochem. Biophys. Res. Commun.*, vol. 503, no. 2, pp. 1168–1173, 2018.
- [11] S. P. Moroney, A. B. Schultz, and J. A. A. Miller, "Analysis and measurement of neck loads," *J. Orthop. Res.*, vol. 6, no. 5, pp. 713–720, Sep. 1988.
- [12] R. Arshad, H. Schmidt, M. El-Rich, and K. Moglo, "Sensitivity of the Cervical Disc Loads, Translations, Intradiscal Pressure, and Muscle Activity Due to Segmental Mass, Disc Stiffness, and Muscle Strength in an Upright Neutral Posture," *Front. Bioeng. Biotechnol.*, vol. 10, no. April, pp. 1–11, 2022.
- [13] S. P. Moroney, A. B. Schultz, A. A. J. Miller, and G. B. J. Andersson, "Load-displacement properties of lower cervical spine motion segments," *J. Biomech.*, vol. 21, no. 9, pp. 769–779, 1988.
- [14] N. Yoganandan, F. A. Pintar, J. Zhang, and J. L. Baisden, "Physical properties of the human head: Mass, center of gravity and moment of inertia," *J. Biomech.*, vol. 42, no. 9, pp. 1177–1192, Jun. 2009.
- [15] J. R. Funk, J. M. Cormier, C. E. Bain, H. Guzman, E. Bonugli, and S. J. Manoogian, "Head and Neck loading in everyday and vigorous activities," *Ann. Biomed. Eng.*, vol. 39, no. 2, pp. 766–776, Feb. 2011.
- [16] N. Bogduk and S. Mercer, "Biomechanics of the Cervical Spine. I: Normal kinematics," *Clin. Biomech.*, vol. 15, pp. 633–648, 2000.
- [17] C. A. M. Jacobs et al., "Biomechanical evaluation of a novel biomimetic artificial intervertebral disc in canine cervical cadaveric spines," *Manuscr. Submitt. Publ.*, 2022.
- [18] C. Jacobs, M. Wijlaars, M. Harries, K. Ito, and L. Kock, "A novel cervical biomimetic artificial intervertebral disc: a mechanical analysis," in *European Society of Biomechanics*, 2019, p. 1.
- [19] N. Anbumani, *Knitting Terms and Functional Elements*. 2007.
- [20] Y. Kyosev, *Warp knitted fabrics construction*. CRC Press, 2019.
- [21] B. Frost, S. Camarero-Espinosa, and E. Foster, "Materials for the spine: anatomy, problems, and solutions," *Materials (Basel)*, vol. 12, no. 2, p. 253, Jan. 2019.
- [22] J. Pospiech, D. Stolke, H. J. Wilke, and L. E. Claes, "Intradiscal pressure recordings in the cervical

- spine," *Neurosurgery*, vol. 44, no. 2, pp. 379–385, 1999.
- [23] K. Wang, Z. Deng, H. Wang, Z. Li, H. Zhan, and W. Niu, "influence of variations in stiffness of cervical ligaments on C5-C6 segment," *J. Mech. Behav. Biomed. Mater.*, vol. 72, no. 1, pp. 129–137, 2017.
- [24] J. H. Werner, J. H. Rosenberg, K. L. Keeley, and D. K. Agrawal, "Immunobiology of periprosthetic inflammation and pain following ultra-high-molecular-weight-polyethylene wear debris in the lumbar spine," *Expert Review of Clinical Immunology*, vol. 14, no. 8, pp. 695–706, 2018.
- [25] C. K. Lee and V. K. Goel, "Artificial disc prosthesis: design concepts and criteria," *Spine J.*, vol. 4, no. 6, Supplement, pp. S209–S218, Nov. 2004.
- [26] M. F. Eijkelkamp, J. M. Huyghe, C. C. van Donkelaar, J. R. van Horn, A. G. Veldhuizen, and G. J. Verkerke, "Requirements for an artificial intervertebral disc," *Int. J. Artif. Organs*, vol. 24, no. 5, pp. 311–321, 2001.
- [27] H. Kienapfel, C. Sprey, A. Wilke, and P. Griss, "Implant fixation by bone ingrowth," *J. Arthroplasty*, vol. 14, no. 3, pp. 355–368, Apr. 1999.
- [28] G. Li et al., "In vitro and in vivo study of additive manufactured porous Ti6Al4V scaffolds for repairing bone defects," *Sci. Rep.*, vol. 6, pp. 1–11, 2016.
- [29] V. Karageorgiou and D. Kaplan, "Porosity of 3D biomaterial scaffolds and osteogenesis," *Biomaterials*, vol. 26, no. 27, pp. 5474–5491, 2005.
- [30] N. Taniguchi et al., "Effect of pore size on bone ingrowth into porous titanium implants fabricated by additive manufacturing: An in vivo experiment," *Mater. Sci. Eng. C*, vol. 59, pp. 690–701, Feb. 2016.
- [31] Z. Chen et al., "Influence of the pore size and porosity of selective laser melted Ti6Al4V ELI porous scaffold on cell proliferation, osteogenesis and bone ingrowth," *Mater. Sci. Eng. C*, vol. 106, no. 110289, pp. 1–13, Jan. 2020.
- [32] J. Augustin et al., "Effect of pore size on tissue ingrowth and osteoconductivity in biodegradable Mg alloy scaffolds," *J. Appl. Biomater. Funct. Mater.*, vol. 20, pp. 1–18, Feb. 2022.
- [33] W. Li et al., "Pore Size of 3D-Printed Polycaprolactone/Polyethylene Glycol/Hydroxyapatite Scaffolds Affects Bone Regeneration by Modulating Macrophage Polarization and the Foreign Body Response," *ACS Appl. Mater. Interfaces*, vol. 14, no. 18, 2022.
- [34] R. Vaishya, A. K. Agarwal, M. Tiwari, A. Vaish, V. Vijay, and Y. Nigam, "Medical textiles in orthopedics: An overview," *J. Clin. Orthop. Trauma*, vol. 9S, pp. S26–S33, Mar. 2018.
- [35] C. A. M. Jacobs, E. E. A. Cramer, A. A. Dias, H. Smelt, S. Hofmann, and K. Ito, "Surface modifications to promote the osteoconductivity of ultra-high-molecular-weight-polyethylene fabrics for a novel biomimetic artificial disc prosthesis: An in vitro study," *J. Biomed. Mater. Res. - Part B Appl. Biomater.*, pp. 1–11, 2022.
- [36] W. Frobin, G. Leivseth, M. Biggemann, and P. Brinckmann, "Vertebral height, disc height, posteroanterior displacement and dens-atlas gap in the cervical spine: Precision measurement protocol and normal data," *Clin. Biomech.*, vol. 17, no. 6, pp. 423–431, 2002.
- [37] I. Busscher, J. J. W. Ploegmakers, G. J. Verkerke, and A. G. Veldhuizen, "Comparative anatomical dimensions of the complete human and porcine spine," *Eur. Spine J.*, vol. 19, no. 7, pp. 1104–1114, Jul. 2010.
- [38] W. Anderst, W. Donaldson, J. Lee, and J. Kang, "Cervical Spine Disc Deformation During In Vivo Three-Dimensional Head Movements," *Ann. Biomed. Eng.*, vol. 44, no. 5, pp. 1598–1612, May 2016.



Chapter 4

Surface modifications to promote the osteoconductivity of UHMWPE fabrics

The contents of this chapter are based on:

C.A.M. Jacobs, E.E.A. Cramer, A.A. Dias, H. Smelt, S. Hofmann, K. Ito. Surface modifications to promote the osteoconductivity of Ultra-High-Molecular-Weight-Polyethylene fabrics for a novel biomimetic artificial disc prosthesis: an *in vitro* study. *Journal of Biomedical Materials Research part B: Applied Biomaterials*, vol. 11, no. 2, p. 442-452 Feb. 2023

DOI: [10.1016/j.spinee.2020.08.007](https://doi.org/10.1016/j.spinee.2020.08.007)

Abstract

A novel biomimetic artificial intervertebral disc (bioAID) for the cervical spine was developed, containing a hydrogel core representing the nucleus pulposus, an UHMWPE fiber jacket as annulus fibrosis, and titanium endplates with pins for mechanical fixation. Osseointegration of the UHMWPE fibers to adjacent bone structures is required to achieve proper biomimetic behavior and to provide long-term stability. Therefore, the aim of this study was to assess the osteoconductivity of several surface modifications of UHMWPE fabrics, 2D weft-knitted, using non-treated UHMWPE fibers (N), plasma treated UHMWPE fibers (PT), 10% hydroxy apatite (HA) loaded UHMWPE fibers (10%HA), plasma treated 10%HA UHMWPE fibers (PT-10%HA), 15%HA loaded UHMWPE fibers (15%HA) and plasma treated 15%HA UHMWPE fibers (PT-15%HA).

Scanning electron microscopy (SEM) was used for surface characterization. Biological effects were assessed by evaluating initial cell attachment (SEM, DNA content), metabolic activity (PrestoBlue assay), proliferation, differentiation (alkaline phosphatase activity) and mineralization (EDX analysis) using human bone marrow stromal cells.

Plasma treated samples showed increased initial cell attachment, indicating the importance of hydrophilicity for cell attachment. However, incorporation only of HA or plasma treatment alone was not sufficient to result in upregulated ALP activity. Combining HA loaded fibers with plasma treatment showed a combined effect, leading to increased cell attachment and upregulated ALP activity. Based on these results, combination of HA loaded UHMWPE fibers and plasma treatment provided the most promising fabric surface for facilitating bone ingrowth.

4.1 Introduction

Cervical artificial intervertebral discs (AIDs) have been developed as a mobility preserving alternative treatment for severely degenerated discs. First generation prostheses were based on traditional synovial joint articulating arthroplasty designs, leading to a mismatch in the motion and kinematics of a natural cervical disc [1], [2]. This mismatch could potentially lead to a hypermobile environment where other anatomical structures need to compensate for this altered loading regime in the spine. It is therefore hypothesized that mimicking the native structure of the cervical intervertebral disc (IVD) would also lead to natural biomechanical properties. As a result, second generation prosthesis have been developed in recent years, that aim to better replicate the anatomy of a natural disc [3]–[7]. One of those is the novel biomimetic cervical AID developed by Peter van den Broek (Figure 4.1) [7]. The design contains a hydrogel core, representing the swelling nucleus pulposus enclosed in a ultra-high-molecular-weight-polyethylene (UHMWPE) fiber jacket mimicking the annulus fibrosus [8]. Although titanium endplates with pins are used to achieve initial stabilization to the vertebrae, direct anchorage or osseointegration of the UHMWPE fibers to the adjacent bone structures is required to achieve proper biomimetic behavior [9]. Moreover, osseointegration is crucial to provide long-term stability, being one of the most important factors influencing clinical success of load bearing prostheses [10]. Although it has good mechanical properties, the disadvantage of pure UHMWPE is that it is inert and hydrophobic, making it less attractive for cells and proteins to attach and facilitate osseointegration [11].

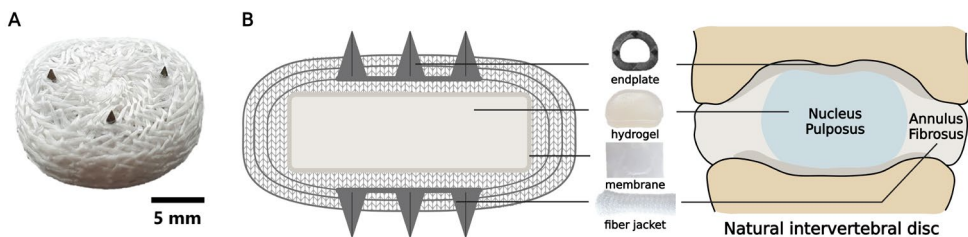


Figure 4.1: A: Biomimetic artificial intervertebral disc (bioAID). B: schematic representation of the design of the bioAID and its biomimicry compared to a natural disc. Created with BioRender.com

To increase the osteoconductivity, defined as a material surface that facilitates bone ingrowth, implant surfaces are often chemically or physically altered [12]. One common approach to increase osteoconductivity is to increase surface roughness. High surface roughness is known to stimulate cell differentiation towards osteoblasts, allow for better biomechanical connection and lead to more bonding spots for host proteins to interconnect with the implant surface [13], [14]. Several methods to increase surface roughness are sand blasting, etching or

oxidation [14]–[16]. Besides surface roughness, an increased hydrophilicity has also shown to promote cell attachment *in vivo* and *in vitro* and thereby promote osseointegration [17]–[21]. Increasing hydrophilicity of the surface can be achieved by methods such as plasma treatment and UV irradiation. The implant surface can also be chemically altered by applying calcium phosphate (CaP) and hydroxyapatite (HA) coatings, which allow for a chemical bonding between the implant and bone surfaces due to the chemical similarities of bone and CaP and HA [22], [23]. Several *in vivo* studies have shown an increase in bone ingrowth for implants coated with HA or CaP [24], [25]. However, there are also concerns with plasma-sprayed coatings. Some studies have shown there is a risk of delamination of the coating from the surface of the implant, resulting in clinical implant failure due to the micromotion caused by debris and loose particles [26], [27]. As a solution, incorporation of HA into the material has shown to be beneficial in providing a mechanically stable surface for facilitating bone ingrowth [28].

Incorporation of ceramics, such as HA, into polymeric materials to increase osteoconductivity is mainly reported for solid surfaces, since spinning of composite materials into fibers is challenging [29]. Fiber production from composite materials can lead to instabilities and frequent breakage during the gel spinning process and unwanted alterations in the bulk mechanical properties. Another potential problem is that the added ceramic particles are often unavailable for biological interaction since most of the particles are covered by the polymeric material due to the production process. In the current article, a novel fiber is introduced that is gel spun out of a composite solution containing UHMWPE and HA. These novel fibers have bioactive surfaces while preserving the desired fiber mechanical properties for orthopedic applications. To increase the exposure of the HA particles at the fiber surface, additional surface treatments can be performed, such as an etching step with plasma.

To date, few studies can be found on physically or chemically altered UHMWPE fabrics used for orthopedic/spinal applications. Most studies have investigated physically or chemically altered metal, since polymers are often avoided at the bone implant interface due to the lower affinity for bone ingrowth [30]. To our knowledge, only one other spinal implant (3D-F) used UHMWPE fibers at the bone-implant surface spray coated with sintered HA or apatite wollastonite glass ceramics granules to increase osteoconductivity [31]–[35]. Initial *in vivo* data showed penetration of scar tissue into the fabric and loss of bioceramic micropowders after implantation [33]. In the following study, *in vivo* results showed that the fibers were directly surrounded by osseous trabeculae [31] and, that the implant was firmly fixed to the vertebral body only when implanted in a stable environment [32].

Due to the limited data available, it is important to get an indication of which surface modifications are most suitable in facilitating osseointegration of the UHMWPE fabric surface of the bioAID. Therefore, this study aimed to assess the initial *in vitro* osteoconductive response of UHMWPE fabrics by modifying the surface roughness, hydrophilicity and/or incorporation of HA particles into the fiber. In the present study, an osteoconductive material is defined as a material that facilitates bone growth on its surface. New tissue formation on a material is mainly promoted by a surface structure that facilitates cell adherence, cell proliferation and production of extracellular matrix. As a result, osteoconductivity was graded based on three characteristics: cell metabolic activity and attachment, osteoblast differentiation and bone matrix production. Human Bone Marrow Stromal cells (hBMSC) were seeded on weft-knitted UHMWPE fabrics *in vitro* to assess the osteoconductive potential of these different surfaces (Figure 4.2).

4.2 Materials & Methods

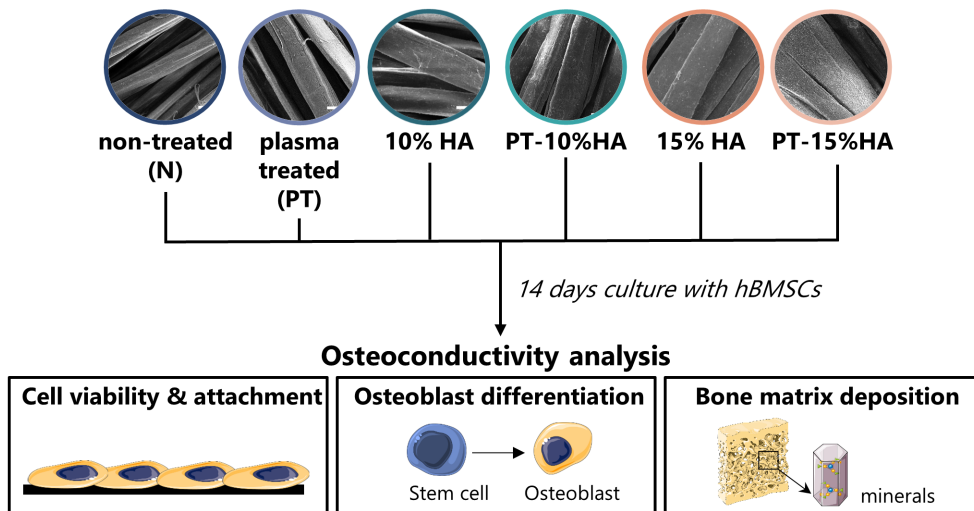


Figure 4.2: Schematic representation of experimental set-up. Weft-knitted fabrics made of untreated (N), plasma treated (PT), 10%HA loaded (10%HA), plasma treated 10%HA loaded (PT-10%HA), 15%HA loaded and, plasma treated 15%HA loaded UHMWPE fibers (PT-15%HA) were cultured with human bone marrow-derived stromal cells (hBMSCs) for 14 days. Osteoconductivity was assessed based on cell viability, attachment, osteogenic differentiation, and mineral deposition. Image created with Servier Medical Art in compliance with the terms of the Creative Commons Attribution 3.0 Unported License.

4.2.1 *Fabric sample preparation*

Six differently modified 2-dimensional (2D) weft-knitted fabrics were prepared: non-treated UHMWPE fibers (N), plasma treated UHMWPE fibers (PT), 10%HA loaded UHMWPE fibers (10%HA), Plasma treated 10%HA UHMWPE fibers (PT-10%HA), 15%HA loaded UHMWPE fibers (15%HA) and plasma treated 15%HA UHMWPE fibers (PT-15%HA). Preparation of the 10% and 15%HA loaded biocomposite UHMWPE fibers was performed using a gel spinning process as described in Dias et al. (2021) and provided by DSM Biomedical, Geleen [36]. Next, untreated UHMWPE fibers (Dyneema Purity® SGX dtex100 TS 100, DSM, Geleen, Netherlands), 10%HA UHMWPE and 15%HA UHMWPE fibers g/m were weft-knitted (Shima Seiki 13 gauge knitting machine) into 2D fabrics using standard large hook needles (GCN 1053A, Groz-Beckert) with areal densities of 75-80 g/m². Depending on the experimental group, select samples were prepared for plasma treatment by winding them around the drum electrode (along the cylinder circumference of 1.8 m) of a pilot-scale web coater. Plasma treatment was performed with argon and oxygen for 40 minutes (40 min, Ar/O, plasma. 160/40 sccm. 1000 W, 1 mbar), resulting in an etching rate of about 25 nm/min. The selected pressure of 1 mbar supports plasma-chemical etching involving rather long-living oxygen species that diffuse along the fibrous surfaces. After surface treatments, all fabrics were cut into circular pieces with a diameter of 9.5 mm. All fabric discs were sterilized by incubation in 0.5 ml isopropanol for 1 hour, followed by evaporation and washing twice for 5 min with 0.5 ml PBS (Dulbecco's Phosphate Buffered Saline, Sigma Aldrich).

4.2.2 *Materials*

Dulbecco's modified Eagle medium (DMEM), non-essential amino acids (NEAA) and antibiotic/antimycotic (Anti-Anti) were from Life Technologies (Bleiswijk, The Netherlands). Trypsin was from Lonza (Breda, The Netherlands). Bovogen fetal bovine serum (FBS) was from PAA laboratories (FBS Gold, Cölbe, Germany). Dexamethasone, ascorbic acid-2-phosphate and β -glycerolphosphate were obtained from Sigma Aldrich (Zwijndrecht, The Netherlands), ITS+ from Corning (Fisher Scientific, Landsmeer, NL).

4.2.3 *Cell culture*

Human Bone Marrow-derived Stromal Cells (hBMSCs) isolation and characterization from human bone marrow (Lonza, Walkersville, MD, USA) was performed as previously described [37]. Passage five hBMSCs were expanded in expansion medium (DMEM; Cat. No. 41966, 10% FBS, 1% anti-anti, 1% NEAA). After the cells reached confluency (day 7), the cells were trypsinized, counted and centrifuged. To prepare cell-laden constructs, hBMSCs were suspended in seeding medium (DMEM, 1%ITS+, 1% anti-anti) at a density of 400,000 cells/ml.

To ensure that cells only attached to fabric constructs and not to the well, cell repellent 48 wells plates were used (Cellstar[®], Greiner Bio One, Frickenhausen, Germany). To prevent the fabric constructs from floating, silicon O-rings (Technirub, O-ring, 9x2 silicone 70 shore rood) were put on top of each fabric construct. Next, the cells were drop seeded on the fabric constructs (20,000 cells/50 μ l) and incubated for 4.5 hours at 37°C, 5%CO₂ to allow for cell attachment before cells were completely submerged with seeding medium with a total volume of 0.5 ml per well. At day 2, 1%ITS+ was replaced with 10% Bovogen FBS in the medium. On day 7, medium was supplemented with osteogenic supplements (50 μ g/mL L-ascorbic-acid-2-phosphate, 100 nM dexamethasone and 10 mM β -glycerophosphate). Samples were cultured for 14 days at 37°C, 5% CO₂, medium was changed every 3 days.

4.2.4 Cell metabolic activity, DNA content and Alkaline Phosphatase activity

To determine metabolic activity of all viable cells, a non-destructive PrestoBlue assay (n=6 per group) was performed at day 2, 7, and 14. PrestoBlue (Thermo Fisher Inc.) was added to each well (10%v/v), including a blank with only medium, and incubated at 37°C, 5% CO₂ for 30 minutes. After incubation, the fluorescence was measured with excitation wavelength at 530-560nm and emission wavelength at 590nm with a plate reader (Synergy[™] HT, BioTek[®] Instruments Inc., Winooski, VT, USA). The measured fluorescence was corrected for the blank, and results are presented as fluorescence intensity. Next, samples were washed in PBS (Dulbecco's Phosphate Buffered Saline, Sigma Aldrich) before performing alkaline phosphatase activity (ALP) assay (day 14) and/or DNA assay (day 2,7 and 14). For the ALP assay, samples were disintegrated in 0.5 mL of 0.2% (v/v) Triton X-100 and 5 mM MgCl₂ solution using steel beads and a MiniBeadbeater[™] (Biospec, USA). After centrifugation at 3000 g for 10 min, the supernatant (80 μ l) was combined with 0.75M 2-amino-2methyl-1-propanol (AMP) buffer solution (20 μ l) and 10 mM p-nitrophenylphosphate substrate solution (100 μ l). This was incubated until a color change was observed (\pm 10 min), then 100 μ l of 0.2 M NaOH was added to stop the conversion of p-nitrophenyl phosphate into p-nitrophenol. Absorbance values were determined at 405 nm with a microplate reader (Synergy[™] HT, BioTek[®] Instruments Inc., Winooski, VT, USA). Absorption values were subtracted from the measured blank. ALP activity was calculated using a standard curve obtained from samples with known p-nitrophenol concentrations, ranging between 0 and 0.9 mmol/ml. The calculated ALP activity was then normalized by the DNA content measured for each construct. Samples for DNA assessment were digested using papain (125 μ g/ml) and DNA content was determined by using Qubit[™] dsDNA HS Assay Kit (Invitrogen, USA), according to the manufacturer's instructions.

4.2.5 SEM/EDX

After 14 days of culture, the cell loaded samples were fixed with 2.5% glutaraldehyde (Sigma Aldrich) in 0.1M Sodium Cacodylate (Sigma Aldrich) buffer for 15 minutes and washed with 0.1M Sodium Cacodylate buffer. Control samples without cells (n=2) and cell loaded samples (n=2) were dehydrated using 0.5 ml of multiple ethanol series (50% twice, 70% twice, 95% twice, 100% three times for 10 minutes) and were dried chemically with hexamethyldisilazane (Sigma Aldrich). Then the samples were washed three times with 0.5 ml ultrapure water for 5 min, dried by air and mounted on specimen stubs. To provide better contrast, only the samples for scanning electron microscopy (SEM) imaging were sputter coated with 8 nm gold (Q3150T, Quorum Technologies). SEM images were obtained using a Quanta 600 SEM (Thermo Scientific Breda, The Netherlands), in a high vacuum ($<1.3 \times 10^{-4}$) at 10 kV with a spot size of 3 using the Everhart-Thornley secondary electron detector (ETD-SE). Similar sample preparation was utilized to perform energy dispersive X-ray (EDX) (Phenom ProX Desktop, ThermoFisher) analysis to evaluate regions in which extracellular matrix depositions were identified (10 kV, backscattered electron detector).

4.2.6 Statistical analysis

Mean and standard deviation were calculated using Microsoft Excel. Comparisons between experimental groups were determined by one-way ANOVA, followed by Tukey's honest post-hoc analysis to determine significant differences. Normal distribution was evaluated using Shapiro-Wilk test and homogeneity of variances was assessed using Levene's test. If the experimental groups did not show homogeneity of variances but had a normal distribution, Welch and Brown-Forsythe ANOVA was used. In all cases $p < 0.05$ was considered as statistically significant. Statistical comparisons between the experiment groups were performed with GraphPad Prism version 8.0.2 for Windows (GraphPad Software, San Diego, California USA).

4.3 Results

4.3.1 Surface characterization

4.3.1.1 *Surface Topography by SEM*

SEM micrographs showed the presence of HA particles (white dots) in the 10%HA, 15%HA, PT-10%HA and PT-15%HA groups, while smooth plain fibers were observed for the N and PT group (Figure 4.3). Application of plasma treatment to the 10%HA and 15%HA fabrics resulted in an increased amount of HA particles being exposed at the surface compared with non-plasma treated fibers of same composition. As a result, the surface roughness also increased due to the increased particles exposed at the surface (only microscopically observed and not quantified). No visible difference in amount of HA particles was microscopically observed between 10%HA and 15%HA. However, more HA particles seem to be exposed on the surface for the PT-15%HA compared with the PT-10%HA surfaces.

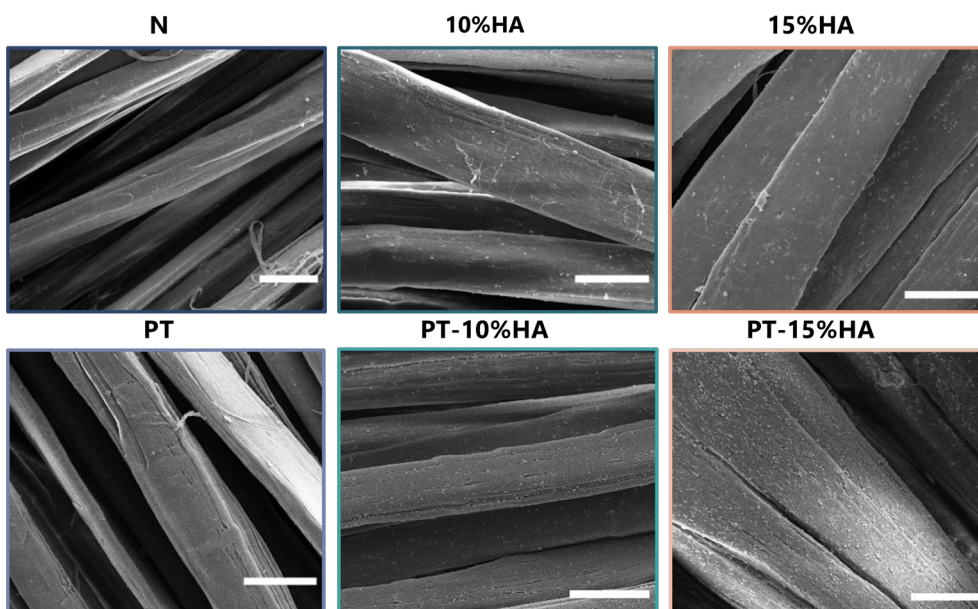


Figure 4.3: Surface characterization by SEM of the untreated (N), plasma treated (PT), 10%HA loaded (10%HA), plasma treated 10%HA loaded (PT-10%HA), 15% loaded and, plasma treated 15%HA loaded fabrics (PT-15%HA). Scale bar: 25 μ m

4.3.2 *In vitro biological response*

4.3.2.1 Cell attachment

Cell attachment was assessed to determine the affinity of hBMSCs to adhere to the material surface. Applying plasma treatment increased the mean initial amount of DNA and overall metabolic activity compared with the same fiber composition without plasma treatment (Figure 4.4, Day 2). However, only PT and PT-10%HA showed a significantly higher amount of DNA compared with the untreated group, while for the overall metabolic activity this held true for all plasma treated groups in comparison to the untreated fabrics. SEM images on day 2 (Figure 4.5) verified the attachment of cells on surfaces in all experimental groups. Adhered hBMSCs showed a similar flattened and spread morphology with numerous filopodia on all surfaces.

4.3.2.2 Cell metabolic activity and proliferation

The normalized metabolic activity on day 2 shows increased activity with the presence of HA particles in the fiber. When looking at the proliferation, over time, a large increase in DNA content and metabolic activity was observed for all groups (Figure 4.4, day 7 and 14). This is also verified with the increased cell density visible on SEM images on day 14 for all samples (Figure 4.5). On day 7, the effect of plasma treatment on increased DNA content and metabolic activity seemed to disappear. On day 14, also no significant difference in DNA content was observed. However, differences in metabolic activity were still present, showing increased mean metabolic activity (overall and normalized to DNA) with increasing HA content.

4.3.2.3 Osteogenic differentiation

ALP activity is often used as an osteoblastic differentiation marker in *in vitro* experiments [38]. At day 14, the HA loaded, and plasma treated fibers (PT-10%HA, PT-15%HA) showed significantly higher ALP activity per cell compared with both the untreated (N) and plasma treated (PT) group (Figure 4.6).

4.3.2.4 Extracellular matrix deposition

SEM images showed matrix deposition in all groups (Figure 4.5). EDX analysis also confirmed the presence of calcium and phosphorus elements, being the major components of calcium phosphate apatite, forming the mineral phase of bone (Figure 4.5). EDX was only used as a method to identify the elements of the nodules, not to evaluate the differences in weight percentage between the groups. However, more nodules containing calcium and phosphate were detected for the HA loaded fibers (10%HA, PT-10%HA, 15%HA and PT-15%HA) and PT group compared with the untreated group (N).

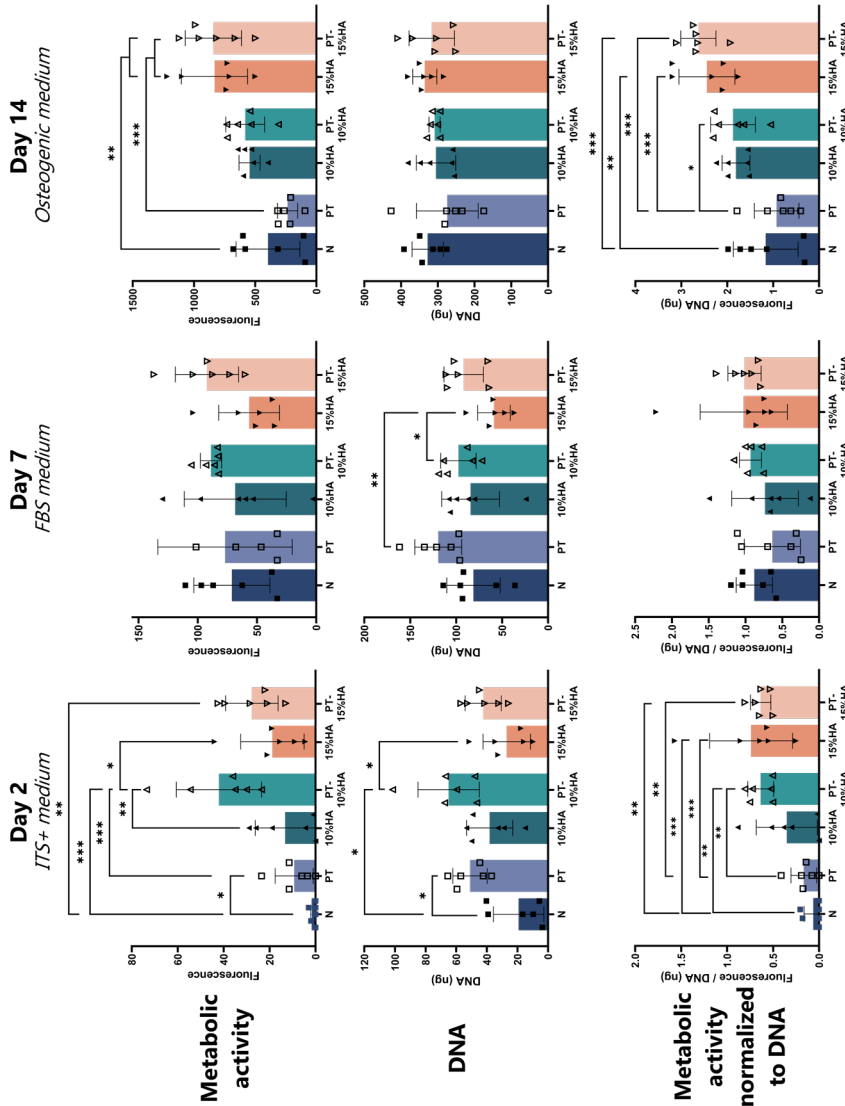


Figure 4.4: Metabolic activity (Fluorescence, mean \pm SD, One way ANOVA (* $p < 0.05$, ** $p < 0.01$, *** $p < 0.001$)) measured by PrestoBlue assay on day 2, 7 and 14. DNA content (ng, mean \pm SD, Brown-Forsythe and Welch ANOVA test (* $p < 0.05$, ** $p < 0.01$, *** $p < 0.001$)) on day 2 showing initial cell adherence and on day 7 and 14 to assess proliferation over time. Metabolic activity normalized for DNA content (fluorescence/ng, mean \pm SD, One way ANOVA ($p < 0.05$, ** $p < 0.01$, *** $p < 0.001$)) on day 2, 7 and 14.

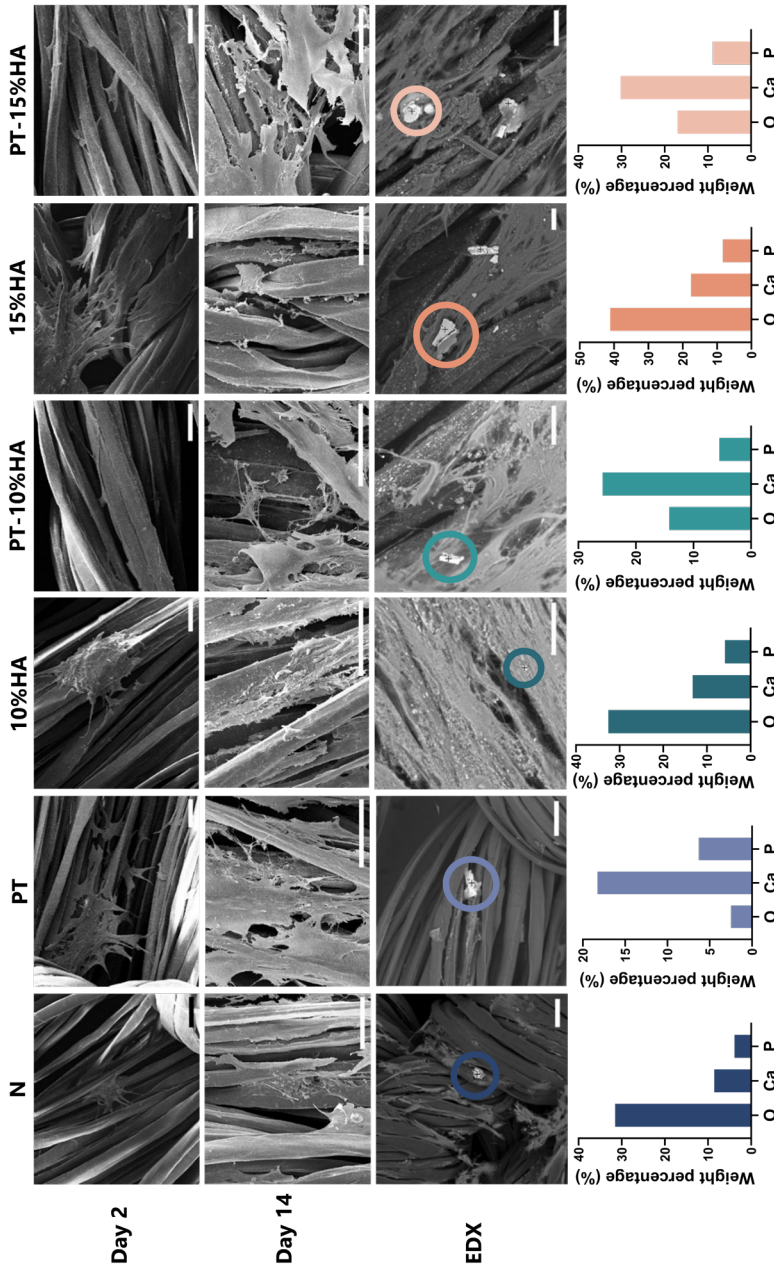


Figure 4.5: SEM images of the differently modified UHMWPE surfaces (N: untreated, PT: plasma treated, 10%HA: 10% hydroxyapatite loaded, PT-10%HA: plasma treated 10%HA loaded, 15%HA: 15% hydroxyapatite loaded, PT-15%HA: plasma treated 15%HA loaded) on day 2 to visualize cell adherence and cell morphology and on day 14 to show cell morphology and matrix deposition. Representative EDX spot analysis of matrix minerals for all groups on day 14 showing the elements of which the spots are composed of. Scale: 50 μ m.

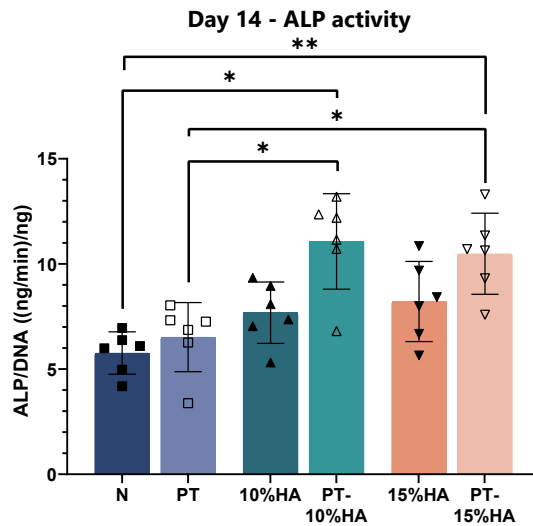


Figure 4.6: ALP activity normalized for DNA content as a marker for osteogenic differentiation ((ng/min)/ng, mean ± SD) on day 14. One way ANOVA (* $p < 0.05$, ** $p < 0.01$, *** $p < 0.001$).

4.4 Discussion

Osseointegration between an implant and the bone surface is of great importance to provide stability and distribute the load. Optimally, the surface of an implant should be able to facilitate bone in-growth to avoid risks of migration and loosening. However, the newly proposed bioAID uses an UHMWPE fiber surface at the bone implant interface, which, due to its inert chemical characteristics and hydrophobic nature, is less attractive for cells and proteins to attach and facilitate osseointegration [39]. Therefore, this study aimed to examine the effect of modifying the surface to increase the osteoconductive properties of UHMWPE by altering the hydrophilicity, chemical composition, and surface roughness.

Plasma treatment increased the hydrophilicity of the surface and led to a higher initial cell attachment compared with the untreated group. Multiple *in vitro* studies have reported similar favorable cellular response when seeded on hydrophilic surfaces compared with hydrophobic surfaces [18], [20], [40], [41]. Zhao et al. (2005) showed a more differentiated phenotype of MG63 osteoblast cells on sand blasted and acid etched titanium surfaces [41]. In another study of Yamamura et al. (2015) it was shown that super hydrophilic treatments of titanium implants increased initial cell attachment, proliferation, and differentiation of MC3T3 osteoblast-like cells [18]. Similarly, Vrekhem et al. (2015) found that plasma treatment of UHMWPE surfaces led to enhanced MC3T3 osteoblast attachment and proliferation [40]. This view is also

supported by Poulsson et al. (2009) who showed that human primary osteoblast-like cells attached and proliferated more on UV/ozone treated UHMWPE surfaces compared with untreated surfaces [11]. However, in the current study, plasma treatment alone did not increase the ALP activity, which is an often-used marker for early-stage osteoblast differentiation [38]. This indicates that only increasing the hydrophilicity of the surface might not be sufficient to support differentiation towards the osteoblastic lineage. Although previous studies have shown increased osteogenic differentiation responses for hydrophilic surfaces, these studies mainly used osteoblast-like cells from several species which already exhibit osteoblastic markers [11], [18], [20], [40], [41]. Therefore, it could be argued that further differentiation *in vitro* can be stimulated more easily by hydrophilicity, while for hBMSCs as used here first an osteoinductive stimulus may also be needed [42]. Osteogenic supplements, being β -glycerolphosphate, dexamethasone and ascorbic acid, are known to have an osteoinductive effect, however, in this study, these were only added to the medium on day 7. It is generally assumed that MSCs supplemented with osteogenic medium need approximately 14 days to reach the peak in ALP activity, marking the progression of differentiation into the osteoblastic lineage [43]. Moreover, the rate and extent of osteoblast differentiation initiated by these osteogenic supplements is dependent on the cell density, which could have been different on day 7 when these were added. It should also be noted that *in vivo*, where this material is intended to be implanted, both osteoblasts and hBMSCs will be present [44].

Besides plasma treatment, incorporation of hydroxyapatite alone also did not result in significant changes in cell attachment and proliferation. It was expected that the incorporation of HA into the fibers would have a dual effect. On one hand, *in vivo* and *in vitro* literature has shown that HA can stimulate osteogenic differentiation by either its geometry, chemical similarities to bone or release of HA ions in the medium [15], [45], [46]. On the other hand, incorporation of HA particles into the fiber has led to an increased surface roughness which has also been suggested to be an important factor influencing cellular behavior by acting as an anchor for cellular adhesion [16], [47], [48]. Deligianni et al. (2000) showed that an increased surface roughness on HA discs led to increased cell adhesion, proliferation, and detachment strength [47]. Likewise, Gittens et al. (2011) found that nano and micro scale roughness on titanium substrates improved osteoblast differentiation [48]. Only few studies have investigated the osteoconductivity of UHMWPE/HA composites *in vitro*, and mainly as bulk materials, showing a beneficial osteoconductive effect of adding HA compared with pure UHMWPE [49]–[53]. Mirsalehi et al. (2016) found that UHMWPE/HA composites with increasing weight percentage of HA resulted in enhanced proliferation and differentiation of MG63 cells [50]. Hermán et al. (2015) found a similar trend showing increased initial cell attachment and highest ALP activity for UHMWPE/HA composite with highest (20%) weight

percentage HA [51]. The results in this study did not show an increased cell attachment and ALP activity for samples with HA, but the data did show increasing metabolic activity with increased HA content for both day 2 and day 14. This gives information on which surface cells are more active, for example forming extracellular matrix, but does not indicate to which type of activity. Based on data of cell attachment and ALP activity alone, the current results seem to suggest that the hydrophobic and inert nature of the UHMWPE has a more dominant effect on the cellular response for non-plasma treated groups. It seems that loading either 10% or 15%HA into the fiber is not sufficient to increase cell attachment and to promote osteogenic differentiation. As also seen by SEM images, loading 10 wt.% or 15 wt.% HA into the fiber only leads to approximately 3-5 wt.% HA exposed at surface, the rest is embedded in the bulk of the fiber [36]. Therefore, the large polymer surface could interfere with cell attachment. Habibovic et al. (2005 and 2006) also postulated that there is an optimal amount of osteoconductive surface area needed to facilitate bone growth [27], [54]. Another explanation for this discrepancy could be that crystalline HA as used here is the most stable and least soluble ceramic. As a result, crystalline HA can function as an anchor for cells but does not allow for a large increase of calcium and phosphate in surrounding medium to attract cells [50], [55]. Moreover, it is generally stated that HA increases protein adsorption from fetal bovine serum such as fibronectin and vitronectin onto the surface, which facilitates cell attachment [56], [57]. In this study, fetal bovine serum was not added in the medium during the first 2 days of culture. Previous research has shown that in absence of an adsorbed protein layer, HA is a poor substrate for initial cell adhesion and cell spreading [58], [59]. Verdanova et al. (2017) reported that in absence of FBS the cells adhere without use of classical focal adhesions that use proteins to anchor them to the surface [57]. It is hypothesized by Verdanova et al. (2017) that cell-surface contact in absence of FBS is mainly mediated by non-specific interactions such as van der Waals bonds, hydrogen bonding or charged interactions between polar groups. This might explain the lack of increased cell attachment for 10%HA and 15%HA samples compared with untreated samples, having mainly hydrophobic surfaces. This seems to confirm that surface hydrophilicity because of the plasma treatment has a larger effect on facilitating cell attachment and subsequent cellular processes than only including HA. Nevertheless, it should be noted that cells in absence of serum proteins absorbed from FBS, will synthesize their own matrix to facilitate cell attachment.

Only the groups that contained HA loaded fibers and were plasma treated resulted in both increased cell attachment and upregulated ALP activity. This indicates a dual effect of applying plasma treatment on the HA containing fabrics, resulting in increased hydrophilicity, more HA particles being exposed at the surface (as also confirmed with SEM) and therefore also

increased surface roughness. Blatt et al. (2018) also found that increasing both surface roughness and hydrophilicity leads to an enhanced effect [16].

The increased number of cells and metabolic activity present for PT-HA groups at day 2 in comparison with non-plasma treated groups disappeared over time when comparing it with data from day 7 and 14. It is hypothesized that this is mainly related to the addition of medium supplements which alter the biological and chemical environment of the cells. It has been stated before in literature that the proliferation and differentiation behavior of hBMSCs is affected by the addition of fetal bovine serum (FBS) resulting in increased proliferation, while β -glycerolphosphate, dexamethasone and ascorbic acid can stimulate differentiation towards osteoblastic lineage and mineralization [60], [61]. Addition of FBS on day 2 indeed resulted in increased cell proliferation for all groups on day 7. It is generally known that FBS stimulates proliferation, and that fibronectin and vitronectin present in FBS can result in a more appealing surface for cells to adhere, which might explain why the DNA content and metabolic activity became more similar between the groups on day 7 and 14. Schakenraad et al. (1986) also found that serum protein coating masks the original surface characteristics, resulting in similar cell spreading and cell growth on different materials [62]. The addition of osteogenic supplements from day 7 onwards resulted in even more proliferation and thus higher DNA content on day 14. It is generally known that proliferation is related to the synthesis of extracellular matrix, confluency, and cell differentiation. High confluency leads to reduced proliferation and vice versa. Accumulation and maturation of the extracellular matrix results in cells being trapped and embedded, leading to reduced proliferation and increased differentiation. *In vivo*, this is all tightly regulated by cellular and molecular mechanisms to maintain homeostasis [63]. *In vitro*, experimental design decisions, such as initial cell seeding density, are important factors influencing cellular behavior [61], [64]. In this study, only 20,000 cells in a minimal volume of 50 μ l were seeded per fabric due to the hydrophobic nature of pure UHMWPE, corresponding to a concentration of 28,000 cells/cm². Cell seeding density can influence cell-cell distance and thereby paracrine signaling that controls cell proliferation and osteogenic differentiation. Previous research has shown that a low cell seeding density led to increased cell proliferation because there is no risk of contact inhibition [64], [65]. The low cell seeding density used could explain the continuous proliferation seen until day 14. Moreover, it might explain the similar amounts of DNA for all experimental groups on day 14, where the non-plasma treated groups are highly proliferative due to low cell seeding combined with the lower initial cell attachment and thus lower confluency compared with plasma treated samples.

Altogether, it can be concluded that both plasma treatment and incorporation of HA had a positive effect on the osteoconductive potential of the surface. However, a direct relationship between the surface chemistry or topography on cellular behavior is difficult to determine. It is often an interplay between multiple factors that leads to the observed cellular behavior which also makes comparisons with previous studies difficult due to differences in used material, topography, applied culture condition and cell source when using primary cells. To elucidate the role of each surface modification on the increased osteoconductive nature of the surface, quantification of extracellular matrix production and verification of osteoblast differentiation should be expanded.

In this study, it is unlikely that the cells have fully differentiated towards osteoblasts since the DNA content increased over the culture period for all experimental groups while osteoblast differentiation is often coupled with a decrease in cell proliferation [66]. Moreover, ALP activity can be upregulated on rough surfaces independent of osteoblast differentiation, and it is an early-stage osteoblast marker which is less expressed in mature osteoblasts [38]. Therefore, to gain more insight on the differentiation of hBMSCs towards the osteoblastic phenotype on the different altered surfaces, increased culture period and upregulation of osteoblast markers such as osteocalcin could be identified with for example immunohistochemistry or PCR analysis. On the other hand, such true bone formation may be better evaluated with *in vivo* implantations.

EDX was used to verify the presence of calcium and phosphorus elements, which are the major components of calcium phosphate apatite, forming the mineral phase of bone. Results showed presence of calcium and phosphorus for all experimental groups. However, EDX is a semiquantitative technique, which can only confirm presence of elements but cannot be used to compare mineral densities. Thus, although more calcium and phosphorus containing spots were detected for PT and/or HA containing groups (not shown), this method cannot elucidate which surface treatment resulted in more mineralization. It is also important to bear in mind that some of the fibers used in this study already contain HA and the addition of β -glycerolphosphate can induce non-specific mineral deposition, making the distinction and quantification of cell-deposited mineralization difficult. To minimize this limitation, only spots in proximity of cells were assumed as cell deposited minerals. As previously mentioned, an increased metabolic activity was measured with increasing HA content that could indicate actively bone depositing cells. Hence, to develop a full picture of the matrix deposition, additional assays that identify collagen synthesis, such as histology, could be valuable.

Since the focus of this study was on the osteoconductive potential of the surface modifications, no extensive surface characterization was included. Nevertheless, an extensive surface characterization was performed on similar fibers as described in the patent publication of Dias et al. (2021) [36]. Results confirmed the presence of HA particles with FTIR-ATR (Fourier transform infrared – attenuated total reflection) spectroscopy and showed that an increase of HA particles increased the roughness, as measured by the yarn-to-yarn coefficient of friction. The patent also describes the effect of the plasma treatment through Atomic Force Microscopy (AFM) and SEM/EDX analysis, verifying the increase of exposed HA particles (3% of area is Ca and Phosphate for 15%HA compared to 16 % for PT-15%HA) and surface roughness. In this study, SEM analysis of the different surfaces also visualize the different densities of HA particles for the different experimental groups, showing the altered roughness. For porous materials it is very difficult to perform contact angle measurements to quantify the hydrophilicity, while it is generally stated that nonporous materials are less capable of providing osteoconductivity [27]. However, addition of medium to the samples clearly visualized the hydrophobic nature of non-plasma treated surface showing droplet formation, and hydrophilic nature of plasma treated samples immediately absorbing the fluid.

In vitro cell culture studies are used to gain insight into cell adhesion, proliferation, and differentiation on implant surfaces. These parameters are valuable initial indicators for the osteoconductive performance of biomaterials *in vivo* [23]. Therefore, this study is useful as initial biological screening of these different surfaces to exclude certain surface modifications and thus reduce the number of *in vivo* experiments. It can, however, not be fully translated to *in vivo* performance. *In vivo* the surface is exposed to heterogenous cell populations, much more complex surrounding fluid and a more representative loading environment. Animal studies remain valuable to provide more accurate data on the dynamics of bone growth on the surface.

4.5 Conclusion

Altogether, the current study shows that incorporating HA in UHMWPE fiber together with plasma treatment provides a surface that allows for cell attachment and supports hBMSCs differentiation towards osteoblasts, thereby increasing the osteoconductive potential of the surface compared with untreated UHMWPE fabrics. These findings suggest that this surface modification would be promising for facilitating bone ingrowth on the cranial and caudal surfaces of the bioAID or for any other orthopedic application using UHMWPE fiber at the bone-implant interface.

Acknowledgements

This publication is part of the project BioAID with project number 16314 of the research program AES Open Technology Program, partly financed by the Dutch Research Council (NWO). We are grateful to DSM Biomedical for providing the different materials used in this publication. Data is available on request from the authors.

References

- [1] A. G. Patwardhan and R. M. Havey, "Prosthesis design influences segmental contribution to total cervical motion after cervical disc arthroplasty," *Eur. Spine J.*, Jul. 2019.
- [2] K. R. Chin, F. J. R. Pencle, L. S. Mustafa, M. S. Mustafa, K. A. Quijada, and J. A. Seale, "Incidence of Fusion Across Total Disc Replacement with Heterotopic Ossification: Are Ball and Socket Disk Replacements Fusing with and Without Radiographic Evidence," *Clin. Spine Surg.*, vol. 32, no. 10, pp. E469–E473, Dec. 2019.
- [3] A. Gloria, T. Russo, U. D'Amora, M. Santin, R. De Santis, and L. Ambrosio, "Customised multiphasic nucleus/annulus scaffold for intervertebral disc repair/regeneration," *Connect. Tissue Res.*, vol. 61, no. 2, pp. 152–162, 2020.
- [4] A. Gloria, R. De Santis, L. Ambrosio, F. Causa, and K. E. Tanner, "A multi-component fiber-reinforced PHEMA-based hydrogel/HAPEXTM device for customized intervertebral disc prosthesis," *J. Biomater. Appl.*, vol. 25, no. 8, pp. 795–810, May 2011.
- [5] A. Gloria, F. Causa, R. De Santis, P. A. Netti, and L. Ambrosio, "Dynamic-mechanical properties of a novel composite intervertebral disc prosthesis," *J. Mater. Sci. Mater. Med.*, vol. 18, no. 11, pp. 2159–2165, Nov. 2007.
- [6] Y. Shikinami, Y. Kotani, B. W. Cunningham, K. Abumi, and K. Kaneda, "A Biomimetic Artificial Disc with Improved Mechanical Properties Compared to Biological Intervertebral Discs," *Adv. Funct. Mater.*, vol. 14, no. 11, pp. 1039–1046, Nov. 2004.
- [7] P. R. Van Den Broek, "Development of a biomimetic artificial intervertebral disc," Eindhoven University of Technology, 2012.
- [8] P. R. Van Den Broek, J. M. Huyghe, and K. Ito, "Biomechanical behavior of a biomimetic artificial intervertebral disc," *Spine (Phila. Pa. 1976)*, vol. 37, no. 6, pp. E367-73, Mar. 2012.
- [9] P. R. van den Broek, J. M. Huyghe, W. Wilson, and K. Ito, "Design of next generation total disk replacements," *J. Biomech.*, vol. 45, no. 1, pp. 134–140, Jan. 2012.
- [10] Z. Ozbek, E. Ozkara, and A. Arslantaş, "Implant Migration in Cervical Disk Arthroplasty," *World Neurosurg.*, vol. 97, pp. 390–397, Jan. 2017.
- [11] A. H. C. Poulsson, S. A. Mitchell, M. R. Davidson, A. J. Johnstone, N. Emmison, and R. H. Bradley, "Attachment of human primary osteoblast cells to modified polyethylene surfaces," *Langmuir*, vol. 25, no. 6, pp. 3718–3727, 2009.
- [12] K. P. Nobles, A. V. Janorkar, and R. S. Williamson, "Surface modifications to enhance osseointegration—Resulting material properties and biological responses," *Journal of Biomedical Materials Research*, vol. 109, no. 11, pp. 1909–1923, 2021.
- [13] Y. Liu et al., "MiR-181d-5p regulates implant surface roughness-induced osteogenic differentiation of bone marrow stem cells," *Mater. Sci. Eng. C*, vol. 121, p. 111801, Feb. 2021.
- [14] M. F. Sola-Ruiz, C. Perez-Martinez, C. Labaig-Rueda, C. Carda, and J. J. Martín De Llano, "Behavior of human osteoblast cells cultured on titanium discs in relation to surface roughness and presence of melatonin," *Int. J. Mol. Sci.*, vol. 18, no. 4, Apr. 2017.
- [15] M. Lukaszewska-Kuska, P. Wirstlein, R. Majchrowski, and B. Dorocka-Bobkowska, "Osteoblastic cell behaviour on modified titanium surfaces," *Micron*, vol. 105, no. November 2017, pp. 55–63, 2018.
- [16] S. Blatt et al., "Early cell response of osteogenic cells on differently modified implant surfaces: Sequences of cell proliferation, adherence and differentiation," *J. Cranio-Maxillofacial Surg.*, vol. 46, no. 3, pp. 453–460, Mar. 2018.
- [17] S. E. More et al., "Surface modification of UHMWPE using ECR plasma for osteoblast and osteoclast differentiation," *Appl. Surf. Sci.*, vol. 506, p. 144665, Nov. 2019.
- [18] K. Yamamura, T. Miura, I. Kou, T. Muramatsu, M. Furusawa, and M. Yoshinari, "Influence of various superhydrophilic treatments of titanium on the initial attachment, proliferation, and differentiation of osteoblast-like cells," *Dent. Mater. J.*, vol. 34, no. 1, pp. 120–127, 2015.

- [19] A. Wennerberg, R. Jimbo, S. Stübinger, M. Obrecht, M. Dard, and S. Berner, "Nanostructures and hydrophilicity influence osseointegration: A biomechanical study in the rabbit tibia," *Clin. Oral Implants Res.*, vol. 25, no. 9, pp. 1041–1050, 2014.
- [20] S. Van Vrekhem et al., "Improving the surface properties of an UHMWPE shoulder implant with an atmospheric pressure plasma jet," *Sci. Rep.*, vol. 8, p. 4720, Dec. 2018.
- [21] P. Cools, S. Van Vrekhem, N. De Geyter, and R. Morent, "The use of DBD plasma treatment and polymerization for the enhancement of biomedical UHMWPE," *Thin Solid Films*, vol. 572, pp. 251–259, 2014.
- [22] A. Elyada, N. Garti, and H. Füredi-Milhofer, "Polyelectrolyte multilayer-calcium phosphate composite coatings for metal implants," *Biomacromolecules*, vol. 15, no. 10, pp. 3511–3521, Oct. 2014.
- [23] R. A. Surmenev, M. A. Surmeneva, and A. A. Ivanova, "Significance of calcium phosphate coatings for the enhancement of new bone osteogenesis - A review," *Acta Biomater.*, vol. 10, no. 2, pp. 557–579, 2014.
- [24] C. Zhu et al., "Titanium-interlayer mediated hydroxyapatite coating on polyetheretherketone: a prospective study in patients with single-level cervical degenerative disc disease," *J. Transl. Med.*, vol. 19, no. 1, Dec. 2021.
- [25] J. H. Lee, H. L. Jang, K. M. Lee, H. R. Baek, K. Jin, and J. H. Noh, "Cold-spray coating of hydroxyapatite on a three-dimensional polyetheretherketone implant and its biocompatibility evaluated by *in vitro* and *in vivo* minipig model," *J. Biomed. Mater. Res. - Part B Appl. Biomater.*, vol. 105B, no. 3, pp. 647–657, Apr. 2017.
- [26] R. Junker, A. Dimakis, M. Thoneick, and J. A. Jansen, "Effects of implant surface coatings and composition on bone integration: A systematic review," *Clinical Oral Implants Research*, vol. 20, no. SUPPL. 4. John Wiley & Sons, Ltd, pp. 185–206, Sep-2009.
- [27] P. Habibovic, T. M. Sees, M. A. Van Den Doel, C. A. Van Blitterswijk, and K. De Groot, "Osteoinduction by biomaterials - Physicochemical and structural influences," *J. Biomed. Mater. Res. - Part A*, vol. 77, no. 4, pp. 747–762, Jun. 2006.
- [28] F. Senatov et al., "Osseointegration evaluation of UHMWPE and PEEK-based scaffolds with BMP-2 using model of critical-size cranial defect in mice and push-out test," *J. Mech. Behav. Biomed. Mater.*, vol. 119, p. 104477, Jul. 2021.
- [29] H. Li and S. Chen, "Biomedical coatings on polyethylene terephthalate artificial ligaments," *J. Biomed. Mater. Res. - Part A*, vol. 103, no. 2, pp. 839–845, Feb. 2015.
- [30] G. C. Causey, G. J. Picha, J. Price, M. H. Pelletier, T. Wang, and W. R. Walsh, "The effect of a novel pillar surface morphology and material composition demonstrates uniform osseointegration," *J. Mech. Behav. Biomed. Mater.*, vol. 123, no. May, 2021.
- [31] Y. Kotani et al., "Artificial Intervertebral Disc Replacement Using Bioactive Three-Dimensional Fabric," *Spine (Phila. Pa. 1976)*, vol. 27, no. 9, pp. 929–935, May 2002.
- [32] M. Takahata et al., "Bone Ingrowth Fixation of Artificial Intervertebral Disc Consisting of Bioceramic-Coated Three-dimensional Fabric," *Spine (Phila. Pa. 1976)*, vol. 28, no. 7, pp. 637–644, Apr. 2003.
- [33] K. Kadoya et al., "Biomechanical and Morphologic Evaluation of a Three-Dimensional Fabric Sheep Artificial Intervertebral Disc," *Spine (Phila. Pa. 1976)*, vol. 26, no. 14, pp. 1562–1569, Jul. 2001.
- [34] M. Hasegawa, A. Sudo, Y. Shikinami, and A. Uchida, "Biological performance of a three-dimensional fabric as artificial cartilage in the repair of large osteochondral defects in rabbit," *Biomaterials*, vol. 20, no. 20, pp. 1969–1975, Oct. 1999.
- [35] Y. Shikinami and H. Kawarada, "Potential application of a triaxial three-dimensional fabric (3-DF) as an implant," *Biomaterials*, vol. 19, no. 7–9, pp. 617–635, Apr. 1998.
- [36] A. A. Dias, N. L. Davison, A. M. Persson, Y. Mengerik, and P. M. De Bueger, "Osteoconductive fibers, Medical Implants comprising such osteoconductive fibers and methods of making US

- Patent 2021/0299332 A1," 2021.
- [37] S. Hofmann et al., "Control of *in vitro* tissue-engineered bone-like structures using human mesenchymal stem cells and porous silk scaffolds," *Biomaterials*, vol. 28, no. 6, pp. 1152–1162, Feb. 2007.
- [38] S. Vimalraj, "Alkaline phosphatase: Structure, expression and its function in bone mineralization," *Gene*, vol. 754, p. 1448, Sep. 2020.
- [39] R. Vaishya, A. K. Agarwal, M. Tiwari, A. Vaish, V. Vijay, and Y. Nigam, "Medical textiles in orthopedics: An overview," *J. Clin. Orthop. Trauma*, vol. 9S, pp. S26–S33, Mar. 2018.
- [40] S. Van Vrekhem et al., "Application of atmospheric pressure plasma on polyethylene for increased prosthesis adhesion," *Thin Solid Films*, vol. 596, pp. 256–263, Dec. 2015.
- [41] G. Zhao et al., "High surface energy enhances cell response to titanium substrate microstructure," *J. Biomed. Mater. Res. - Part A*, vol. 74, no. 1, pp. 49–58, Jul. 2005.
- [42] K. Anselme and M. Bigerelle, "Role of materials surface topography on mammalian cell response," *International Materials Reviews*, vol. 56, no. 4, pp. 243–266, Jul-2011.
- [43] E. Castrén et al., "Osteogenic differentiation of mesenchymal stromal cells in two-dimensional and three-dimensional cultures without animal serum," *Stem Cell Res. Ther.*, vol. 6, no. 1, p. 167, Dec. 2015.
- [44] J. M. Kim, C. Lin, Z. Stavre, M. B. Greenblatt, and J. H. Shim, "Osteoblast-Osteoclast Communication and Bone Homeostasis," *Cells*, vol. 9, no. 9, p. 2073, Sep. 2020.
- [45] Y. Cai et al., "Accelerated bone growth *in vitro* by the conjugation of BMP2 peptide with hydroxyapatite on titanium alloy," *Colloids Surfaces B Biointerfaces*, vol. 116, pp. 681–686, Apr. 2014.
- [46] M. Roy, A. Bandyopadhyay, and S. Bose, "Induction plasma sprayed nano hydroxyapatite coatings on titanium for orthopaedic and dental implants," *Surf. Coatings Technol.*, vol. 205, no. 8–9, pp. 2785–2792, Jan. 2011.
- [47] D. D. Deligianni, N. D. Katsala, P. G. Koutsoukos, and Y. F. Missirlis, "Effect of surface roughness of hydroxyapatite on human bone marrow cell adhesion, proliferation, differentiation and detachment strength," *Biomaterials*, vol. 22, no. 1, pp. 87–96, Jan. 2000.
- [48] R. A. Gittens et al., "The effects of combined micron-/submicron-scale surface roughness and nanoscale features on cell proliferation and differentiation," *Biomaterials*, vol. 32, no. 13, pp. 3395–3403, May 2011.
- [49] D. L. P. Macuvelo et al., "Advances in ultra high molecular weight polyethylene/hydroxyapatite composites for biomedical applications: A brief review," *Mater. Sci. Eng. C*, vol. 76, pp. 1248–1262, 2017.
- [50] S. A. Mirsalehi, M. Sattari, A. Khavandi, S. Mirdamadi, and M. R. Naimi-Jamal, "Tensile and biocompatibility properties of synthesized nano-hydroxyapatite reinforced ultrahigh molecular weight polyethylene nanocomposite," *J. Compos. Mater.*, vol. 50, no. 13, pp. 1725–1737, 2016.
- [51] V. Hermán et al., "Biocompatibility studies of HDPE–HA composites with different HA content," *Polym. Bull.*, vol. 72, no. 12, pp. 3083–3095, Dec. 2015.
- [52] F. Senatov et al., "Biomimetic UHMWPE/HA scaffolds with rhBMP-2 and erythropoietin for reconstructive surgery," *Mater. Sci. Eng. C*, vol. 111, p. 110750, Jun. 2020.
- [53] Y. F. Huang, J. Z. Xu, D. Zhou, L. Xu, B. Zhao, and Z. M. Li, "Simultaneous reinforcement and toughening of polymer/hydroxyapatite composites by constructing bone-like structure," *Compos. Sci. Technol.*, vol. 151, pp. 234–242, Oct. 2017.
- [54] P. Habibovic, H. Yuan, C. M. Van Der Valk, G. Meijer, C. A. Van Blitterswijk, and K. De Groot, "3D microenvironment as essential element for osteoinduction by biomaterials," *Biomaterials*, vol. 26, no. 17, pp. 3565–3575, Jun. 2005.
- [55] Q. Hu et al., "Effect of crystallinity of calcium phosphate nanoparticles on adhesion, proliferation, and differentiation of bone marrow mesenchymal stem cells," *J. Mater. Chem.*, vol. 17, no. 44, pp. 4690–4698, Nov. 2007.

- [56] S. Vohra, K. M. Hennessy, A. A. Sawyer, Y. Zhuo, and S. L. Bellis, "Comparison of mesenchymal stem cell and osteosarcoma cell adhesion to hydroxyapatite," *J. Mater. Sci. Mater. Med.*, vol. 19, no. 12, pp. 3567–3574, Dec. 2008.
- [57] M. Verdanova, P. Sauerova, U. Hempel, and M. H. Kalbacova, "Initial cell adhesion of three cell types in the presence and absence of serum proteins," *Histochem. Cell Biol.*, vol. 148, no. 3, pp. 273–288, Sep. 2017.
- [58] A. A. Sawyer, K. M. Hennessy, and S. L. Bellis, "Regulation of mesenchymal stem cell attachment and spreading on hydroxyapatite by RGD peptides and adsorbed serum proteins," *Biomaterials*, vol. 26, no. 13, pp. 1467–1475, May 2005.
- [59] A. A. Sawyer, K. M. Hennessy, and S. L. Bellis, "The effect of adsorbed serum proteins, RGD and proteoglycan-binding peptides on the adhesion of mesenchymal stem cells to hydroxyapatite," *Biomaterials*, vol. 28, no. 3, pp. 383–392, Jan. 2007.
- [60] M. J. Coelho and M. H. Fernandes, "Human bone cell cultures in biocompatibility testing. Part II: Effect of ascorbic acid, β -glycerophosphate and dexamethasone on osteoblastic differentiation," *Biomaterials*, vol. 21, no. 11, pp. 1095–1102, Jun. 2000.
- [61] M. A. Yassin et al., "Cell seeding density is a critical determinant for copolymer scaffolds-induced bone regeneration," *J. Biomed. Mater. Res. - Part A*, vol. 103, no. 11, pp. 3649–3658, Nov. 2015.
- [62] J. M. Schakenraad, H. J. Busscher, C. R. H. Wildevuur, and J. Arends, "The influence of substratum surface free energy on growth and spreading of human fibroblasts in the presence and absence of serum proteins," *J. Biomed. Mater. Res.*, vol. 20, no. 6, pp. 773–784, Jul. 1986.
- [63] J. S. Kenkre and J. H. D. Bassett, "The bone remodelling cycle," *Annals of Clinical Biochemistry*, vol. 55, no. 3. SAGE Publications Ltd, pp. 308–327, 01-May-2018.
- [64] K. Kim, D. Dean, A. G. Mikos, and J. P. Fisher, "Effect of initial cell seeding density on early osteogenic signal expression of rat bone marrow stromal cells cultured on cross-linked poly(propylene fumarate) disks," *Biomacromolecules*, vol. 10, no. 7, pp. 1810–1817, Jul. 2009.
- [65] M. Bitar, R. A. Brown, V. Salih, A. G. Kidane, J. C. Knowles, and S. N. Nazhat, "Effect of cell density on osteoblastic differentiation and matrix degradation of biomimetic dense collagen scaffolds," *Biomacromolecules*, vol. 9, no. 1, pp. 129–135, 2008.
- [66] A. Bigi et al., "*In vitro* culture of mesenchymal cells onto nanocrystalline hydroxyapatite-coated Ti13Nb13Zr alloy," *J. Biomed. Mater. Res. - Part A*, vol. 82, no. 1, pp. 213–221, Jul. 2007.



Chapter 5

Biomechanical evaluation in canine cervical cadaveric spines

The contents of this chapter are based on:

C.A.M. Jacobs, R.J.P Doodkorte, S.A. Kamali, A.M. Abdelgawad, S. Ghazanfari, S. Jockenhoewel, J.J.C. Arts, M.A. Tryfonidou, B.P. Meij, K. Ito. Biomechanical evaluation of a novel biomimetic artificial intervertebral disc in canine cervical cadaveric spines. *JOR Spine*. p. 1-10, Feb. 2023

DOI: [10.1002/jsp2.1251](https://doi.org/10.1002/jsp2.1251)

Abstract

Cervical disc replacement (CDR) aims to restore motion of the treated level to reduce the risk of adjacent segment disease (ASD) compared with spinal fusion. However, first-generation articulating devices are unable to mimic the complex deformation kinematics of a natural disc. Thus, a biomimetic artificial intervertebral CDR (bioAID), containing a hydroxyethyl methacrylate (HEMA) – sodium methacrylate (NaMA) hydrogel core representing the nucleus pulposus, an ultra-high-molecular-weight-polyethylene fiber jacket as annulus fibrosus, and titanium endplates with pins for primary mechanical fixation, was developed. To assess the initial biomechanical effect of the bioAID on the kinematic behavior of the canine spine, an *ex vivo* biomechanical study in 6-degrees-of-freedom was performed.

Six cadaveric canine specimens (C3-C6) were tested in flexion-extension (FE), lateral bending (LB) and axial rotation (AR) using a spine tester in three conditions: intact, after C4-C5 disc replacement with bioAID, and after C4-C5 interbody fusion. A hybrid protocol was used where first the intact spines were subjected to a pure moment of ± 1 Nm, whereafter the treated spines were subjected to the full range of motion (ROM) of the intact condition. 3D segmental motions at all levels were measured while recording the reaction torsion. Biomechanical parameters studied included ROM, neutral zone (NZ), and intradiscal pressure (IDP) at the adjacent cranial level (C3-C4).

The bioAID retained the sigmoid shape of the moment-rotation curves with a NZ similar to the intact condition in LB and FE. Additionally, the normalized ROMs at the bioAID-treated level were not statistically different from intact during FE and AR while slightly decreased in LB. At the two adjacent levels, ROMs showed similar values for the intact compared to the bioAID for FE and AR and an increase in LB. In contrast, levels adjacent to the fused segment showed an increased motion in FE and LB as compensation for the loss of motion at the treated level. The IDP at the adjacent C3-C4 level after implantation of bioAID was close to intact values. After fusion, an increased IDP was found compared with intact but it did not reach statistical significance.

This study indicates that the bioAID can mimic the kinematic behavior of the replaced intervertebral disc and preserves that for the adjacent levels better than fusion. As a result, CDR using the novel bioAID is a promising alternative treatment for replacing severely degenerated intervertebral discs.

5.1 Introduction

Currently, the golden standard to treat severely degenerated intervertebral discs (IVDs) is anterior cervical discectomy and fusion (ACDF). ACDF has shown promising clinical results, but several limitations remain to fuse the vertebrae [1]–[7]. It is hypothesized that adjacent segments need to compensate for the altered loading pattern due to the loss of motion at the index level. Research has shown that 92% of patients showed radiographic degeneration of the adjacent segments five years post fusion surgery [8]. Other studies have reported different rates for the incidence of symptomatic adjacent segment disease (ASD). One study found the prevalence of symptomatic ASD in 6.2% of the cases after single level ACDF at different follow-up periods ranging between 5 and 15 years [9]. At 5 years follow-up, the rate of ASD after ACDF was found to be 10.9% [10]. On the other hand, Wu et al. (2019) only found 2.9% of the patients that needed a second surgery to treat ASD at 16 years follow-up [11]. As a result, cervical disc replacement (CDR) has been proposed as an alternative treatment that aims to restore motion of the treated spinal level to reduce the risk of adjacent segment pathology compared with fusion. Xie et al. (2016) compared data of 20 randomized controlled trials with a total of 4004 patients with a follow-up of two years; results indeed showed that CDR was statistically superior to ACDF in the development of adjacent segment disease (ASD) with a risk ratio of 0.62 and a 95% confidence interval (0.43, 0.88) [1]. This conclusion is supported by Wu et al. (2017) who also reported fewer rates of ASD in the CDR group compared to ACDF, although, according to the authors, based on relatively low-quality evidence [5]. Besides ASD, other clinical outcomes such as arm and neck pain, and patient satisfaction have also shown to be more favorable for CDR compared to ACDF [1], [3], [12], [13].

Despite these promising outcomes, first-generation articulating ball-and-socket disc replacements cannot mimic the complex deformational kinematics of natural IVDs [14]–[16]. The design of these first-generation prostheses is often derived from large synovial joint arthroplasties and thus is mainly based on sliding motions, whereas the natural IVD allows motion based on deformation [17], [18]. Previous research has shown that, a first-generation ball-and-socket implant could not reproduce the kinematic signature of an intact spinal segment, unlike a second-generation with a deformable viscoelastic component [18]. Another advantage of these second-generation devices is that these devices have a variable center of rotation (COR), therefore being less susceptible to correct positioning [19]–[21]. Although these second-generation devices are already an improvement when compared to first-generation devices, none of the currently available implants can mimic the osmotic swelling pressure known to be crucial for the biomechanical properties of the IVD tissue, needed to provide its compressive resistance [14], [17]. To better replicate the biomechanical properties of the natural IVD, a biomimetic artificial IVD (bioAID) was developed [22], [23]. This novel

prosthesis mimics a number of aspects of the native structure of the IVD and aims to mimic its biomechanical properties. The bioAID design contains a hydrogel core wrapped in a membrane, representing the contained gelatinous swelling nucleus pulposus, a stiff ultra-high-molecular-weight-polyethylene (UHMWPE) fiber jacket mimicking the tensile load-bearing of the annulus fibrosus, and a titanium endplate with pins to prevent initial device migration (Figure 5.1) [22]–[24]. The combination of the hydrogel wrapped with fiber jacket aims to imitate the properties of a natural IVD, like non-linear viscoelastic behavior, osmotic pressure resulting in pre-stress of fibers, creep, relaxation, and intradiscal pressure (IDP). Furthermore, it offers stability and shock absorbance while allowing semi-constrained motion based on deformation [22].

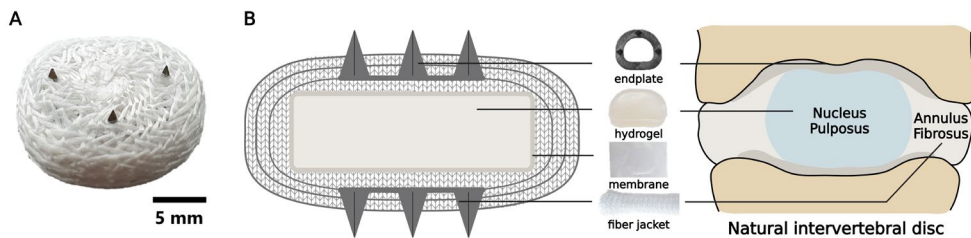


Figure 5.1: A: biomimetic artificial intervertebral disc (bioAID). B: schematic representation of the design of the bioAID and its biomimicry compared to a natural disc. Created with BioRender.com

Since the primary rationale of CDR is to preserve and restore the natural range of motion (ROM), it is of great importance to assess the bioAID's capability to restore the physiological kinematics of the spine. It is hypothesized that the biomimetic structure of the bioAID can maintain normal kinematics at the treated and adjacent levels, thereby minimizing the risk of adjacent segment pathologies in the long term. Therefore, this *ex vivo* biomechanical study in 6-degrees-of-freedom (6-DOF) was performed to assess the initial biomechanical effect of the bioAID on the kinematic behavior of the treated and adjacent canine cervical spine segments.

5.2 Materials & Methods

5.2.1 Device design

The first prototypes were developed for the lumbar spine, while clinical need, market size, interest of industry, and clinicians showed more feasibility for the cervical spine [22], [23]. As a consequence, the cervical bioAID prosthesis (21 x 14.5 x 5 mm) consisting of an ionized hydrogel surrounded by a membrane and three layers of fiber jacket was re-sized and re-designed (Figure 5.1). This was again resized for a canine model as cervical disc degeneration is also problematic in dogs and the size of the cervical vertebrae is not too different from small

humans. Moreover, a canine model will also be used later for *in vivo* proof-of-concept studies. Canine dimensions (14.5 x 13.5 x 4.5 mm) were determined based on CT scans of mixed breed dogs. The hydrogel was prepared by dissolving its components in ultra-pure water (Table 5.1). Next, a disc of polyurethane foam (diameter 10 cm x height 0.2 cm, MCF.03, Corpura B.V., Etten-Leur, The Netherlands) was soaked with the hydrogel solution and polymerized under UV light (UVP XX15L, 365 nm, Analytik Jena, Upland, CA USA) for two hours. It was subsequently heated to 45°C for 14 hours to complete polymerization. After polymerization, the hydrogel core (14 x 13 x 2 mm) was punched out. This hydrogel was sealed (thermal cutter, HSG-0, HSGM, Walluf, Germany) into an UHMWPE pouch (38 µm thick, 5 g/m², 0.9 µm pore, membrane, DSM Biomedical, Geleen, the Netherlands) to contain the hydrogel. A tube was warp-knitted (2x1 lapping, 8 stitch/cm, Centexbel, Grâce-Hollogne, Belgium) from multifilament UHMWPE yarn (Dyneema Purity[®] SGX, dtex110, TS 100, DSM Biomedical, Geleen, Netherlands). The core was then enclosed in 3 layers of this tubing and manually sewn closed with Dyneema purity[®] yarn to form an outer jacket. Before closure, a wire-eroded titanium endplate ring (9 x 8 x 0.3 mm) with 2 mm pins was placed above the innermost layer of the jacket, such that the pins protruded out of the jacket. Prior to implantation in the cadaveric spines, the bioAIDs were swollen under a 50N load in PBS (Dulbecco's Phosphate Buffered Saline, Sigma Aldrich) for seven days to reach swelling equilibrium and mimic the compressive load of a natural spine due to the weight of the head [25].

Table 5.1: Chemical components of the HEMA-NaMA hydrogel solution.

Components of the monomer solution	Function	Mol ratio	Weight (g)
Distilled water	Solvent	0.80	35.74
Sodium methacrylate 99% (NaMA)	Monomer	0.02	5.09
2-hydroxyethyl methacrylate 97% (HEMA)	Monomer	0.18	55.2
Poly (ethylene glycol) dimethacrylate, average molecular weight 550 nM	Cross-linker	0.00001	5.75
2,2' azobis (2-methylpropionamidine) dihydrochloride, 97%	Initiator	0.0001	0.054

5.2.2 Specimen preparation

Six fresh-frozen cadaveric cervical canine spines were obtained from donated animals of the Faculty of Veterinary Medicine, Utrecht University, the Netherlands that became available from unrelated experiments. The cadaveric cervical canine spines were thawed at room temperature, and all paraspinal musculature was removed while preserving the IVDs, facet joints, and ligaments. Radiographical screening was performed to exclude specimens with any spinal pathology. Thereafter, the spinal columns were wrapped in PBS-soaked gauzes and

stored overnight in the fridge. Two standard woodscrews were drilled in the cranial (C3) and caudal (C6) endplate to improve the embedding fixation. Next, the spine was vertically aligned using a line laser before embedding it in polymethylmethacrylate resin (Technovit 3040, Heraeus Kulzer GmbH, Wehrheim, Germany). During the experiment, the specimens were kept hydrated by applying PBS.

5.2.3 Biomechanical testing

The cadaveric canine specimens (C3-C6) were subjected to cyclic application ($1^\circ/\text{sec}$) of flexion-extension (FE), lateral bending (LB), and axial rotation (AR) in random order using an electronic 6-DOF spine testing system capable of applying unconstrained pure moments (Figure 5.2) (FS21; Applied Test Systems, Buttlar, PA, USA) [26]. Each spinal specimen was tested in three conditions: intact, after total disc replacement with the bioAID, and after fusion using an anchored cage (C-LOX, Rita Leibinger Medical, Muehlheim, Germany) at level C4-C5. A hybrid protocol was used where the intact spines were first subjected to a pure moment of ± 1 Nm for five cycles whereafter the instrumented spines were subjected to the full ROM of the intact condition [27].

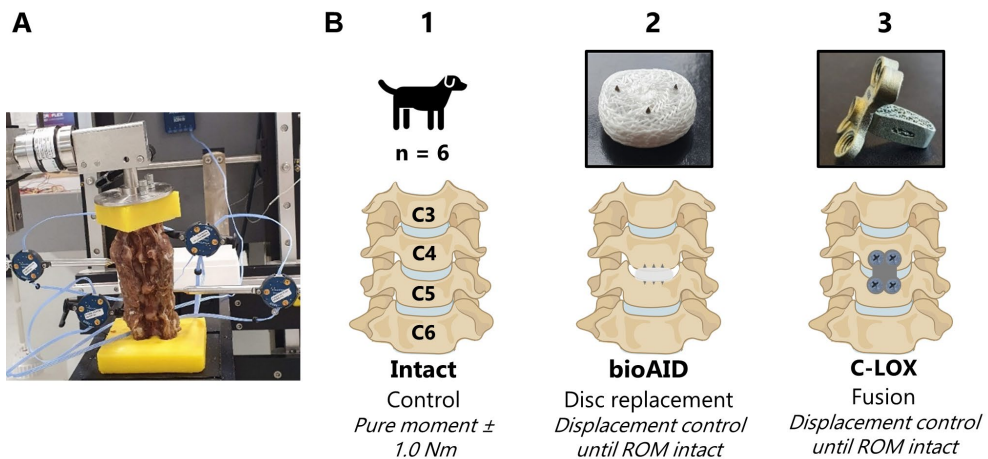


Figure 5.2: A: ventral (anterior in humans) view of intact cervical cadaveric canine spine embedded in polymethylmethacrylate resin including insertion of the triplet markers subjected to ± 1 Nm pure moment using a 6-DOF spine tester. B: schematic representation of the hybrid test protocol in the following three conditions: intact, after replacement of C4-C5 disc with bioAID, and after C4-C5 fusion using an anchored cage (C-LOX). ROM = range of motion. This figure was partly generated using Servier Medical Art, provided by Servier, licensed under a Creative Commons Attribution 3.0 unported license.

A moment of 1 Nm was selected because it is capable of producing physiologic motions without the risk of damaging spinal structures [28]. As a result of the low loads applied (± 1 Nm) and the flexibility of the cervical spine, the resistances present in the linear actuators on top of the actual weight of the sliding mechanisms could have influenced the natural coupling of motions. It is therefore important to bear in mind that the experimental protocol used in this study cannot fully replicate the *in vivo* motion behavior of the cervical spine. Motions of the individual vertebrae were obtained with triplet LED-markers rigidly fixed to each vertebra with custom-made pins and tracked using an optical registration system (Optotrak Certus, Northern Digital, Waterloo, Ontario, Canada). The data was automatically gathered by the spine tester software (FS21; Applied Test Systems, Buttlar, PA, USA) and segmental rotations were calculated using a custom-written algorithm based on Tait-Bryan angle sequence (MATLAB R2018b, MathWorks, Natick, MA, USA) [29]. Based on these calculations, data of the fourth cycle was used to determine the segmental ROM in all three degrees of freedom, defined as the difference in rotation at maximum and minimum load. Moment-Rotation curves were plotted and used to define the neutral zone (NZ), being the region of intervertebral motion around the neutral posture where there is the least resistance. The boundaries of the NZ were defined as the deflection points of compliance in the moment-rotation curves as described previously [30]. Data analysis was performed by a customized MATLAB (MathWorks, Natick, MA, USE) script.

5.2.4 Surgical procedure

After testing the intact specimens, the spines were subjected to a near-complete C4-C5 discectomy, removing the ventral (anterior in humans) annulus fibrosus and inner layers of the lateral and dorsal (posterior in humans) annulus but leaving the dorsal longitudinal ligament intact. Next, the cartilaginous endplates were scraped using a curette. Before implantation of the bioAID, (only 4 devices, so 2 spines were implanted with used implants) a custom-made trial guide was used to drill holes using 1 mm k-wires into the adjacent vertebral bodies matching the exact locations of the bioAID endplate pins. After testing the spinal specimens with the bioAID, the implant was removed. Next, a smooth trial guide was used to assess the appropriate size of the anchored cage (C-LOX, Rita Leibinger Medical, Muehlheim, Germany). The appropriate size cage with spikes was then attached to an insertion tool and hammered into the correct position within the disc space and fixated with four titanium locking screws before being tested with the spine tester.

5.2.5 *Intradiscal pressure*

A pressure measuring sensor (type CTN0 4F HP, Gaeltec Devices Ltd, Dunvegan, Isle of Skye, Scotland, UK) was positioned in the C3-C4 IVD to assess changes in IDP of intact compared to treated spines. A 1.2 mm-diameter needle was manually pushed through the ventral (anterior in humans) annulus fibrosus into the center of the nucleus pulposus. The needle was removed, and the pressure transducer needle was inserted into the created channel. During the loading cycles, the voltage outputs of the pressure sensor were recorded continuously using a universal amplifier (MPAQ, IDEE/Maastricht Instruments, Maastricht, The Netherlands). Peak pressures of the fourth loading cycle were reported.

5.2.6 *Statistical analysis*

ROM and NZ data were normalized to the intact condition to account for differences between specimens. Mean values and standard deviation were calculated for each parameter. Comparisons between experimental groups of ROMs, NZ, and IDP data were determined by repeated measures ANOVA (with Geisser-Greenhouse correction since multiple measurements over time were performed), or mixed effect analysis when there were missing values, followed by Tukey's honest post-hoc analysis (GraphPad Prism version 8.0.2 for Windows, San Diego, California USA). Normal distribution was evaluated using quantile-quantile plots. In all cases $p < 0.05$ was defined as a statistically significant difference.

5.3 Results

5.3.1 *Segmental ROM*

The bioAID provided similar ROM compared with the intact segment during FE (105 ± 14 % of intact) at the treated level (Figure 5.3 and Table 5.2). In AR, an increase in mean ROM was observed at C4-C5, showing 249 ± 154 % of the intact ROM after disc replacement with the bioAID. Also at the adjacent levels, the ROM was preserved and not significantly different from intact after replacement with the bioAID for both FE (C3-C4, 95 ± 8 % of intact; C5-C6, 94 ± 9 % of intact) and AR (C3-C4, 122 ± 57 % of intact; C5-C6, 76 ± 22 % of intact). During LB, 84 ± 6 % of the intact ROM was found at level C4-C5 for the bioAID, being significantly lower than the intact condition. The reduced motion at the treated level led to increased motion at the adjacent levels (C3-C4, 111 ± 9 % of intact; C5-C6, 108 ± 5 % of intact).

In contrast to replacing the IVD with the bioAID, fusing the spine at level C4-C5 led to a significant loss of motion in FE (17 ± 8 % of intact) and LB (18 ± 5 % of intact). In direct relation to this loss of motion at the treated level, levels adjacent to fused segments showed a significantly increased motion in FE (C3-C4, 133 ± 6 % of intact; C5-C6, 132 ± 6 % of intact)

and LB (C3-C4, $111 \pm 9\%$, and C5-C6 ($129 \pm 5\%$ of intact). However, in AR, the ROM at C4-C5 remained close to the intact condition ($93 \pm 75\%$ of intact). As a result, also at the adjacent level, the ROM in AR was not significantly different from intact (C3-C4, $122 \pm 9\%$ of intact; C5-C6, $84 \pm 17\%$ of intact).

Table 5.2: Normalized mean range of motion \pm standard deviation (SD), and mean moment \pm SD during spine testing in 3 directions for intact C4-C5 disc, after replacement with bioAID at C4-C5 and after C4-C5 fusion. (n=6) Significantly different compared with intact measured with repeated ANOVA, Tukey Post-Hoc: * $p < 0.05$ ** $p < 0.01$ *** $p < 0.001$.

	Flexion/Extension			Lateral Bending			Axial Rotation		
	intact	bioAID	fusion	intact	bioAID	fusion	intact	bioAID	fusion
Mean moment	1.05	0.91	1.80*	1.03	1.23	2.26**	1.13	0.80*	1.31
SD	0.03	0.45	0.56	0.06	0.33	0.59	0.06	0.70	0.29
Normalized ROM	-	1.05	0.17***	-	0.84**	0.18***	-	2.49	0.93
SD	-	0.14	0.08	-	0.06	0.05	-	1.54	0.75

Table 5.2 shows the amount of torque (Nm) required to achieve the intact ROM after disc replacement with the bioAID and after fusion. After disc replacement with the bioAID, the moment data was close to the intact moment in FE and LB, but approximately 30% less in AR. The fused specimens required the highest torque to achieve the intact ROM in all directions. This was only significant in FE and LB where the required moment was almost double the moment seen in the intact condition.

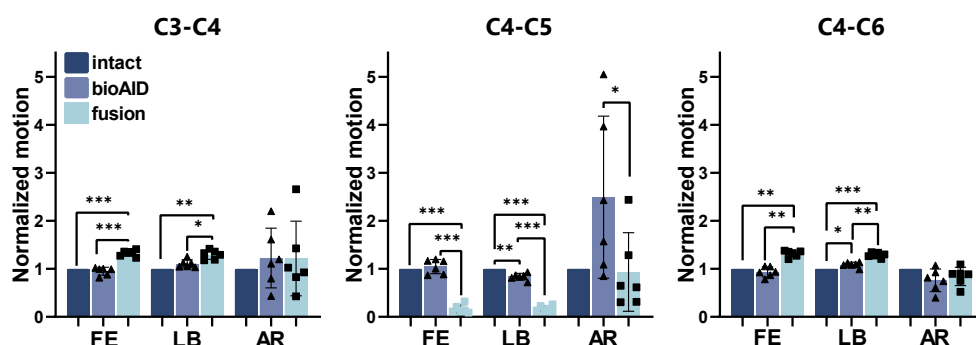


Figure 5.3: Normalized segmental range of motion \pm standard deviation for spinal levels between C3-C6 in flexion/extension (FE), lateral bending (LB), and axial rotation (AR) for intact C4-C5 disc, after replacement with bioAID, and after C4-C5 fusion in intact specimens, with bioAID and fusion at C4-C5. (Repeated measures ANOVA, Tukey Post-Hoc: * $p < 0.05$ ** $p < 0.01$ *** $p < 0.001$).

5.3.2 Neutral zone

Based on the moment-rotation graphs (Figure 5.4A), the bioAID exhibited non-linear behavior with a neutral and elastic zone comparable to what was seen in the intact condition at the treated level for both LB and FE. When quantifying the normalized NZ, results showed that the bioAID indeed had a NZ close to intact in FE (Figure 5.4B). However, a significantly smaller NZ was observed in LB for the bioAID (Figure 5.4B). For the fused segments, no NZ could be identified for FE and LB. A small NZ in AR was detected for all three conditions (Figure 5.4B)

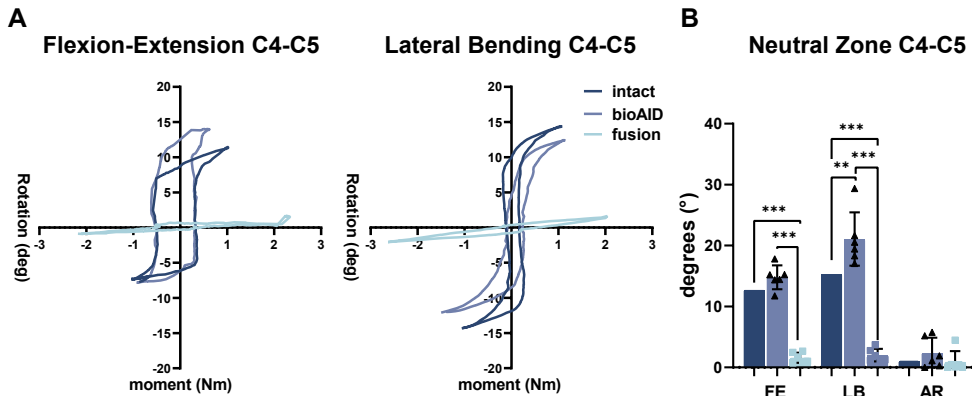


Figure 5.4: Representative moment-rotation curves (A) and mean normalized neutral zone \pm standard deviation (B) for intact C4-C5 disc, after replacement with bioAID at C4-C5 and after C4-C5 fusion. (Repeated measures ANOVA, Tukey Post-Hoc: ** $p < 0.01$ *** $p < 0.001$).

5.3.3 Intradiscal pressure

After implantation of the bioAID, the peak IDP was similar at the adjacent cranial level compared with intact in all directions (Figure 5.5). An increase in the mean IDP was observed

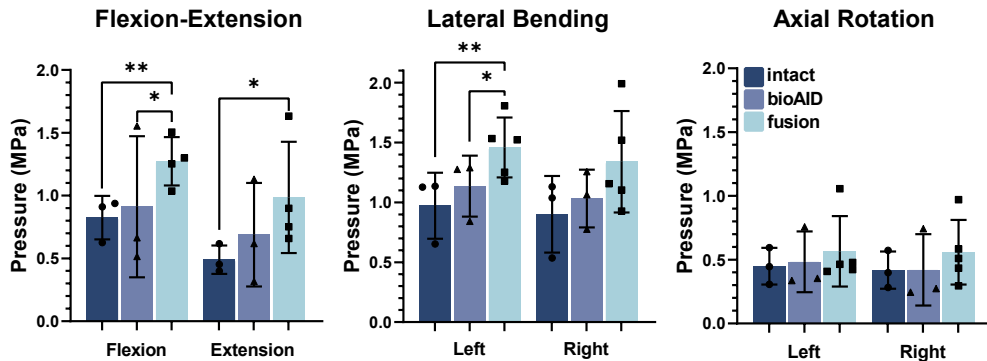


Figure 5.5: Intradiscal pressure (MPa, mean \pm standard deviation) at C3-C4 for intact, after replacement of C4-C5 with bioAID and after C4-C5 fusion. (Mixed effect analysis, Tukey Post-Hoc: * $p < 0.05$, ** $p < 0.01$).

for all three DOF at the adjacent cranial level of the fused specimens compared with the intact spines, although only significant in FE and LB.

5.4 Discussion

To assess the initial biomechanical effect of the bioAID on the kinematic behavior of the spine an *ex vivo* biomechanical study in 6-DOF was performed. The current study found that the bioAID can preserve motion at treated and adjacent levels and shows similar non-linear behavior including a NZ as seen for the intact condition, indicating its potential to restore physiological kinematics and similar ROM allowed by the spinal segments. Unlike fusion, by preserving this kinematic signature and adjacent intradiscal pressures, the bioAID might reduce overloading of the surrounding structures, thereby potentially reducing the risk of adjacent segment disease.

The most important and most reported parameters to assess the biomechanical similarities between intact and treated specimens are the ROM and neutral zone [31]. Within the context of disc replacement, the NZ is often seen as a clinically relevant measure for the quality of motion, giving information about the region of intervertebral motion where there is the least resistance. It is hypothesized that alterations in the sigmoid curve, also called the kinematic signature, can result in altered stresses on the spinal musculature and ligaments that stabilize the spinal segment [32]. The similarities in the sigmoid curve observed seem to indicate that the bioAID allows for similar semi-constrained motion as the native disc and thus can better replicate the kinematics of the intact condition compared to spinal fusion.

Besides the similarities in FE and the sigmoid shape of the moment-rotation curves, significant differences in ROM during LB and AR were observed. Similar to Patwardhan (2012) and Snyder (2007), the decrease in LB after CDR with the bioAID could be attributed to the fact that a small part of the lateral and dorsal borders of the annulus fibrosus (or equivalent anatomical locations) was preserved to reduce risk of migration and preserve additional stability [21], [33].

However, the most distinct difference in *ex vivo* motions between the bioAID and the intact condition was during AR, where especially two specimens show a much higher ROM compared to the other results. This difference could be explained by the lack of initial fixation since these two specimens were instrumented with previously implanted bioAIDs due to the limited availability of bioAIDs, resulting in flattened pins due to the retraction procedure. This instability mainly affected AR since this motion results in a shearing force. Within this context, the fibers of the jacket play an important role in resisting shearing motion, similar to Sharpey's fibers of the natural annulus [34]. To mimic the kinematic behavior of a natural IVD, shearing

needs to be transferred through the jacket, which cannot be achieved without proper interconnection between vertebrae and fibers of the jacket. This can also explain why even for the samples with intact pins, a slight increase in AR for the bioAID compared to intact was observed. Previous finite element modeling research on the bioAID also found that, especially for AR, bone ingrowth over the whole cranial and caudal surface of the implant is required to mimic the motion of the intact condition [24]. *In vivo*, osseointegration between the jacket's fibers and the vertebrae is lacking immediately post-surgery. As bone ingrowth takes time, the current fixation system is probably still sufficient as initial fixation, providing similar motion characteristics in FE and LB.

After fusing the spines at level C4-C5, the ROM was redistributed over the three segments, similar to what has been reported in other studies that utilized a hybrid protocol [35]–[38]. It is hypothesized that the altered motion pattern at the treated level often leads to a compensatory mechanism at the adjacent levels, which can increase the risk of adjacent segment disease in the long term [8], [35]. Surprisingly, in AR, no significant reduction in ROM was observed. Other studies have also reported the least difference in AR after fusing the segment [39], [40], but contradictory results have also been reported [36], [37], [41]–[44]. A possible explanation for the reported discrepancies could be the use of different cage designs and the lack of bone ingrowth which could lead to motion at the interface.

By using the hybrid protocol, the measurements performed on the instrumented spines can result in different peak torques acting on the specimens for reaching the same global ROM as the intact condition. Comparing the ROM alone is therefore not sufficient to verify similarities between instrumented and intact spines. Based on the results, the fused specimens needed much higher moments to reach the same global ROM, indicating that an increased force is required to preserve cervical physiological ROM after fusion similar to what has been observed in other *in vivo* and *in vitro* research [8], [35], [36], [38], [45]. This hybrid protocol was chosen based on the hypothesis of Panjabi et al. (2007), stating that a modification, in this case, a disc replacement with the bioAID or fusion, will result in a compensatory mechanism of the adjacent levels resulting in a redistribution of the loads to reach the intact condition [27]. Many other studies utilize the flexibility protocol, in which a constant pure moment is applied in all three conditions while measuring the resulting ROM [39], [40], [42], [43], [46], [47]. However, the flexibility method is unable to evaluate the effect on the adjacent levels since it applies an equal moment at all spinal levels and thus is less suitable to identify if there are alterations in the overall kinematic behavior of the spine after treatment.

Lastly, the IDP provides more insight into the adjacent level kinematics and the redistribution of biomechanical stresses acting on the spine after treatment. The preserved IDP after disc replacement with the bioAID indicates there is a similar distribution of biomechanical stresses as in an intact spine. Previous studies have also shown that preserving motion has a positive effect on preserving IDP at the adjacent levels [35], [48]–[51]. After fusing the segment, the loss of motion at the fused level led to elevated IDPs at the adjacent level compared with intact in all directions. These observations again demonstrate that adjacent segments are compensating for the loss of motion and that there is an altered loading pattern in the spine, as also seen in ROM, coupled motion, and NZ data. Other studies also observed that loss of motion at the treated level leads to compensation mechanisms at the adjacent level, such as elevated IDPs [35], [52].

There are several study limitations and considerations to the interpretation of the current results which also make a direct comparison with other studies difficult due to differences in specimen origin, specimen quality, testing protocol, surgical procedure, and testing apparatus.

First of all, the bioAIDs were implanted in a swollen condition giving the bioAID a final height of approximately 6 mm. This could have led to over distraction of the disc space imposing increased tension on soft spinal structures that potentially limit ROM. This was done to best replicate the motion behavior after reaching swelling equilibrium *in vivo* since unconstrained swelling of the hydrogel can take up to 6 days in a physiologic salt solution [53]. Ultimately, the bioAID will be implanted unswollen to avoid this and allow swelling until equilibrium under physiological loading. Moreover, differences in height between the bioAID and fusion cages could have affected soft tissue tensioning between the two conditions, potentially influencing the kinematics.

This experiment only used one size of the implant while, in general, the implant is adjusted to the dimensions of the patient. As a result, for some spinal specimens, the implant was slightly too big, potentially hampering the ROM. This could explain the variations observed, but it did not affect the overall trend seen.

It must also be mentioned that in the current study the use of a follower load to replicate the muscle forces that act on the cervical spine was omitted. In general, including a follower load leads to stiffening of the IVD and thus often results in decreased ROM and NZ and increased IDPs, especially in FE [50], [52], [54]. This effect might be even more prominent for the bioAID, since this design contains a compressible core, which is seen as one of the advantages, giving the device its shock absorption capability. However, it is also speculated that incorporating a

follower load in an *ex vivo* setting might result in applying unphysiological forces, especially during rotation [55]. Although a follower load was not incorporated in this research, current results still illustrate that the bioAID design allowed motion based on deformation and was able to mimic both the ROM in FE, NZ and IDP as seen in the intact condition.

The serial nature of this repeated-measures experiment could have introduced iatrogenic changes during the intact and/or bioAID conditions influencing the results of the fusion condition. Although this is unlikely under such low loads, future work should be carried out to confirm this.

Lastly, this study cannot fully elucidate its benefits compared with first-generation ball-and-socket designs. The rationale of the bioAID design is that by mimicking the structure of the natural IVD, it can better replicate the kinematics of a native IVD compared with first-generation ball-and-socket designs. Based on the data of this study, it can be suggested that the bioAID can restore motion and allow for non-linear behavior similar to an intact spine at both the adjacent and treated level. Despite these promising results, actual improvements in this design compared with ball-and-socket first-generation devices cannot be deduced from this study. To assess differences between these designs, clinical trials with long-term follow-up data are necessary. Both design categories can maintain motion, but the biomimetic design aims to reduce compensatory mechanisms at the adjacent levels with the hypothesis that this will lead to a reduced risk of adjacent segment disease in the long term.

5.5 Conclusion

In spite of its limitations, the results obtained in this research illustrate that the bioAID may preserve the adjacent level IDPs and segmental kinematics close to the intact condition. These findings support the hypothesis that CDR using the novel bioAID can be a promising alternative treatment for replacing severely degenerated IVDs. By maintaining normal kinematics and stresses at the treated and adjacent levels, the bioAID might minimize the risk of adjacent segment disease. However, further preclinical work based on *in vivo* evaluation in a large animal model is needed prior to making valid conclusions regarding its safety and efficacy in comparison to other current treatment options.

Acknowledgments

This publication is part of the project BioAID with project number 10025453 of the research program AES Open Technology Program, partly financed by the Dutch Research Council (NWO). The authors are grateful to DSM Biomedical for providing the UHMWPE fibers used in this publication and Dr. Arjan Loenen for helping with the data analysis of the segmental rotations.

References

- [1] L. Xie, M. Liu, F. Ding, P. Li, and D. Ma, "Cervical disc arthroplasty (CDA) versus anterior cervical discectomy and fusion (ACDF) in symptomatic cervical degenerative disc diseases (CDDDs): an updated meta-analysis of prospective randomized controlled trials (RCTs)," *SpringerPlus*, vol. 5, no. 1. Springerplus, p. 1188, 01-Dec-2016.
- [2] J. A. Youssef et al., "Outcomes of posterior cervical fusion and decompression: a systematic review and meta-analysis," *Spine Journal*, vol. 19, no. 10. *Spine J*, pp. 1714–1729, 01-Oct-2019.
- [3] T. F. M. Boselie, P. C. Willems, H. Van Mameren, R. A. De Bie, E. C. Benzel, and H. Van Santbrink, "Arthroplasty versus fusion in single-level cervical degenerative disc disease," *Spine (Phila. Pa. 1976)*, vol. 38, no. 17, pp. E1096–E1107, 2013.
- [4] D. Turkov, A. Job, C. Iturriaga, and R. B. Verma, "Current Concepts of Cervical Disc Arthroplasty," *Int. J. Spine Surg.*, vol. 15, no. 6, pp. 1174–1183, Dec. 2021.
- [5] T. K. Wu et al., "Multilevel cervical disc replacement versus multilevel anterior discectomy and fusion: A meta-analysis," *Med. (United States)*, vol. 96, no. 16, pp. 1–9, 2017.
- [6] M. Boakye, C. G. Patil, J. Santarelli, C. Ho, W. Tian, and S. P. Lad, "Cervical spondylotic myelopathy: Complications and outcomes after spinal fusion," *Neurosurgery*, vol. 62, no. 2, pp. 455–461, 2008.
- [7] D. Coric, J. Cassis, J. D. Carew, and M. O. Boltes, "Prospective study of cervical arthroplasty in 98 patients involved in 1 of 3 separate investigational device exemption studies from a single investigational site with a minimum 2-year follow-up: Clinical article," *J. Neurosurg. Spine*, vol. 13, no. 6, pp. 715–721, Dec. 2010.
- [8] J. Goffin et al., "Long-term follow-up after interbody fusion of the cervical spine," *J. Spinal Disord.*, vol. 17, no. 2, pp. 79–85, Apr. 2004.
- [9] F. Wang, H. T. Hou, P. Wang, J. T. Zhang, and Y. Shen, "Symptomatic adjacent segment disease after single-lever anterior cervical discectomy and fusion," *Med. (United States)*, vol. 96, no. 47, 2017.
- [10] J. You, X. Tang, W. Gao, Y. Shen, W. Y. Ding, and B. Ren, "Factors predicting adjacent segment disease after anterior cervical discectomy and fusion treating cervical spondylotic myelopathy: A retrospective study with 5-year follow-up," *Med. (United States)*, vol. 97, no. 43, pp. 2–6, 2018.
- [11] J. C. Wu, H. K. Chang, W. C. Huang, and Y. C. Chen, "Risk factors of second surgery for adjacent segment disease following anterior cervical discectomy and fusion: A 16-year cohort study," *Int. J. Surg.*, vol. 68, pp. 48–55, Aug. 2019.
- [12] Z. Ma, X. Ma, H. Yang, X. Guan, and X. Li, "Anterior cervical discectomy and fusion versus cervical arthroplasty for the management of cervical spondylosis: a meta-analysis," *Eur. Spine J.*, vol. 26, no. 4, pp. 998–1008, Apr. 2017.
- [13] R. C. Sasso, P. A. Anderson, K. D. Riew, and J. G. Heller, "Results of cervical arthroplasty compared with anterior discectomy and fusion: four-year clinical outcomes in a prospective, randomized controlled trial," *J. bone Jt. Surg.*, vol. 93-A, no. 18, pp. 1684–1692, 2011.
- [14] B. Frost, S. Camarero-Espinosa, and E. Foster, "Materials for the spine: anatomy, problems, and solutions," *Materials (Basel)*, vol. 12, no. 2, p. 253, Jan. 2019.
- [15] F. Galbusera, C. M. Bellini, M. Brayda-Bruno, and M. Fornari, "Biomechanical studies on cervical total disc arthroplasty: A literature review," *Clin. Biomech.*, vol. 23, no. 9, pp. 1095–1104, Nov. 2008.
- [16] V. V. Patel et al., "Cervical facet force analysis after disc replacement versus fusion," *Clin. Biomech.*, vol. 44, pp. 52–58, May 2017.
- [17] C. A. M. Jacobs, C. J. Siepe, and K. Ito, "Viscoelastic cervical total disc replacement devices: Design concepts," *Spine Journal*, vol. 20, no. 12. Elsevier, pp. 1911–1924, Aug-2020.
- [18] A. G. Patwardhan and R. M. Havey, "Prosthesis design influences segmental contribution to total cervical motion after cervical disc arthroplasty," *Eur. Spine J.*, Jul. 2019.
- [19] J. Lazennec, A. Aaron, O. Ricart, and J. P. Rakover, "The innovative viscoelastic CP ESP cervical disk

- prosthesis with six degrees of freedom: biomechanical concepts, development program and preliminary clinical experience," *Eur. J. Orthop. Surg. Traumatol.*, vol. 26, no. 1, pp. 9–19, Jan. 2016.
- [20] R. D. Guyer et al., "Kinematic assessment of an elastic-core cervical disc prosthesis in one and two-level constructs," *JOR Spine*, vol. 1, no. 4, pp. 1–10, Dec. 2018.
- [21] A. G. Patwardhan et al., "Primary and coupled motions after cervical total disc replacement using a compressible six-degree-of-freedom prosthesis," *Eur. Spine J.*, vol. 21, no. S5, pp. S618–S629, Jun. 2012.
- [22] P. R. Van Den Broek, J. M. Huyghe, and K. Ito, "Biomechanical behavior of a biomimetic artificial intervertebral disc," *Spine (Phila. Pa. 1976)*, vol. 37, no. 6, pp. 367–373, 2012.
- [23] P. R. van den Broek, J. M. Huyghe, W. Wilson, and K. Ito, "Design of next generation total disk replacements," *J. Biomech.*, vol. 45, no. 1, pp. 134–140, Jan. 2012.
- [24] P. R. Van Den Broek, "Development of a biomimetic artificial intervertebral disc," Eindhoven University of Technology, 2012.
- [25] N. Yoganandan, F. A. Pintar, J. Zhang, and J. L. Baisden, "Physical properties of the human head: Mass, center of gravity and moment of inertia," *J. Biomech.*, vol. 42, no. 9, pp. 1177–1192, Jun. 2009.
- [26] E. M. Mannen, S. S. Ranu, A. M. Villanueva, and E. A. Friis, "Validation of a novel spine test machine," *J. Med. Devices, Trans. ASME*, vol. 9, no. 1, p. 011002, Mar. 2015.
- [27] M. M. Panjabi, "Hybrid multidirectional test method to evaluate spinal adjacent-level effects," *Clin. Biomech.*, vol. 22, no. 3, pp. 257–265, Mar. 2007.
- [28] M. M. Panjabi et al., "Mechanical properties of the human cervical spine as shown by three-dimensional load-displacement curves," *Spine (Phila. Pa. 1976)*, vol. 26, no. 24, pp. 2692–2700, 2001.
- [29] R. J. P. Doodkorte, A. K. Roth, J. J. Arts, L. M. A. Lataster, L. W. van Rhijn, and P. C. Willems, "Biomechanical comparison of semirigid junctional fixation techniques to prevent proximal junctional failure after thoracolumbar adult spinal deformity correction," *Spine J.*, vol. 21, no. 5, pp. 855–864, 2021.
- [30] T. H. Smit, M. S. Van Tunen, A. J. Van Der Veen, I. Kingma, and J. H. Van Dieën, "Quantifying intervertebral disc mechanics: A new definition of the neutral zone," *BMC Musculoskelet. Disord.*, vol. 12, 2011.
- [31] H. J. Wilke, K. Wenger, and L. Claes, "Testing criteria for spinal implants: Recommendations for the standardization of *in vitro* stability testing of spinal implants," *Eur. Spine J.*, vol. 7, no. 2, pp. 148–154, 1998.
- [32] M. M. Panjabi, "The stabilizing system of the spine. Part II. neutral zone and instability hypothesis," *J. Spinal Disord.*, vol. 5, no. 4, pp. 390–397, 1992.
- [33] J. T. Snyder et al., "Effect of uncovertebral joint excision on the motion response of the cervical spine after total disc replacement," *Spine (Phila. Pa. 1976)*, vol. 32, no. 26, pp. 2965–2969, 2007.
- [34] A. White and M. Panjabi, *Clinical Biomechanics of the Spine*, 2nd ed. London: Lip pincott Company, 1990.
- [35] A. E. Dmitriev, B. W. Cunningham, N. Hu, G. Sell, F. Vigna, and P. C. McAfee, "Adjacent level intradiscal pressure and segmental kinematics following a cervical total disc arthroplasty: An *in vitro* human cadaveric model," *Spine (Phila. Pa. 1976)*, vol. 30, no. 10, pp. 1165–1172, May 2005.
- [36] B. W. Cunningham, N. Hu, C. M. Zorn, and P. C. McAfee, "Biomechanical comparison of single- and two-level cervical arthroplasty versus arthrodesis: effect on adjacent-level spinal kinematics," *Spine J.*, vol. 10, no. 4, pp. 341–349, Apr. 2010.
- [37] K. O. Colle, J. B. Butler, P. M. Reyes, A. G. U. S. Newcomb, N. Theodore, and N. R. Crawford, "Biomechanical evaluation of a metal-on-metal cervical intervertebral disc prosthesis," *Spine J.*, vol. 13, no. 11, pp. 1640–1649, Nov. 2013.
- [38] A. A. Gandhi, S. Kode, N. A. Devries, N. M. Grosland, J. D. Smucker, and D. C. Fredericks, "Biomechanical analysis of cervical disc replacement and fusion using single level, two level, and

- hybrid constructs," *Spine (Phila. Pa. 1976)*, vol. 40, no. 20, pp. 1578–1585, Oct. 2015.
- [39] D. Daentzer et al., "In vitro-analysis of kinematics and intradiscal pressures in cervical arthroplasty versus fusion - A biomechanical study in a sheep model with two semi-constrained prosthesis," *Biomed. Eng. Online*, vol. 14, no. 1, pp. 27 (1–15), Dec. 2015.
- [40] P. C. McAfee et al., "Cervical disc replacement—porous coated motion prosthesis," *Spine (Phila. Pa. 1976)*, vol. 28, no. 20S, pp. S176–S185, 2003.
- [41] D. J. DiAngelo et al., "In vitro biomechanics of cervical disc arthroplasty with the ProDisc-C total disc implant," *Neurosurg. Focus*, vol. 17, no. 3, p. E7, 2004.
- [42] Y. Kotani et al., "Multidirectional flexibility analysis of cervical artificial disc reconstruction: in vitro human cadaveric spine model," *J. Neurosurg. Spine*, vol. 2, no. 2, pp. 188–194, Feb. 2005.
- [43] N. R. Crawford, S. Baek, A. G. U. Sawa, S. Safavi-Abbasi, V. K. H. Sonntag, and N. Duggal, "Biomechanics of a fixed-center of rotation cervical intervertebral disc prosthesis," *Int. J. Spine Surg.*, vol. 6, no. 1, pp. 34–42, 2012.
- [44] T. Terai, A. Faizan, K. Saiyo, and V. K. Goel, "Operated and adjacent segment motions for fusion versus cervical arthroplasty: A pilot study," in *Clinical Orthopaedics and Related Research*, 2011, vol. 469, no. 3, pp. 682–687.
- [45] A. S. Hilibrand, G. D. Carlson, M. A. Palumbo, P. K. Jones, and H. H. Bohlman, "Radiculopathy and myelopathy at segments adjacent to the site of a previous anterior cervical arthrodesis," *J. Bone Jt. Surg. - Ser. A*, vol. 81, no. 4, pp. 519–528, Apr. 1999.
- [46] C. C. Yu et al., "Biomechanical analysis of a novel prosthesis based on the physiological curvature of endplate for cervical disc replacement," *PLoS One*, vol. 11, no. 6, p. e0158234, 2016.
- [47] J. Lou, Y. Li, B. Wang, Y. Meng, Q. Gong, and H. Liu, "Biomechanical evaluation of cervical disc replacement with a novel prosthesis based on the physiological curvature of endplate," *J. Orthop. Surg. Res.*, vol. 13, no. 41, pp. 1–8, Feb. 2018.
- [48] C. Barrey, S. Campana, S. Persohn, G. Perrin, and W. Skalli, "Cervical disc prosthesis versus arthrodesis using one-level, hybrid and two-level constructs: an in vitro investigation," *Eur. Spine J.*, vol. 21, no. 3, pp. 432–442, Mar. 2012.
- [49] W. Womack, P. D. Leahy, V. V. Patel, and C. M. Puttlitz, "Finite element modeling of kinematic and load transmission alterations due to cervical intervertebral disc replacement," *Spine (Phila. Pa. 1976)*, vol. 36, no. 17, pp. E1126–E1133, Aug. 2011.
- [50] C. C. Wigfield, D. Skrzypiec, A. Jackowski, and M. A. Adams, "Internal stress distribution in cervical intervertebral discs," *J. Spinal Disord. Tech.*, vol. 16, no. 5, pp. 441–449, Oct. 2003.
- [51] A. Faizan, V. K. Goel, A. Biyani, S. R. Garfin, and C. M. Bono, "Adjacent level effects of bi level disc replacement, bi level fusion and disc replacement plus fusion in cervical spine- a finite element based study," *Clin. Biomech.*, vol. 27, no. 3, pp. 226–233, Mar. 2012.
- [52] J. Pospiech, D. Stolke, H. J. Wilke, and L. E. Claes, "Intradiscal pressure recordings in the cervical spine," *Neurosurgery*, vol. 44, no. 2, pp. 379–385, 1999.
- [53] F. Pizzocolo, J. M. Huyghe, and K. Ito, "Mode I crack propagation in hydrogels is step wise," *Eng. Fract. Mech.*, vol. 97, no. 1, pp. 72–79, 2013.
- [54] A. G. Patwardhan et al., "Load-carrying capacity of the human cervical spine in compression is increased under a follower load," *Spine (Phila. Pa. 1976)*, vol. 25, no. 12, pp. 1548–1554, 2000.
- [55] P. A. Crompton, S. B. Bruehlmann, T. E. Orr, T. R. Oxland, and L. P. Nolte, "In vitro axial preload application during spine flexibility testing: Towards reduced apparatus-related artefacts," *J. Biomech.*, vol. 33, no. 12, pp. 1559–1568, Dec. 2000.

Chapter 6

Mechanical characterization of the bioAID

The contents of this chapter are based on:

C.A.M. Jacobs, S.A. Kamali, A.M. Abdelgawad, B.P. Meij, S. Ghazanfari, S., M.A. Tryfonidou, Jockenhoevel, K. Ito. Mechanical characterization of a novel biomimetic artificial disc for the cervical spine. . *Journal of the Mechanical Behavior of Biomedical Materials*, Apr. 2023
DOI: 10.1016/j.jmbbm.2023.105808

Abstract

A novel biomimetic artificial intervertebral disc (bioAID) replacement implant has been developed containing a swelling hydrogel representing the nucleus pulposus, a tensile strong fiber jacket as annulus fibrosus and titanium endplates with pins to primarily secure the device between the vertebral bodies. In this study, the design safety of this novel implant was evaluated based on several biomechanical parameters, namely compressive strength, shear-compressive strength, risk of subsidence and device expulsion as well as identifying the diurnal creep-recovery characteristics of the device.

The bioAID remained intact up to 1 kN under static axial compression and only 0.4 mm of translation was observed under a physiological compressive shear load of 20 N, being both within the physiological range. No subsidence was observed after 0.5 million cycles of sinusoidal compressive loading between 50 – 225 N. After applying 400 N in antero-posterior direction under 100 N axial compressive preload, approximately 2 mm displacement was found, being within the range of displacements reported for other commercially available cervical disc replacement devices. The diurnal creep recovery behavior of the bioAID closely resembled what has been reported for natural intervertebral discs in literature.

Overall, these results indicate that the current design, under physiological loading, is withstanding (shear-)compression and is able to remain fixed in a mechanical design resembling the vertebral bodies. Moreover, it is one of the first implants that can closely mimic the poroelastic and viscoelastic behavior of natural disc under a diurnal loading pattern.

6.1 Introduction

Currently, anterior cervical discectomy and fusion (ACDF) is still the golden standard to treat patients with cervical myelopathy due to severely degenerated cervical discs. During ACDF, the diseased intervertebral disc is removed and replaced by a cage or allograft to restore disc height and with the aim of spinal fusion of the two adjacent vertebrae resulting in little mobility. The loss of motion at the treated level leads to compensatory increased motion at the adjacent levels which are hypothesized to elevate the risk of adjacent segment disease [1]–[4]. This has motivated the search for alternative, motion-preserving, treatments.

Similar to total hip and knee replacement preserving joint motion, cervical disc replacement (CDR) can preserve mobility of the cervical spinal unit. However, the first attempts of these artificial disc replacements still suffer from several limitations because the designs are too simplistic compared to the complex structure of the natural intervertebral disc. The disc provides motion based on deformation and exhibits viscoelastic and poroelastic behavior as a result of the osmotic pressure inside the disc, giving it its shock absorbance capacity. Most of these first-generation devices have a ball-and-socket design, consisting of a metallic or plastic core sandwiched between two metal endplates [5]–[8]. In these devices, the kinematics are based on articulation where one surface can slide relative to the other with limited constraint in the range of motion. Due to the stiff materials used in these designs, very limited shock absorption is facilitated which is needed to avoid overloading of the surrounding anatomical structures. Multiple studies have confirmed that implantation of such devices altered the kinematic behavior, resulting in facet overloading and increased risk of adjacent segment disease in the long-term [9]–[12]. This implies that the quality of motion might be more important than only preserving motion, probably one of the reasons why the superiority of CDR to ACDF is still under debate.

Therefore, a novel disc replacement was developed with the hypothesis that mimicking the structure of a natural intervertebral disc would lead to similar biomechanics and reduce the risk of altering the loading pattern of adjacent spinal units [13], [14]. The biomimetic artificial intervertebral disc (bioAID) contains a gelatinous swelling hydrogel representing the nucleus pulposus, a tensile strong ultra-high-molecular weight polyethylene (UHMWPE) fiber jacket as annulus fibrosis and titanium endplates with pins to replicate the connection between the disc and adjacent vertebrae (Figure 1.1). The design of the bioAID aims to mimic the non-linear viscoelastic behavior, osmotic intradiscal pressure and creep - relaxation behavior. A previous study has already shown how the bioAID can preserve the motion at the treated and adjacent level and replicate the non-linear characteristic of an intact motion segment [15].

Another unique feature of this design is that it can replicate the poroelasticity seen in a natural disc, being the fluid flow throughout the porous tissue. In the bioAID, the hydrogel core contains a negative charged backbone, resulting in a difference in ion concentration between the material and surrounding solution. This results in a Donnan osmotic pressure gradient, that attracts water into the hydrogel, giving it its osmotic swelling capacity [16]. This osmotic swelling is restricted by the fiber jacket, resulting in a high intradiscal pressure responsible for the device's compressive strength. Due to continuous loading during the day, the bioAID will experience fluid outflow that results in a reduced disc height, while during the night, the lower loading will lead to disc height recovery.

Besides preserving motion, another goal of cervical disc replacement surgery is restoration of the disc height. It is therefore important to assess if the bioAID also preserves the disc height under diurnal loading regime and determine how similar this diurnal creep-recovery behavior is compared with a natural disc. However, mechanical performance of the design is also of importance to ensure safety before introducing it clinically and to avoid common problems associated with current disc replacements such as dislocation, migration, and subsidence. Especially since the hydrogels such as the one used in this novel design do not have a long history in orthopedic applications. Thus, the goal of this study was to evaluate the design of the bioAID based on biomechanical parameters, namely compressive strength, shear-compressive strength, risk of subsidence and device expulsion as well as identifying the diurnal creep-recovery characteristics of the device.

6.2 Materials and Methods

6.2.1 Implant design

The cervical bioAID prosthesis (human size: 22 x 15.5 x 5 mm, canine size 14.5 x 13.5 x 5 mm) consists of an ionized hydrogel surrounded by a membrane and three layers of fiber jacket (Figure 6.1). The hydrogel was prepared by dissolving its components in ultra-pure water (Table 6.1). The hydrogel consists of two monomers, 2-hydroxyethyl methacrylate (HEMA) and sodium methacrylate (NaMA). When exposed to an aqueous environment, the sodium ion (Na^+) of NaMA dissolves, resulting in a negatively charged backbone giving the hydrogel a fixed charged density responsible for the Donnan osmotic swelling. After dissolving the hydrogel components, a disc of polyurethane foam (\varnothing 10 x 0.2 cm, MCF.03, Corpura B.V., Etten-Leur, The Netherlands) was soaked with the hydrogel solution and polymerized under UV light (UVP XX15L, 365 nm, Analytik Jena, Upland, CA USA) for 2 hours. It was subsequently heated to 45°C for 14 hours to complete polymerization. After polymerization, the hydrogel core (human size: 21 x 14.5 x 2 mm, canine size: 14 x 13 x 2 mm) was punched out. This

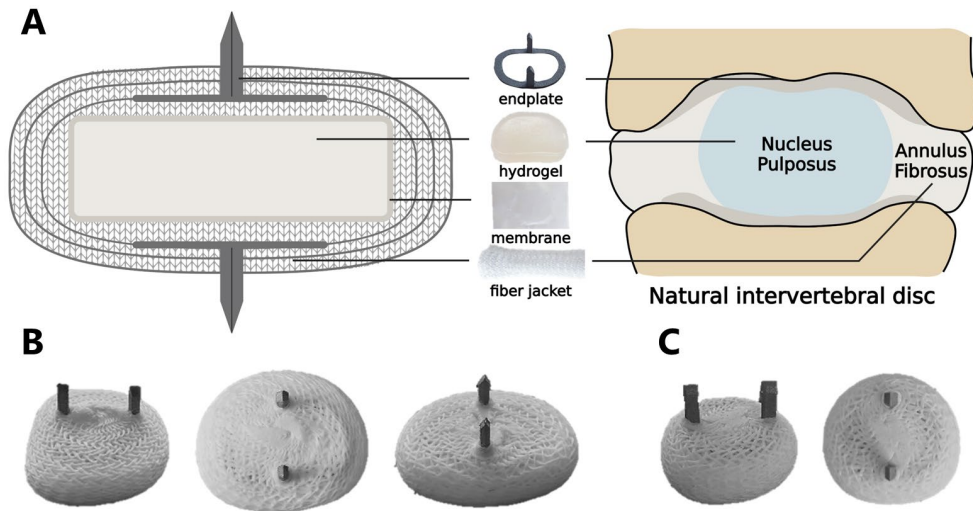


Figure 6.1: A) Schematic representation (coronal plane) of the bioAID design and its mimicry to a natural intervertebral disc. B) Image of human sized bioAID. (22 x 15.5 x 5 mm) C) Image of canine sized bioAID (14 x 13 x 5 mm). Created with BioRender.com

hydrogel was sealed (thermal cutter, HSG-0, HSGM, Walluf, Germany) into a loose UHMWPE pouch (38 μm thick, 5 g/m^2 , 0.9 μm pore, membrane, DSM Biomedical, Geleen, the Netherlands) to contain the hydrogel. A textile tube was warp-knitted (2x1 lapping, 10 stitch/cm, Dept. of Biohybrid & Medical Textiles (BioTex), Helmholtz Institute Aachen, Germany) from multifilament UHMWPE yarn (10%HA Dyneema Purity[®] SGX, dtex110, TS 100, DSM Biomedical, Geleen, Netherlands). The core was then enclosed in 3 layers of this tubing and manually sewn closed with 10%HA Dyneema purity[®] yarn to form an outer jacket. Before closure, a 3D printed titanium endplate ring (9 x 8 x 0.3 mm, 3D-MetalPrint, Houlle, France) with 2 mm pins was placed above the innermost layer of the jacket, such that the pins protruded out of the jacket.

Table 6.1: Chemical components of the HEMA-NaMA hydrogel solution.

Components of the monomer solution	Function	Mol ratio	Weight (g)
Distilled water	Solvent	0.80	35.74
Sodium methacrylate 99% (NaMA)	Monomer	0.02	5.09
2-hydroxyethyl methacrylate 97% (HEMA)	Monomer	0.18	55.2
Poly (ethylene glycol) dimethacrylate, average molecular weight 550 nM	Cross-linker	0.00001	5.75
2,2' azobis (2-methylpropionamide) dihydrochloride, 97%	Initiator	0.0001	0.054

Before further testing, all devices were swollen in Phosphate Buffered Saline (PBS, Dulbecco's Phosphate Buffered Saline, Sigma Aldrich) at 37°C under a static load of 50 N, representing the weight of the human head, for 7 days to reach swelling equilibrium [17].

6.2.2 Compression and shear-compression strength

The set-up of the static axial compression test and shear-compression test was custom-made according to the American Society for Testing and Materials (ASTM) method for static and dynamic characterization of spinal artificial disc (F2346-05) [18] and performed with a material test system (MTS; criterion model 42, MTS Systems corporation, Eden Prairie, MN USA) using a load cell of 5 kN (MTS, Model LSB.503, sensitivity of 2.227 mV/V). A motion segment was simulated via a gap between two titanium alloy (TiAl6V4) blocks (3D printed, Materialise, Leuven, Belgium) having slight concave surfaces with holes where the pins can sink in to match how the device is intended to fit between the vertebrae without considering bone ingrowth and intervertebral ligaments. Strength measurements of human sized implants (n=5) were performed in displacement control in 37°C PBS at a quasi-static rate of 0.001 mm/s until failure or limit of the load cell. Failure was defined as a force drop of >5% at constant displacement, or when 50% of the initial disc height was reached. Load and displacement data were continuously recorded at 10 Hz and used to calculate the stiffness, failure load, and ultimate load. Stiffness was defined as the slope of the load-displacement curve between physiological loads in the cervical spine of 80 and 180 N, and between 180 N and the failure load representing more extreme cervical loading regimes. Ultimate load was defined as the maximum force the bioAID could withstand without functional failure (no drop in force).

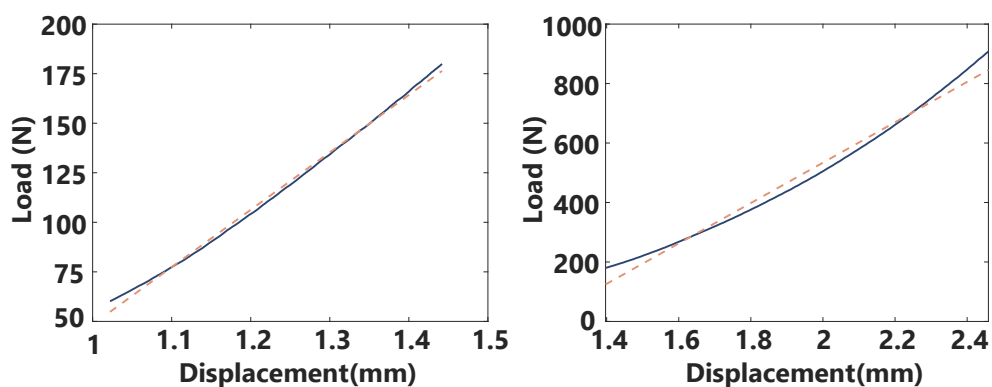


Figure 6.2: Representative plot visualizing how the slope (dotted line) of the load-displacement curve (blue line) was determined between physiological cervical loads of 80-180 N (left) and for more extreme cervical loading regimes between 180 N – failure load (right).

For the shear-compression test, the testing blocks were rotated $+45^\circ$ in the z-axis about the y-axis such that the sample experiences a combined compression and lateral shear load (Figure 6.3). To mimic bone ingrowth, the human sized implants were glued (Aquarium Munster Orca Gel Superglue) to the testing blocks and loaded in displacement mode in 37°C PBS at a rate of 0.01 mm/sec until failure, limit of the load cell or limit of the test set-up. Failure was defined as a force drop of $>5\%$. Load and displacement data were recorded continuously at a speed of 10 Hz . The displacement value at the vertical component of the physiological shear load of 28 N ($20\text{ N}/\cos 45^\circ$) was reported and should be within the range of lateral translation under shear loading found *in vivo*, being between $0 - 1.4\text{ mm}$ [19], [20].

After compression and shear-compression testing, damage to the outer part of the fiber jacket, hydrogel and endplate was macroscopically inspected.

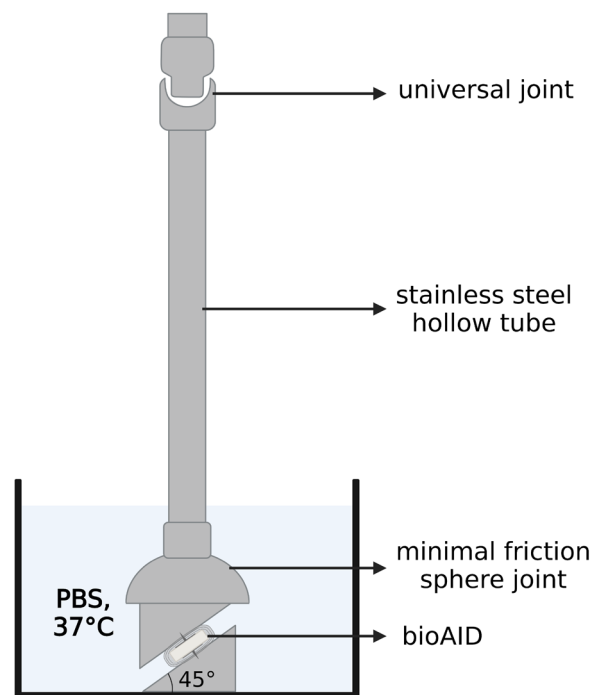


Figure 6.3: Schematic representation of shear-compression test set-up based on ASTM F2346-05. Created with BioRender.com

6.2.3 Subsidence test

Subsidence is defined as the amount of displacement the implant sinks into the adjacent vertebral bodies and its onset often occurs within the first months after implantation [21]. Therefore, a dynamic compression testing protocol was conducted until 0.5 million cycles, representing approximately 6 months *in vivo*. It is known from literature that after 6 months, osseous integration has taken place decreasing the risk of subsidence [22]. This test was performed on canine implants (n=5) as preparation for *in vivo* study in canines. These canine implants were placed between two pieces of rigid polyurethane foam (15 x 22 x 15 mm, Sawbones[®], density 0.24 g/cc, compressive modulus 4.9 MPa, Malmö, Sweden) as defined in ASTM F1839-01 [23], matching dimensions of cervical vertebrae, similar to how the device would be implanted *in vivo*. During the implantation procedure, a channel of 1 mm width and 5.5 mm depth was created in the cranial and caudal vertebrae and the keels of the bioAID endplates were inserted in ventrodorsal direction. The keels had a width of 1 mm dorsally and 1.3 mm ventrally to maximize contact surface and diminish the risk of anterior expulsion. Next, the samples were loaded in sinusoidal cycles at 2 Hz between 50 – 225 N, representing physiological loads in the cervical spine [24], [25], using a MTS (Acumen Electrodynamic test system, MTS Systems corporation, loadcell 3 kN, (MTS, Model 661.18SE-02)). The amount of subsidence was assessed using a μ CT scanner (CT 100, Scanco Medical, Brüttisellen, Switzerland) with an energy level of 70 kVp, intensity level of 200 μ A, integration time of 200 ms and one-fold frame average. Scans were performed at high resolution mode, using a voxel size of 51 μ m. CT scans were analyzed using Fiji [26] to identify the surface area that had less than 0.2 mm subsidence and less than 0.7 mm subsidence. First, the images were binarized, whereafter the pores in the image were filled to measure the area without taking into consideration the porous structure of the PU foam. The percentage of non-subsided area was then calculated by dividing the area in the transverse plane at 0.2- or 0.7-mm depth by the total area at 2 mm depth.

6.2.4 Device expulsion test

Canine samples (n=5) were used to assure safety before starting animal trials. The samples were positioned between two polyurethane foam blocks (Sawbones[®], density 0.24 g/cc, compressive modulus 4.9 MPa, Malmö, Sweden) as defined in ASTM F1839-01 [23], to mimic the mechanical properties of the vertebral bodies. An axial pre-load of 100 N was applied using a spring system (4 springs, C0480-045-0500, spring constant of 5.11 N/mm, Amatec, Alphen aan den Rijn, The Netherlands) to mimic the physiological axial compressive load, whereafter implants were loaded with an indenter matching the width of the implant (in the dorsal to ventral direction with regard to the bioAID) with a MTS (criterion model 42, MTS Systems corporation, 500 N load cell) at a loading rate of 0.1 mm/s until 10 mm displacement

or 400 N (Figure 6.4). Push out load was defined as the maximum load recorded. Displacement of the implant was manually determined with a caliper by measuring the distance between the implant's location before and after the test to exclude plastic deformation of the sample. Video recordings were used to define the minimal push out load at which displacement of the implant started to occur. After the test, damage to the outer part of the fiber jacket, hydrogel and endplate was macroscopically inspected.

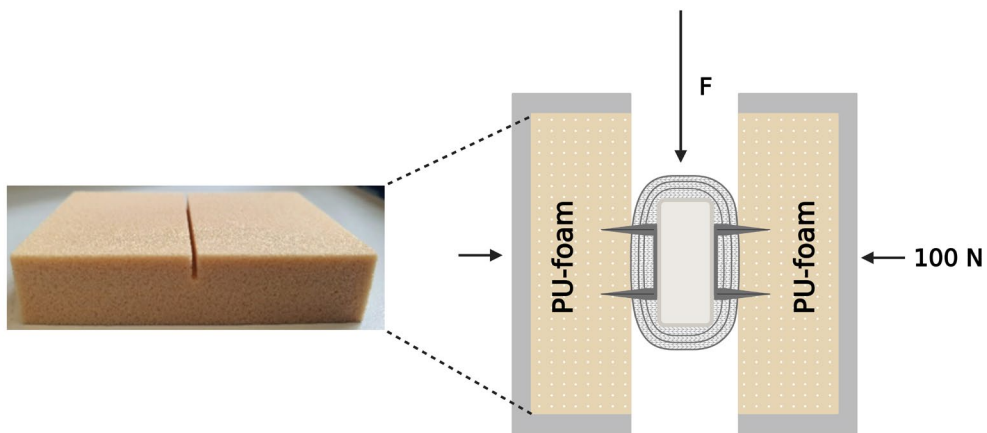


Figure 6.4: Schematic representation of the bioAID expulsion set up, using polyurethane (PU) foam blocks to mimic the mechanical properties of the vertebral bodies. Push out load is depicted by F and the bioAID was axially pre-loaded by 100 N. Created with BioRender.com

6.2.5 Diurnal creep-recovery behavior

Diurnal load was simulated by 8 hours at 60 N, hereafter referred to as night-loading, followed by quasi-static axial compression for 16 hours at a load magnitude alternating every 30 minutes between 60 N and 180 N, hereafter referred to as day-loading (Figure 6.5). Loading magnitudes were based on *in vivo* measurement of cervical discs in healthy human subjects performing normal neck movements [24], [25]. Three diurnal loading cycles were performed, where the load-displacement values were continuously recorded at a frequency of 20 Hz. The first cycle was used as a preconditioning cycle and used to normalize measurements of cycle 2 and 3. Biomechanical parameters were calculated on the last (3rd) cycle using Matlab (MATLAB R2018b, MathWorks, Natick, MA, USA). The overall disc height loss was defined as the difference in height at the start of the diurnal load cycle and the end of the diurnal load cycle relative to the start of the experiment (Figure 6.6). The creep during the day-loading phase is the difference in disc height at the beginning and end of the day-loading phase, while recovery is defined as the difference in disc height between the beginning and end of the night-loading phase (Figure 6.6). The rate of recovery was also calculated during the second

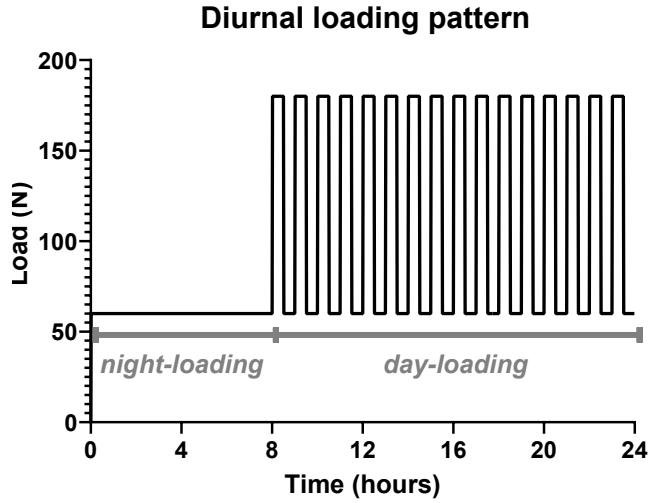


Figure 6.5: One cycle of the diurnal loading pattern to evaluate the bioAID's creep-recovery behavior.

half hour of the night-loading phase (the change during the first half hour was predominantly elastic deformation) and the last half hour of the night-loading phase (Figure 6.6). The long-term time constant was obtained by fitting the displacement data to a double Voight model (Eq. 6.1) using a least squares method [27], where L/S_1 is the deformation of the fast Voight model at infinity, τ_1 is the time constant of the fast Voight model, L/S_2 is the deformation of the slow Voight model at infinity and τ_2 the corresponding time constant. L/S_E describes the deformation prior to the creep phase which was not included since all parameters were calculated from the time point when the load was constant.

$$x(t) = L \left[\frac{1}{S_1} \left(1 - e^{-\left(\frac{t}{\tau_1}\right)} \right) + \frac{1}{S_2} \left(1 - e^{-\left(\frac{t}{\tau_2}\right)} \right) + \frac{1}{S_E} \right] \quad (6.1)$$

The water content, swelling capacity and Fixed Charged Density (FCD) were also determined by measuring the weight after production of implants (M0), after pre-load (M1), after diurnal loading cycle (M2) and after freeze-drying (Md). The water content at each timepoint was then calculated by the following formula: $(M1,2 - Md)$, which in turn was used to calculate the FCD with Equation 6.2. m_{NaMA} is the mass of sodium methacrylate, Z_{NaMA} mol-charges of sodium methacrylate, MW_{NaMA} is molecular weight of sodium methacrylate and m_{H_2O} is mass of water at each timepoint. The swelling capacity was determined by $(M1,2-Md)/Md * 100$ to get the increase in weight in percentage.

$$FCD = \frac{m_{NaMA} \left(\frac{z_{NaMA}}{MW_{NaMA}} \right) * \frac{100 \text{ mEq}}{\text{mol charge}}}{m_{H_2O}} \quad (6.2)$$

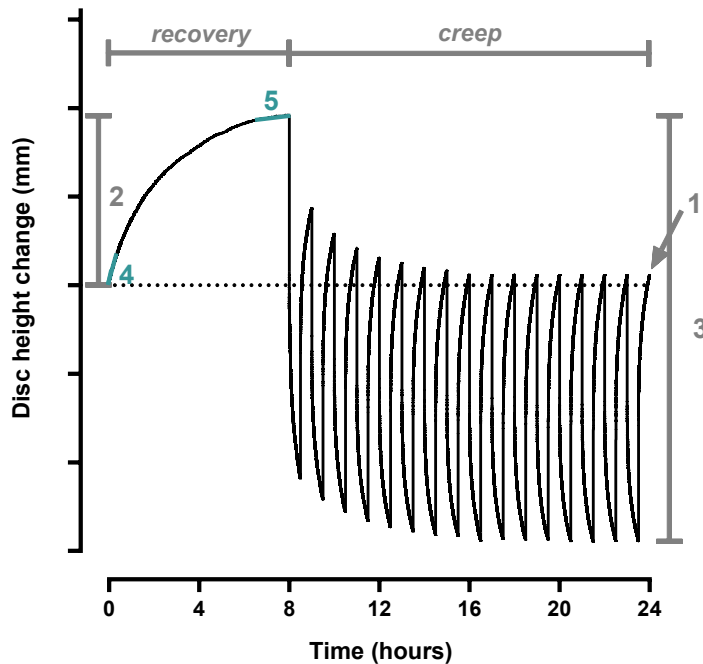


Figure 6.6: Biomechanical parameters that were calculated from the diurnal creep-recovery test. 1=overall disc height loss; 2=recovery; 3=creep; 4=rate of recovery during the second half hour of the night-loading phase; 5=rate of recovery during the last half hour of the night-loading phase.

6.2.6 Statistical analysis

Mean and standard deviation were calculated using Microsoft Excel. To determine differences between experimental groups, one-way ANOVA, followed by Tukey's honest post-hoc analysis was performed. Normal distribution was assessed using Shapiro-Wilk test and homogeneity of variance by Bartlett's test. A $p < 0.05$ was considered statistically significant. All statistical comparisons between groups were performed using GraphPad Prism version 8.02 for Windows (GraphPad Software). To determine the quality of the fit for the recovery results, a calculated R^2 of > 0.97 was considered sufficient (MATLAB R2018b, MathWorks, Natick, MA, USA).

6.3 Results

6.3.1 Compression and shear-compression strength

The average failure load of the bioAID at 50% of the initial height of the device was 973 ± 55 N. Functional failure of the bioAID did not occur even up to 5 kN (limit of the load cell). After the test, no macroscopic failure of the jacket or membrane was observed upon disassembly.

Although the hydrogel did show multiple cracks after the test, all hydrogel particles were contained within the UHMWPE membrane pouch. The average stiffness under physiological load (60-180N) was found to be 301 ± 49 N/mm (Table 6.2). Stiffness above physiological loads was found to be between 584 – 724 N/mm (Table 6.2).

Shear-compression properties of the bioAID were evaluated by reporting the amount of displacement under the physiological shear load. The average displacement under 28 N (vertical component of physiological lateral shear load) was 0.41 ± 0.12 mm.

Table 6.2: Mechanical properties (mean \pm SD) of the bioAID under quasi-static axial compression.

Failure load (N)	Ultimate load (kN)	Stiffness (N/mm)	
		60 - 180 N	180 N - failure
973 ± 55	5	301 ± 49	658 ± 55

6.3.2 Subsidence test

Figure 6.7 shows the area of the polyurethane foam surface that had less than 0.2 mm or less than 0.7 mm subsidence. Approximately 10 % of the surface has subsided more than 0.2 mm (Figure 6.7). There was a significant difference between the cranial and caudal surfaces. Less than 1.5% of the area has a subsidence greater than 0.7mm (Figure 6.7).

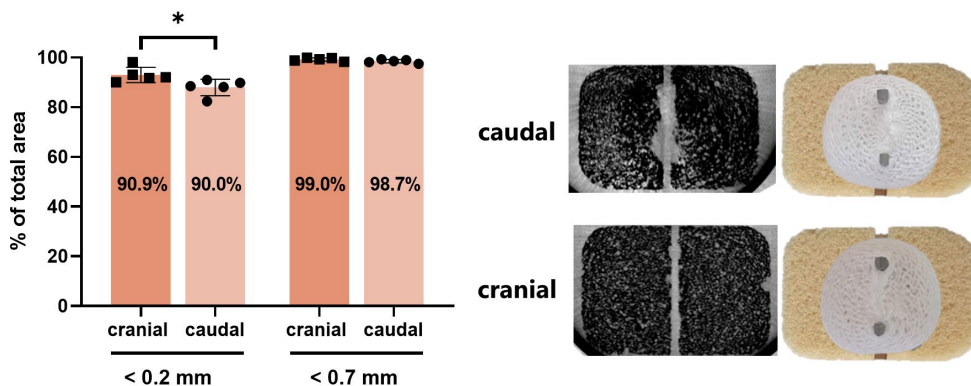


Figure 6.7: Left: Area of polyurethane foam surface (% mean \pm SD, one way ANOVA with Tukey's post-hoc ($*p < 0.05$)) with less than 0.2 or less than 0.7mm subsidence for both the cranial and caudal block. Right: Visualization of the CT scans of polyurethane foam blocks and image of the corresponding configuration during the test showing the difference in subsided area between cranial and caudal.

6.3.3 Device expulsion test

Device expulsion test was performed to determine the amount of displacement in the dorsal-ventral direction under loading of 400 N, as well as the minimal force needed for device migration. After applying a dorsal-ventral load of 400 N an average displacement of 2.11 ± 0.39 mm was found. Based on the video recording, the minimum force observed to cause device migration was approximately 150 N (Figure 6.8). Although the pins appeared to be slightly bended, the endplate remained intact. No damage of the fiber jacket was observed while the hydrogel exhibited cracks.

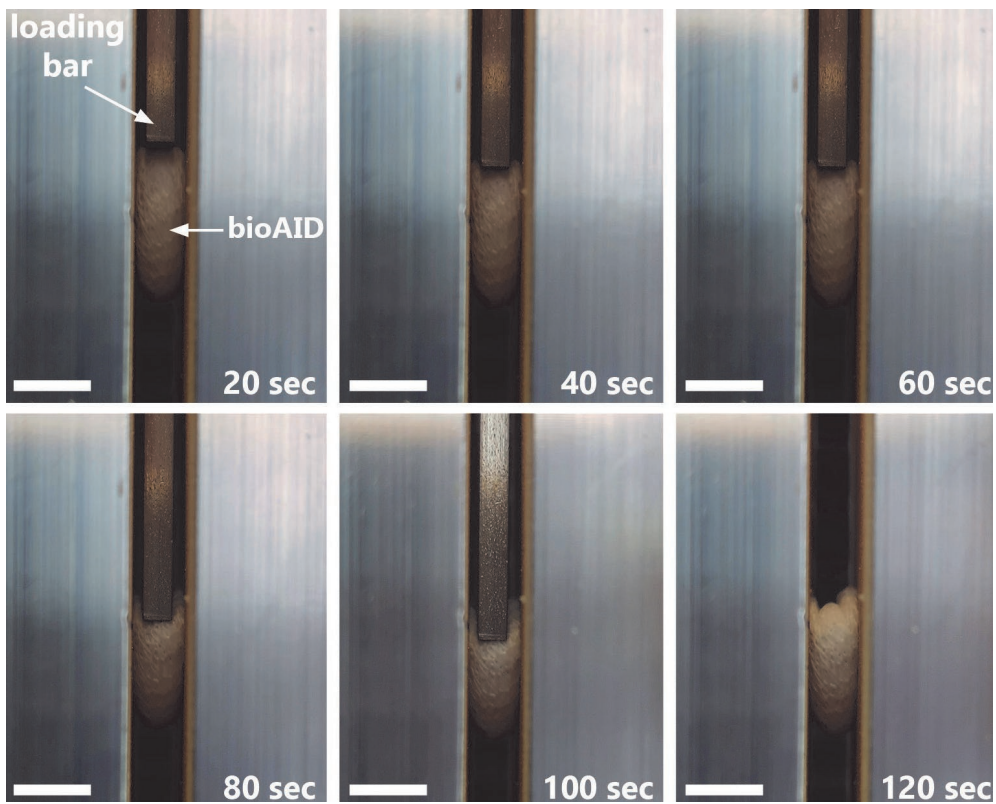


Figure 6.8: Lateral view of a representative time lapse of the device expulsion test showing the resistance to shear load and the plastic deformation occurring during the test. BioAID starts to migrate after approximately 60 seconds, which corresponds to a minimum value of 150 N in the load-displacement data. Scalebar: 7 mm.

6.3.4 Diurnal creep-recovery behavior

The poroelastic and viscoelastic properties of the bioAID under a diurnal loading pattern were evaluated. The FCD is a measure for the amount of negative charges within the hydrogel,

which is dependent on the water content and thus varies throughout the diurnal loading pattern. The FCD of the bioAID during the diurnal loading pattern ranged between 0.46 ± 0.05 and 0.37 ± 0.04 mEq/g, with a corresponding swelling capacity of 64 ± 0.1 and 79 ± 0.1 %.

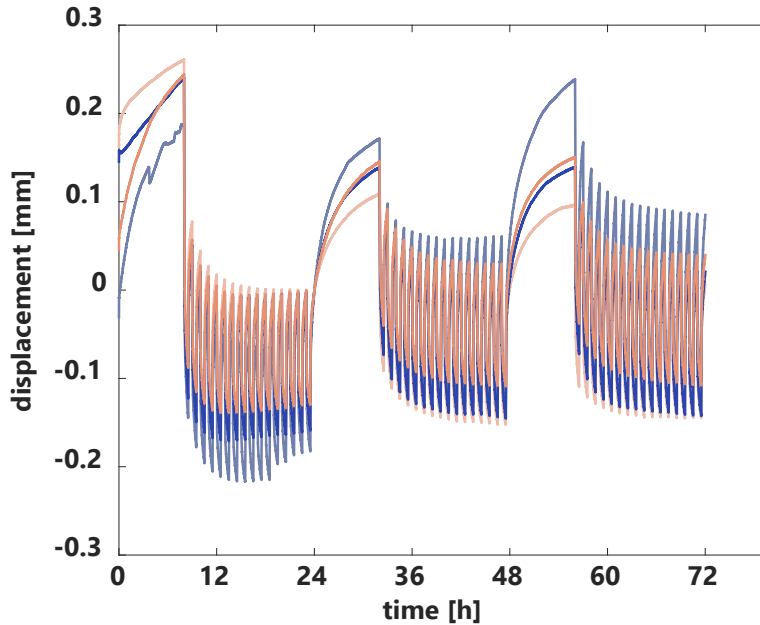


Figure 6.9: Displacement data over the three diurnal cycles for each of the tested samples (each color represents a different sample). Data is normalized to the end of day 1.

Table 6.3: Diurnal creep - recovery characteristics of the bioAID of the third cycle of diurnal loading.

overall disc height loss (mm)	Time constant (h)	rate of recovery (mm/h)		recovery (mm)	creep (mm)
		second half hour	last half hour		
0.04 ± 0.03	3.00 ± 0.35	0.05 ± 0.01	0.004 ± 0.001	0.29 ± 0.05	0.28 ± 0.04

The j-shaped creep and recovery curves show that disc height change during the day-time loading (creep) reached equilibrium, while the recovery of the disc height change during the night did not (Figure 6.9). Although the recovery did not reach equilibrium, the rate of recovery decreased between the second-half hour and last-half hour of the night-loading. Moreover, the day-time creep was almost fully compensated during the recovery phase since the overall disc height loss was close to zero (Table 6.3). Based on the Double-Voight model, the long-term time constant of the bioAID was approximately 3 hours (average R^2 of 0.99 ± 0.003) (Table 6.3).

6.4 Discussion

This study evaluated the mechanical performance of the cervical bioAID in compression, shear compression, as well as its risk for subsidence and device expulsion. Although many different loads act on the spine, the main loading direction in the spine is axial compression [28]. In the current study, the bioAID design did not fail (50% of initial height) until approximately 1 kN, being well above the estimated cervical physiological disc load of 50 – 150 N found in neutral posture [19], [29]–[31]. Although hydrogel cracks were visible after compression up to 5 kN, no functional failure and no hydrogel particles were extruded from the samples. This seems to indicate that even for peak loads, or impact loads reported to range between 100-1200 N the bioAID is mechanically safe [25], [32], [33]. Similar to what has been found here, the compressive stiffness for a natural intervertebral disc has been reported to range between 500 – 800 N/mm when subjected to 700 N of compressive load [33]. Stiffness within the physiological loading region is also in close agreement with previous studies, shown to range between 128 – 500 N/mm [32], [33].

Although the aim of this design concept is to replicate biomechanical properties of the native situation, comparison to existing, clinically used devices is often performed to predict clinical success. Other CDR devices have shown no failure up to 1.7 – 25 kN of compression [34]–[38]. These devices consist mainly out of hard polymers and metals, known to have higher strength and stiffer mechanical properties [39]. Moreover, in this study, a very low strain rate of 0.001 mm/sec was applied to reduce the effect of viscous dissipation, while other CDR devices were tested at much higher rates (0.2 – 0.4 mm/sec), which can have a big effect on the failure load and stiffness of the bioAID due to its viscoelastic properties [40], [41]. In general, increasing the strain rate will result in an increased stiffness and increased failure load of viscoelastic materials.

If the translation under a physiological shear load is higher than observed *in vivo*, it will result in overloading of surrounding anatomical structures such as the facet joints [42], [43]. In this study, only 0.4 mm of translation was observed under a physiological shear load of 20 N, being within the physiological range of 0 – 1.4 mm [19], [20]. Unfortunately, in this study, it was not possible to assess the ultimate compressive-shear failure of the device due to limitations in the test set-up. The maximum shear-compressive load tested here was around 100 N while maximum shear loads *in vitro* have been reported to be 135 N, and under low-speed frontal impacts *in vivo* were measured between 225 – 232 N [24]. Therefore, additional research should be carried out to establish the complete failure mechanism under compressive shear loading.

To compare shear-compression results to clinically available first-generation CDR devices, first, a distinction between unconstrained and semi-constrained designs has to be made. Unconstrained implants have a variable center of rotation (COR) and allow translations in all directions, whereas semi-constrained implants have a fixed COR and only allow minimal coupled translation. Both designs are unable to resist shear in a similar fashion as a natural disc [9], [44]. Semi-constrained designs, such as SECURE-C, Prestige LP, PCM and Mobi-C, report 2 % yield loads in the range between 100 – 500 N and maximum loads of 5 kN [34]–[37]. This seems to indicate that these designs are extremely safe in resisting shear loading. However, *in vivo*, these more constrained designs distribute shear loads between the bone-implant interface and the facet joints, with the risk of overloading the facet joints when the implant is not properly fixated to the adjacent vertebrae. Moreover, the ability of these semi-constrained designs to distribute shear loads depends on the location of the COR, which is extremely sensitive to correct placement [44]. On the other hand, unconstrained devices, such as the Charité and DISCOVER, do not support shear loading at all, increasing the risk of developing facet arthrosis [44]. Instead of solely assessing the ultimate loads under shear-compression loading, it might be valuable to also assess disc translations of CDR devices in cadavers to get more insight in the initial contact mechanism and loading of facet joints.

The results of the device expulsion and subsidence test suggest that the current design of the bioAID has a good primary stability with low risk of migration and subsidence. Based on video recordings of the device expulsion test, the minimal force needed to initiate displacement was 150 N, being above the physiological shear load of 20 N and maximum physiological shear load in anterior-posterior direction (equivalent to ventrodorsal direction in canines) of 135 N [29]. However, in extreme situations, such as those measured by Vives-Torres (2021) et al., shear loads of up to 232 N have been reported [24].

After applying 400 N, approximately 2 mm displacement was found, being within the range of displacements reported for other commercially available cervical disc replacement devices (0.93 for mm Mobi-C, subluxation test 2.19 mm and core expulsion of 1.75 mm for PCM) [34], [37]. Average push-out loads reported for other CDR devices are within the range of 127 – 289 N. Unfortunately, due to differences in test set-up protocol and the limited available data, it is very difficult to compare the performance of the primary fixation with other cervical disc replacement devices. Due to the usage of ‘soft’ materials in the design of the bioAID, it is impossible to replicate the test analysis done on other CDR devices. Moreover, the risk of device expulsion is often increased under a certain degree of extension, which was not replicated in this test set-up. Nevertheless, the load applied in this study is 20 times higher

than the physiological shear load in the cervical spine [29]. This test is therefore not suitable to predict *in vivo* behavior but serves as a test scenario for assessing safety.

Risk of subsidence was assessed under 0.5 million cycles of axial compression to simulate 6 months of daily activities. It was hypothesized that the risk of subsidence is minimal after 6 months due to bone remodeling and that its risk of occurrence increases during dynamic compressive loading compared to static loading, which is most often performed to assess safety of CDR devices [34], [35], [37], [45]. In the current study, less than 1.5% of the surface was subsided more than the 0.7 mm threshold chosen based on the average thickness of a native human vertebral cortical endplate [46], [47]. This small portion of subsidence, mainly visible until 0.2 mm depth, can be attributed to the width of the keels (1 mm dorsal and 1.3 mm ventral) which are pressed into the 1 mm drilled channel of the PU foam. The reasoning behind this implantation procedure is to reduce the risk of anterior expulsion, while avoiding over distraction of the disc space. The difference between the cranial and caudal surface can be explained by the suture knot of the bioAID, being only present at the caudal side of the bioAID. The largest factors that increase the risk of subsidence are low bone density and footprint mismatch between the device and the surface area of the vertebral endplate [48]–[51]. Although the PU foam does not replicate the human geometry and density distribution, the previous study has shown that the PU foam could replicate subsidence measures of middle-aged human vertebrae [52]. To best match the geometry, the foam blocks were cut into dimensions comparable to human cervical vertebrae [49].

Assessment of the primary fixation, evaluated by the subsidence and device expulsion test, was only performed on canine implants to ensure primary stability before starting (planned) animal trials. Since only the area of the ring, and not the dimension of the keels is adjusted to match the human implants, it is expected that these results can be extrapolated to the human devices. It can therefore be assumed that the current design of the bioAID has very little subsidence risk when being implanted *in vivo*.

These standardized testing procedures are mainly used as a mechanical comparison to other CDR devices, and do not give insight into the implant's performance under *in vivo* loads and motions [18]. It is often used as a measure for assuring safety after implantation. As already indicated in the previous paragraph, it is often difficult to compare the obtained data to other CDR devices due to large differences in materials, design and thus biomechanical properties. Even more challenging is that interpretation of the described method differs between studies while only limited information is reported about test conditions and results, further complicating the comparison between devices. Another aspect that hampers comparison is

that each company defines its own safety threshold and testing procedure, which is often a worst-case scenario and does not predict the device's biomechanical behavior *in vivo*. Continued efforts are needed to define more physiological standardized testing methods that include safety thresholds based on data of natural discs and clinically successful CDR devices such that more biomimetic devices can be developed that potentially improve long-term risks such as adjacent segment disease.

One of the unique features of the bioAID, is its ability to create an osmotic swelling pressure due to the negative charges of the hydrogel, giving it poroelastic properties. This poroelasticity is important for the biomechanical behavior of the bioAID, being responsible for preserving disc height and stiffness, regulating load distribution, and giving its energy absorbing and cushioning ability under axial compression. Therefore, this study also investigated the creep-recovery behavior under a diurnal loading pattern. When comparing the results of this research with data of natural intervertebral discs, it can be concluded that the bioAID can replicate a similar displacement – time curve [53]. Biomechanical parameters, such as creep, recovery, rate of recovery and overall disc height loss, were derived from this curve to be able to make a quantitative comparison with the native condition.

The overall disc height loss was close to zero, indicating that the bioAID can fully restore the daily creep during the night. Consistent with observations for natural discs, swelling equilibrium was only reached during day-loading and not during the night-loading recovery period. Similar to *in vivo*, the disc is in a steady-state condition where swelling equilibrium is often not achieved [54]. The difference in mechanism between mechanically applied fluid outflow and pressure related fluid inflow has been proposed as a possible explanation [55]–[57]. Moreover, during the recovery phase, the swelling is ultimately limited by tensioning of the fiber jacket, which could act as a 'sudden' stop in the transient swelling response. As hypothesized for a natural disc, the bioAID also seems to remain closer to the loading swelling equilibrium in comparison to the unloading equilibrium [57]. In general, fluid flow is slower towards the swelling equilibrium state, which could explain why swelling equilibrium was not reached during the night-loading compared to the day-loading [57]. This is also reflected in the rate of recovery, where there is a significant reduction from the second half hour compared to the last half hour. Another potential explanation for the longer time constant of the recovery phase compared to the creep phase is that permeability, and thus fluid flow, is strain dependent, which is much lower at the start of the recovery phase.

Overall, the long-term time constant for the recovery phase in this study was within the same order of magnitude as reported for a natural disc under a similar loading regime [53]. Within

the bioAID, the fluid flow is mainly dependent on the permeability of the membrane, since the jacket has significantly larger pores (860 μm pores in the jacket vs 0.9 μm pores in the membrane). Although current results show promising similarities to the native disc, it is possible to use a membrane with either bigger or smaller pores to tune its poroelastic properties.

The absolute change of disc height of the bioAID was 0.28 mm on average, while changes in disc height for a natural disc under a similar loading pattern have been reported to be around 0.4 mm [53]. This is most likely related to differences in the experimental set-up, using *ex vivo* thoracolumbar goat intervertebral discs including the endplates under a dynamic testing regime in a bioreactor. Calculating the percentage of disc height change, the results seem to be more comparable, showing 6 % change in this study compared to 6 – 10 % change (assuming lumbar goat disc height of approximately 4-6 mm [58]) [53]. In literature, there is an even larger variation in reported creep for natural discs using *in vitro* test set-ups, ranging between 0.2 – 3.5 mm [59]. Most of these variations arise from differences in specimen preparation, specimen species, loading regime and testing environment [59].

As previously mentioned, the FCD is responsible for the swelling pressure and dependent on the water content, which varies throughout the diurnal loading pattern, also varying the disc height. The FCD found in this study (0.37-0.46 mEq/g) is within the range of the nucleus pulposus of natural disc, known from literature to range between 0.35 – 0.6 mEq/g [60]–[62]. The water content was also comparable to what has been reported for the native situation during creep experiments [53], [63]. This seems to indicate that the ratio between hydroxyethyl-methacrylate and sodium-methacrylate is optimal to replicate the poroelastic behavior of the bioAID, which if needed, could be easily tuned. Nevertheless, in this research, the resultant intradiscal pressure of the bioAID and how it compares to the natural situation was not assessed. It is believed that since the FCD is within the natural range, it will also result in similar intradiscal pressure values.

6.5 Conclusion

Overall, these results indicate that the current design, under physiological loads, is mechanically withstanding (shear-)compression and is able to remain fixated between the vertebral bodies. Moreover, it is one of the first implants that can closely mimic the poroelastic and viscoelastic behavior of natural disc under a diurnal loading pattern.

Acknowledgements

This publication is part of the project BioAID with project number 10025453 of the research program AES Open Technology Program, partly financed by the Dutch Research Council (NWO). The authors are grateful to Jurgen Bultink for his assistance in developing the test setup.

References

- [1] C. Findlay, S. Ayis, and A. K. Demetriades, "Total disc replacement versus anterior cervical discectomy and fusion," *Bone Jt. J.*, vol. 100B, no. 8, pp. 991–1001, Aug. 2018.
- [2] S. Xu, Y. Liang, Z. Zhu, Y. Qian, and H. Liu, "Adjacent segment degeneration or disease after cervical total disc replacement: A meta-analysis of randomized controlled trials," *Journal of Orthopaedic Surgery and Research*, vol. 13, no. 1. *J Orthop Surg Res*, 03-Oct-2018.
- [3] Q. li Wang et al., "Long-term Results Comparing Cervical Disc Arthroplasty to Anterior Cervical Discectomy and Fusion: A Systematic Review and Meta-Analysis of Randomized Controlled Trials," *Orthop. Surg.*, vol. 12, no. 1, pp. 16–30, Feb. 2020.
- [4] A. S. Hilibrand, G. D. Carlson, M. A. Palumbo, P. K. Jones, and H. H. Bohlman, "Radiculopathy and myelopathy at segments adjacent to the site of a previous anterior cervical arthrodesis," *J. Bone Jt. Surg. - Ser. A*, vol. 81, no. 4, pp. 519–528, Apr. 1999.
- [5] M. D. Staudt, K. Das, and N. Duggal, "Does design matter? Cervical disc replacements under review," *Neurosurg. Rev.*, vol. 41, no. 2, pp. 399–407, Apr. 2018.
- [6] M. H. Pham, V. A. Mehta, A. Tuchman, and P. C. Hsieh, "Material Science in Cervical Total Disc Replacement," *BioMed Research International*, vol. 2015. Hindawi Limited, 2015.
- [7] F. Galbusera and H.-J. Wilke, Chapter 18: Motion Preservation. Elsevier Ltd., 2018.
- [8] P. B. Derman and J. E. Zigler, "Cervical disc arthroplasty: Rationale and history," *Int. J. Spine Surg.*, vol. 14, no. s2, pp. S5–S13, Aug. 2020.
- [9] M. A. Rousseau, D. S. Bradford, R. Bertagnoli, S. S. Hu, and J. C. Lotz, "Disc arthroplasty design influences intervertebral kinematics and facet forces," *Spine Journal*. 2006.
- [10] C. S. Shim et al., "CHARITI versus ProDisc: A comparative study of a minimum 3-year follow-up," *Spine (Phila. Pa. 1976)*, vol. 32, no. 9, pp. 1012–1018, 2007.
- [11] Z. Mo, Y. Zhao, C. Du, Y. Sun, M. Zhang, and Y. Fan, "Does Location of Rotation Center in Artificial Disc Affect Cervical Biomechanics?," *Spine (Phila. Pa. 1976)*, vol. 40, no. 8, pp. E469–E475, 2015.
- [12] S. H. Lee, Y. J. Im, K. T. Kim, Y. H. Kim, W. M. Park, and K. Kim, "Comparison of cervical spine biomechanics after fixed- and mobile-core artificial disc replacement: A finite element analysis," *Spine (Phila. Pa. 1976)*, vol. 36, no. 9, pp. 700–708, 2011.
- [13] P. R. van den Broek, J. M. Huyghe, K. Ito, "Biomechanical Behavior of a Biomimetic Artificial Intervertebral disc," *Spine (Phila. Pa. 1976)*, vol. 37, no. 6, pp. E367--373, Mar. 2012.
- [14] P. R. van den Broek, J. M. Huyghe, W. Wilson, and K. Ito, "Design of next generation total disk replacements," *J. Biomech.*, vol. 45, no. 1, pp. 134–140, Jan. 2012.
- [15] C. A. M. Jacobs et al., "Biomechanical evaluation of a novel biomimetic artificial intervertebral disc in canine cervical cadaveric spines," *Manuscr. Submitt. Publ.*, 2022.
- [16] N. Žuržul, A. Ilseng, V. E. Prot, H. M. Sveinsson, B. H. Skallerud, and B. T. Stokke, "Donnan contribution and specific ion effects in swelling of cationic hydrogels are additive: Combined high-resolution experiments and finite element modeling," *Gels*, vol. 6, no. 3, pp. 1–20, 2020.
- [17] N. Yoganandan, F. A. Pintar, J. Zhang, and J. L. Baisden, "Physical properties of the human head: Mass, center of gravity and moment of inertia," *J. Biomech.*, vol. 42, no. 9, pp. 1177–1192, Jun. 2009.
- [18] ASTM F2346-05, "Standard Test Methods for Static and Dynamic Characterization of Spinal Artificial," 2012.
- [19] R. Arshad, H. Schmidt, M. El-Rich, and K. Moglo, "Sensitivity of the Cervical Disc Loads, Translations, Intradiscal Pressure, and Muscle Activity Due to Segmental Mass, Disc Stiffness, and Muscle Strength in an Upright Neutral Posture," *Front. Bioeng. Biotechnol.*, vol. 10, no. April, pp. 1–11, 2022.
- [20] T. Whyte, J. B. Barker, D. S. Cronin, G. A. Dumas, L. P. Nolte, and P. A. Cripton, "Load-sharing and kinematics of the human cervical spine under multi-axial transverse shear loading: Combined experimental and computational investigation," *J. Biomech. Eng.*, vol. 143, no. 6, 2021.

- [21] J. Y. Choi and K. H. Sung, "Subsidence after anterior lumbar interbody fusion using paired stand-alone rectangular cages," *Eur. Spine J.*, vol. 15, no. 1, pp. 16–22, Feb. 2006.
- [22] M. F. Eijkelkamp, J. M. Huyghe, C. C. van Donkelaar, J. R. van Horn, A. G. Veldhuizen, and G. J. Verkerke, "Requirements for an artificial intervertebral disc," *Int. J. Artif. Organs*, vol. 24, no. 5, pp. 311–321, 2001.
- [23] ASTM, "Standard Specification for Rigid Polyurethane Foam for Use as a Standard Material for Testing Orthopaedic Devices and Instruments. ASTM F1839-08," ASTM International, vol. 15, p. 6, 2016.
- [24] C. M. Vives-Torres et al., "Comparison of Upper Neck Loading in Young Adult and Elderly Volunteers During Low Speed Frontal Impacts," *Front. Bioeng. Biotechnol.*, vol. 9, p. 682974, 2021.
- [25] J. R. Funk, J. M. Cormier, C. E. Bain, H. Guzman, E. Bonugli, and S. J. Manoogian, "Head and Neck loading in everyday and vigorous activities," *Ann. Biomed. Eng.*, vol. 39, no. 2, pp. 766–776, Feb. 2011.
- [26] J. Schindelin et al., "Fiji: An open-source platform for biological-image analysis," *Nat. Methods*, vol. 9, no. 7, pp. 676–682, Jun. 2012.
- [27] A. J. Van der Veen, A. Bisschop, M. G. Mullender, and J. H. van Dieën, "Modelling creep behaviour of the human intervertebral disc," *J. Biomech.*, vol. 46, no. 12, pp. 2101–2103, Aug. 2013.
- [28] N. Bogduk and S. Mercer, "Biomechanics of the Cervical Spine. I: Normal kinematics," *Clin. Biomech.*, vol. 15, pp. 633–648, 2000.
- [29] S. P. Moroney, A. B. Schultz, and J. A. A. Miller, "Analysis and measurement of neck loads," *J. Orthop. Res.*, vol. 6, no. 5, pp. 713–720, Sep. 1988.
- [30] J. M. Barrett, C. McKinnon, and J. P. Callaghan, "Cervical spine joint loading with neck flexion," *Ergonomics*, vol. 63, no. 1, pp. 101–108, Jan. 2020.
- [31] S. Kumaresan, N. Yoganandan, F. A. Pintar, D. J. Maiman, and V. K. Goel, "Contribution of disc degeneration to osteophyte formation in the cervical spine: a biomechanical investigation," *J. Orthop. Res.*, vol. 19, pp. 977–984, 2001.
- [32] S. P. Moroney, A. B. Schultz, A. A. J. Miller, and G. B. J. Andersson, "Load-displacement properties of lower cervical spine motion segments," *J. Biomech.*, vol. 21, no. 9, pp. 769–779, 1988.
- [33] Yoganandan, S. Kumaresan, and F. A. Pintar, "Biomechanics of the cervical spine Part 2. Cervical spine soft tissue responses and biomechanical modeling," *Clin. Biomech.*, vol. 16, no. 1, pp. 1–27, 2001.
- [34] I. LDR Spine USA, "Summary of Safety and Effectiveness Data Mobi-C," 20013.
- [35] I. Globus Medical, "Summary of Safety and Effectiveness Data: Prestige LP," pp. 1–18, 2012.
- [36] FDA, "Summary of Safety and Effectiveness Data - SECURE C," U.S. Food Drug Adm., p. 39, 2007.
- [37] NuVasive, "summary of safety and effectiveness data: PCM," 2012.
- [38] I. Spinal Kinetics, "Summary of safety and effectiveness data M6-C."
- [39] M. Navarro, A. Michiardi, O. Castaño, and J. A. Planell, "Biomaterials in orthopaedics," *Journal of the Royal Society Interface*, vol. 5, no. 27. The Royal Society, pp. 1137–1158, 06-Oct-2008.
- [40] N. Newell, G. Grigoriadis, A. Christou, D. Carpanen, and S. D. Masouros, "Material properties of bovine intervertebral discs across strain rates," *J. Mech. Behav. Biomed. Mater.*, vol. 65, no. June 2016, pp. 824–830, 2017.
- [41] N. Newell, D. Carpanen, G. Grigoriadis, J. P. Little, and S. D. Masouros, "Material properties of human lumbar intervertebral discs across strain rates," *Spine J.*, vol. 19, no. 12, pp. 2013–2024, 2019.
- [42] F. Cornaz, J. Widmer, N. A. Farshad-Amacker, J. M. Spirig, J. G. Snedeker, and M. Farshad, "Biomechanical Contributions of Spinal Structures with Different Degrees of Disc Degeneration," *Spine (Phila. Pa. 1976)*, vol. 46, no. 16, pp. E869–E877, 2021.
- [43] N. V. Jaumard, W. C. Welch, and B. A. Winkelstein, "Spinal facet joint biomechanics and mechanotransduction in normal, injury and degenerative conditions," *J. Biomech. Eng.*, vol. 133, no. 7, pp. 071010 (1–31), 2011.

- [44] J. J. Yue, R. Bertagnoli, P. C. McAfee, and H. S. An, "Motion Preservation Surgery of the Spine: Advanced Techniques and Controversies," *Am. J. Neuroradiol.*, vol. 30, no. 9, pp. E134–E134, Oct. 2008.
- [45] ASTM, "Standard Test Method for Measuring Load Induced Subsidence of Intervertebral Body Fusion Device Under Static Axial Compression 1," no. Reapproved 2011. pp. 1–7, 2014.
- [46] B. Berg-Johansen, A. J. Fields, E. C. Liebenberg, A. Li, and J. C. Lotz, "Structure-function relationships at the human spinal disc-vertebra interface," *J. Orthop. Res.*, vol. 36, no. 1, pp. 192–201, Jun. 2017.
- [47] K. Wade, Chapter 8 - Vertebral Endplates. Elsevier Ltd., 2018.
- [48] C. K. Lee, "Osteopenia and Total Disc Prosthesis Subsidence: Inclusion/Exclusion Criteria for Total Disc Replacement," *SAS J.*, vol. 1, no. 2, pp. 82–84, 2007.
- [49] J. Lou, H. Liu, X. Rong, H. Li, B. Wang, and Q. Gong, "Geometry of inferior endplates of the cervical spine," *Clin. Neurol. Neurosurg.*, vol. 142, pp. 132–136, 2016.
- [50] M. Thaler, S. Hartmann, M. Gstöttner, R. Lechner, M. Gabl, and C. Bach, "Footprint mismatch in total cervical disc arthroplasty," *Eur. Spine J.*, vol. 22, no. 4, pp. 759–765, 2013.
- [51] S. Karaca, A. O. Akpolat, A. Oztermeli, M. N. Erdem, and M. Aydogan, "Discrepancy between cervical disc prostheses and anatomical cervical dimensions," *Acta Orthop. Traumatol. Turc.*, vol. 50, no. 5, pp. 544–547, 2016.
- [52] A. G. Au, A. K. Aiyangar, P. A. Anderson, and H. L. Ploeg, "A new bone surrogate model for testing interbody device subsidence," *Spine (Phila. Pa. 1976)*, vol. 36, no. 16, pp. 1289–1296, 2011.
- [53] P. P. A. Vergroesen, K. S. Emanuel, M. Peeters, I. Kingma, and T. H. Smit, "Are axial intervertebral disc biomechanics determined by osmosis?," *J. Biomech.*, vol. 70, pp. 4–9, Mar. 2018.
- [54] D. H. Cortes, N. T. Jacobs, J. F. DeLucca, and D. M. Elliott, "Elastic, permeability and swelling properties of human intervertebral disc tissues: A benchmark for tissue engineering," *J. Biomech.*, vol. 47, no. 9, pp. 2088–2094, Jun. 2014.
- [55] A. J. van der Veen, M. Mullender, T. H. Smit, I. Kingma, and J. H. van Dieën, "Flow-related mechanics of the intervertebral disc: the validity of an *in vitro* model," *Spine (Phila. Pa. 1976)*, vol. 30, no. 18, pp. 534–539, 2005.
- [56] G. D. O'Connell, N. T. Jacobs, S. Sen, E. J. Vresilovic, and D. M. Elliott, "Axial creep loading and unloaded recovery of the human intervertebral disc and the effect of degeneration," *J. Mech. Behav. Biomed. Mater.*, vol. 4, no. 7, pp. 933–942, Oct. 2011.
- [57] P. P. A. Vergroesen, A. J. van der Veen, K. S. Emanuel, J. H. van Dieën, and T. H. Smit, "The poroelastic behaviour of the intervertebral disc: A new perspective on diurnal fluid flow," *J. Biomech.*, vol. 49, no. 6, pp. 857–863, Apr. 2016.
- [58] M. Krijnen, D. Mensch, J. Van Dieen, P. Wuisman, and T. Smit, "Primary spinal segment stability with a stand-alone cage: *In vitro* evaluation of a successful goat model," *Acta Orthop.*, vol. 77, no. 3, pp. 454–461, 2006.
- [59] M. Yang, D. Xiang, S. Wang, and W. Liu, "*In vitro* Studies for Investigating Creep of Intervertebral Discs under Axial Compression: A Review of Testing Environment and Results," *Materials*, vol. 15, no. 7. Multidisciplinary Digital Publishing Institute (MDPI), p. 2500, 28-Mar-2022.
- [60] E. Salzer, V. H. M. Mouser, M. A. Tryfonidou, and K. Ito, "A bovine nucleus pulposus explant culture model," *J. Orthop. Res.*, vol. 40, no. 9, pp. 2089–2102, 2022.
- [61] S. S. Sivan et al., "Injectable hydrogels with high fixed charge density and swelling pressure for nucleus pulposus repair: Biomimetic glycosaminoglycan analogues," *Acta Biomater.*, vol. 10, no. 3, pp. 1124–1133, 2014.
- [62] B. G. M. Van Dijk, E. Potier, and K. Ito, "Long-term culture of bovine nucleus pulposus explants in a native environment," *Spine J.*, vol. 13, no. 4, pp. 454–463, Apr. 2013.
- [63] C. P. L. Paul et al., "Simulated-physiological loading conditions preserve biological and mechanical properties of caprine lumbar intervertebral discs in *ex vivo* culture," *PLoS One*, vol. 7, no. 3, p. e33147, Mar. 2011



Chapter 7

General discussion

7.1 General discussion

Cervical disc replacement (CDR) prostheses have been developed in recent years as an alternative treatment for severe disc degeneration. The rationale of CDR is to replace the diseased intervertebral disc while preserving motion, thereby reducing the risk of adjacent segment disease. A remaining challenge in the development of these implants is to ensure that the kinematics are restored as close as possible to avoid surrounding tissues and anatomical structures from compensating, and the subsequent pathologies related to this. In this thesis, a biomimetic artificial intervertebral disc (bioAID) was further developed by optimizing both the biomaterials and biomechanical properties to better replicate the biomechanics of the natural disc. This chapter provides an overview of the main findings, remaining challenges, future research directions and overall conclusion of this thesis.

7.1.1 *Main findings and implications*

In **Chapter 2**, an overview is given of all the viscoelastic total disc replacements that are currently on the market. In this chapter, the design of each of these devices were categorized based on their characteristics and reviewed for their design related advantages and disadvantages. The biggest advantage of using viscoelastic devices is that these implants preserve motion based on deformation, similar to what is seen for a natural disc. Another advantage is that most of these viscoelastic implants have a variable center of rotation (COR), making them less prone to mispositioning, and reducing the risk of facet overloading. However, a potential risk of these viscoelastic devices is that there is limited long-term clinical data available of these viscoelastic materials. Currently, only standardized testing methods are used to compare material characteristics of newly developed implants with clinically available prostheses. However, these testing methods are often based on assessing ball-and-socket devices, and thus are not always applicable to these second-generation viscoelastic devices.

As already indicated in chapter 2, many of the materials and how they are used in these new generation implants do not have an extensive history in orthopedics. This is also the case for the knitted ultra-high-molecular-weight-polyethylene (UHMWPE) fabric that forms the outer part of the bioAID. To further develop the design of this fiber jacket, several different textile structures and assembly configurations were assessed in **Chapter 3**. Four different stitch patterns were assessed for their suitability within the bioAID, namely 2x1 lapping, 1x1 lapping, 2x1 lapping with pillar stitch and 1x1 lapping with pillar stitch. Both fabric mechanical properties and complete device mechanical properties showed to be most favorable for four layers of the 2x1 lapping configuration. Although both isolated fabric and complete device properties were investigated, this study did not give a full picture of the jacket's performance under different spinal movements.

As stated in the introduction, it is hypothesized that the combination of the fiber jacket and hydrogel give the bioAID its load bearing capacity and semi-constrained motion. Therefore, in **Chapter 5** the kinematic behavior of the bioAID was assessed in cadaveric spines and compared it to the intact condition and to the gold standard anterior cervical discectomy and fusion (ACDF) procedure. This is of interest since the main rationale of using the biomimetic design is to better replicate the kinematic behavior of a natural disc. In this study, it was shown that, unlike fusion, the bioAID could indeed replicate the sigmoid moment-rotation curves as seen for a natural disc. These results indicated that the bioAID can provide motion based on deformation, and that this is most likely related to the symbiotic relationship between the hydrogel and jacket. Although the results shown in chapter 5 were very promising, the kinematic behavior in axial rotation was substantially different compared to the intact situation. The main reason was thought to be the absence of osseointegration, required to transfer the rotational and shear loads through the jacket and hydrogel. These results already indicated the importance of osseointegration between the jacket and adjacent vertebral bodies to replicate the biomechanical behavior.

It is the UHMWPE textile surface which is exposed at the bone-implant interface. However, UHMWPE is known to be inert and hydrophobic, and thus unsuitable to facilitate bone ingrowth. Therefore, in **Chapter 4**, several different surface modifications were assessed to increase the jacket's osteoconductive potential. The combination of including hydroxyapatite (HA) with plasma treatment was found to be most optimal for facilitating bone ingrowth. Although *in vitro* models are extensively used as a first screening method to assess biological responses, it will never provide a full answer. Therefore, animal trials should be carried out to confirm that this surface modification is sufficient to facilitate osseointegration.

In **Chapter 6**, the latest design of the bioAID was evaluated based on several biomechanical parameters, namely compressive strength, shear-compressive strength, risk of subsidence and risk of device expulsion. The results were very promising in comparison with mechanical data of the natural intervertebral disc reported in literature, indicating the design is mechanically safe and there is a low risk of migration. In addition, one of the unique features of the bioAID, is its capability to replicate the poroelastic properties seen in a natural disc. Therefore, in this chapter, the viscoelastic and poroelastic characteristics were also investigated under a diurnal loading pattern. The observations in this study indicate that the hydrogel composition can closely replicate the Donnan osmotic pressure and resultant poroelastic properties as seen in natural discs.

7.1.2 *Remaining challenges and future research perspectives*

7.1.2.1 *Design optimizations*

The aim of this biomimetic design was to replace each natural component with a synthetic one to better replicate the biomechanics of the native situation. Although the current thesis has shown promising results, several design optimizations steps are still needed.

Fiber jacket

In the current design, the fiber jacket is one knitted stocking, so it does not replicate the lamellar structure with altering fiber orientations per layer as seen in the annulus fibrosus. However, due to twisting of the jacket, there will be a slight alteration in textile structure orientation per layer. Moreover, only four different knitting patterns were assessed in this thesis, all being relatively simple structures while the annulus fibrosus is a complex structure [1]. The usage of more advanced textile techniques could be used to achieve more biomimicry, but would also increase complexity, costs, and availability. In this thesis, UHMWPE yarns were used to create the jacket component. Although other yarns could be used within this application, it is believed that the UHMWPE yarn is suitable due to its excellent strength and abrasion resistance [2]. Nevertheless, in the current design of the bioAID, the jacket is a tube that is wrapped multiple times around the hydrogel. As a result, the separate UHMWPE textile layers could rub against each other during spinal movements when there is no osseointegration yet, potentially causing wear debris. Previous research on the 3D-F implant, made solely out of UHMWPE fibers, did not observe any wear debris both *in vitro* after 63 million cycles and *in vivo* up to 24 months [3]–[5]. Nevertheless, due to differences in the design, it is suggested to assess the wear characteristics of the bioAID under different spinal motions.

Hydrogel

The combination of the hydrogel and jacket give the bioAID its unique biomechanical properties. As shown in this thesis, the hydrogel encapsulated within the jacket results in similar stiffness and creep characteristics as a natural disc. Moreover, it shows non-linear behavior under different ranges of motion within the cervical spine. The most unique feature of the bioAID is that the current hydrogel composition can closely mimic the time-dependent viscoelastic and poroelastic properties observed within a natural disc. To the best of our knowledge, this is the first synthetic disc replacement that not only preserves the range of motion (ROM) but also replicates the time-dependent biomechanics. An additional benefit of the swelling hydrogel, is that the device can be implanted unswollen, reducing the risk of over distracting the disc space that could induce laxity in surrounding muscles and ligaments. Despite these promising results, the hydrogel is also the main weak spot in the design. The

hydrogel has not been evaluated for its long-term behavior and mechanical safety under combined loading conditions. Therefore, continued efforts are needed to assess all failure mechanisms of the hydrogel, such as durability testing under various loading conditions. To improve the mechanical stability of the hydrogel, the current polymer ratio and cross-linker density could be adjusted and/or using other reinforcement materials. In this research, polyurethane foam was used as reinforcement of the hydrogel. Many other possibilities are described in literature, such as fiber reinforcement using polyethylene terephthalate (PET) within a poly(2-hydroxyethyl methacrylate)-poly(methyl methacrylate) (PHEMA-PMMA) hydrogel, shown to result in high endurance and long-term resistance to compressive creep [6], [7]. Another example previously reported is a carrageenan gel-infused polycaprolactone scaffold assessed as nucleus replacement [8]. Lastly, changing the structure of the foam by for example, 3D printed polyurethane or using a polyurethane foam with different pore sizes, could also be used to adjust the mechanical strength [9], [10].

Endplate

The last component within the design is the endplate, which merely serves as a fixation method to assure stability between the adjacent vertebral bodies. During the course of this thesis, multiple design iterations have been tested (not reported), which were mainly based on optimizing the implantation procedure. In the latest design, a kidney shaped ring was 3D printed (0.3 mm thick) out of titanium alloy (TiAlV) with two keels. Although the ring is covered with multiple layers of jacket, the keels are in direct contact with the adjacent vertebrae. Therefore, the usage of titanium alloy is beneficial to stimulate the osseointegration of the keels to the adjacent vertebral bodies [11]. Moreover, the 3D printing method allows to scale up the production process. A potential disadvantage of 3D printing at such small scales (0.3 mm thickness) is that it can affect the mechanical stability of the construct, which has not been assessed in this thesis. The purpose of the endplate is, however, not to carry load, but only to serve as a connection between the implant and adjacent vertebral bodies. During the implantation, a 0.65 mm wide channel is drilled in the adjacent vertebral bodies to be able to slide the bioAID into the disc space, in which the two centrally positioned keels of the endplate are used for correct positioning. To prevent ventral expulsion, the anterior keels (1.3 mm) are slightly thicker than the posterior keels (1 mm). To further reduce the expulsion risk, hydroxyapatite particles could be used to fill up the remaining empty channel or a synthetic flexible anterior ligament could be designed. The disadvantage is that it will increase complexity and surgery time. Based on the data presented within this thesis, the final design of the endplate seems suitable to preserve stability between the adjacent vertebral bodies.

Production procedure

In the current assembly procedure, the twisting of the tubular jacket serves as the main method for holding the different components together. As a result, the amount of tensioning of the jacket plays a large role in the degree of movement possible between the different components. This lack of integration/bonding between the three components might form a potential failure mechanism and can affect the consistency. However, based on all the gathered data within this thesis, it seems that even though there is no bonding between the components, it can still provide motion in a similar manner as the intact condition and can withstand physiological mechanical loads. Moreover, only little differences are (described by the standard deviations) observed between the manual assembled samples under various loading conditions. Another challenge that remains to be solved due to the current manual assembly procedure is its scalability. At the moment, the membrane, fiber jacket and endplate are produced in a scalable manner. Only the hydrogel is manually prepared but could be easily automated by using an injection molding process. However, the assembly of all separate components into one device remains manual. The critical steps in this assembly procedure are the twisting of the jacket to create multiple layers and the suture closure of the jacket.

To make the twisting redundant, the way the multiple layers are currently created could be adjusted. A possible solution would be as described for the 3D-F, where a very complex textile technology was utilized to create a complete fibrous implant without the need of intermediate steps [12]. The disadvantage of this production procedure is that damage of one yarn could lead to disintegration of the complete device. Moreover, by increasing the complexity of the production procedure, the associated production time and costs will increase as well. Another option would be to use an electrospinning process to immediately cover the hydrogel. As a consequence, a different yarn needs to be utilized, resulting in a lot of optimization steps. Another approach, shown to be successful as a biomimetic cartilage replacement, is the usage of a spacer fabric, where a similar Donnan osmotic principle was achieved by incorporating the hydrogel within the spacer fabric [13]. A potential problem within this design is the incorporation of a primary fixation component.

To keep the twisting during assembly, some sort of robotic tool that does the twisting in a controlled and automated manner could be created, ruling out any variations introduced by the manual assembly. To improve the closure of the jacket, a purse string suture principle could be utilized within the design to reduce the thickness of the suture knot. Another potential solution is to create a similar concept as seen for the NeoDisc, where fabric flanges are used as anterior plates to fixate the device between the vertebral bodies.

Geometry

In this thesis, only one size was designed for the human application and one size for the canine application. However, as seen for all commercially available CDR devices, multiple sizes are available to best match the disc space of the patient [14]–[18]. The dimensions of the implant, and its fit within the disc space can influence the final behavior of the bioAID. For this reason, testing the smallest version, assumed as the worst-case-scenario, is therefore suggested by the FDA to assure proper functioning of all sizes [19]. Eventually, after finalizing the design, it would be desirable to produce multiple sizes of the bioAID and test the smallest version.

The initial prototype was designed for the lumbar region [20], however, based on based on clinical need, market size (two thirds of global disc market is cervical based on GMInsights Market Research Group, 2020) and interest of industry and clinicians, the bioAID in this thesis was evaluated for the cervical region. To achieve this, the initial prototype was mainly downscaled to fit the cervical region in terms of dimensions, while the intervertebral disc anatomy in the cervical region slightly differs from lumbar region [21], [22]. The biggest difference is that the cervical vertebrae are curved in the sagittal plane [21]. To better match with the physiological curvature in the cervical disc, a wedged shape hydrogel could be produced, such as is seen within the Freedom implant [23]. This could enhance the fit within the disc space, maintain the lordosis, and improve the contact area with the adjacent vertebral bodies.

7.1.2.2 Osseointegration

Previous research of Peter van den Broek et al. (2012) already highlighted the importance of anchoring the fibers to the bone to replicate natural motion [20]. Therefore, in the present thesis, one of the goals was to investigate several surface modifications that would control bone ingrowth. Controlling bone ingrowth refers to the ability to selectively facilitate osseointegration on the cranial and caudal sides of the device, while bone formation would be inhibited on the lateral sides. Based on the *in vitro* data, it was seen that the HA loaded fibers in combination with plasma treatment were most suitable to facilitate osseointegration. The issue then remained how to introduce this knowledge within the bioAID design. Two different options are proposed, both having advantages and disadvantages. The first option would be to produce tubular fiber jackets with the 10 % HA loaded fiber, whereafter assembly only the cranial and caudal surfaces are plasma treated. This will result in increased hydrophilicity, and increased exposure of HA at the cranial and caudal surface compared to the lateral surfaces. The advantage is that the production procedure is preserved, which is beneficial for the scalability and production costs. Nevertheless, there is a risk of bone deposition at the lateral sides due to the presence of HA particles. In the worst-case-scenario,

this could lead to a reduced ROM and ultimately a complete fusion. For the patient, pain will still be relieved and clinical outcomes are often preserved on the short term [24], [25]. However, on the long term, the lack of motility can lead to adjacent segment disease which is the main rationale of performing a motion preserving surgery. A possible, but more complex option would be to use untreated UHMWPE fibers to knit the jacket, then embroider 10 % HA fibers on the cranial and caudal side of the bioAID after assembly, whereafter only the cranial and caudal sides are plasma treated. In this way, the risk of facilitating bone ingrowth on lateral sides is limited due to the hydrophobic and inert nature of untreated UHMWPE. However, this adds an extra step, complicating the production procedure, production time and associated costs. Moreover, only the top layer of the jacket will contain HA particles, potentially limiting the bone anchorage into the underlying jacket layers.

These proposed design alterations are purely based on *in vitro* obtained data, using a highly simplified 2D set-up, while previous research has shown that there is a poor correlation between *in vitro* and *in vivo* testing of biomaterials [26]. Usage of more physiological 3D model could be a promising alternative approach for evaluating the performance of these surface modifications. A disadvantage is that this would lead to more complexity and more parameters that could influence the outcome. Although *in vitro* testing is useful to get more insight on the initial biological response of the material, it will never provide a complete insight into the *in vivo* response, including the mid and long-term *in vivo* response of surrounding tissue. As a result, animal testing remains an essential final step in gaining a better understanding of the materials biological response.

Within the current project, an *in vivo* study using canines has been planned. Although multiple studies have suggested that canines are a suitable animal model, there are also some limitations [27], [28]. Previous research has shown that quadrupeds have a higher bone mineral density, and thus have stronger vertebrae compared to humans [27]. As a result, the amount of subsidence could be underestimated when tested in canines. In relation to this, some studies have suggested that the disc also experiences higher loads in quadrupeds than in humans [29]. This has also been reported as one of the reasons why bone fusions are often successful in canine models but fail in humans. Caution is therefore advised when interpreting *in vivo* data obtained using animal models.

7.1.2.3 Biocompatibility and sterilization

Before the bioAID can be implanted *in vivo*, it is important to ensure that none of the materials elicit an undesirable inflammatory response. Both the UHMWPE yarn and UHMWPE membrane are of medical grade and have proven to be biocompatible and sterilizable in

several ways [30]. The endplate was 3D printed using medical grade TiAlV which is commonly used in orthopedic devices [31]. Therefore, the HEMA-NaMA hydrogel is the only critical component that could potentially form a problem. Fortunately, the intervertebral disc has no synovial tissue, which contains synoviocytes, being the primary source of cytokines in peripheral joints [32]. Hence, a large inflammatory response of any debris is not expected. To further reduce the risk of eliciting a foreign body response, the hydrogel is encapsulated in the UHMWPE membrane, shown to be able to contain all hydrogel particles under high static compressive loadings. It is, however, unknown if the membrane will also stay intact when exposed to various combined loadings present in the spine. As such, it is desirable to ensure biocompatibility of the hydrogel in case of a membrane rupture. All the components of the hydrogel have been previously used in biomedical applications. Polyurethane foam has been widely employed as wound dressings and proven to be biocompatible, although only for external use [33], [34]. HEMA together with PeGdiMa as cross-linker is a frequently reported hydrogel for biomedical applications, such as for contact lenses [35]–[37]. Park et al. (2005) showed good biocompatibility, both *in vitro* and *in vivo*, of HEMA-NaMA hydrogels using PEGdiMa and ammonium persulfate as cross-linker and initiator respectively [38]. In addition, a preliminary study has previously been performed where murine fibroblasts (L929) were cultured in the presence of the HEMA-NaMA hydrogel. After 24 hours, cell viability was evaluated showing 91.5 % mean cell viability, indicating there was no cytotoxic effect. Therefore, biocompatibility is not expected to be a problem.

Another critical point of using a hydrogel is that conventional sterilization procedures are known to affect the mechanical, physical, and chemical properties [39]. There are two possible processes to sterilize the implant, either by aseptic processing or by terminal sterilization. By aseptic processing, each individual component is sterilized whereafter the assembly is performed in a sterile environment (e.g. safety cabinet). The disadvantage is that this requires multiple steps that are not required when using a terminal sterilization procedure. Therefore, terminal sterilization is preferred, where the implant is sterilized after assembly. Two things are important for determining the sterilization method. First of all, the sterilization process should remove micro-organisms to meet the sterilization process assurance level [40]. When using a terminal sterilization procedure, this means that the sterilization method should be able to penetrate through the center of the implant. Secondly, it should not lead to severe loss of mechanical and structural properties of the device.

During this project, the influence of gamma irradiation and autoclaving on the mechanical properties of hydrogel were examined in a preliminary study. Although both treatments introduced some variation in the swelling behavior and compressive strength of the hydrogel,

the differences were most severe for gamma irradiation. As a next step, ethylene oxide and autoclavation were evaluated for their influence on the mechanical properties of the complete device. Minor differences were observed, favoring ethylene oxide sterilization. As a preliminary validation for sterility, ethylene oxide sterilized implants, intact and deconstructed, were put on culture and assessed for the presence of aerobic bacteria, anaerobic bacteria, yeast and fungi. Results confirmed that both intact and individual components were uncontaminated. While these findings help to bring this novel design closer to the clinical application, additional work should be carried out to establish and validate the entire sterilization process, including packaging, and confirmation of the hydrogel's biocompatibility.

7.1.3 Restoring the biomechanical properties

The design of the bioAID is based on the hypothesis that mimicking the natural structure of the intervertebral disc would lead to biomechanical properties comparable to the native disc, thereby improving clinical outcome, and reducing the risk of adjacent segment disease compared to first generation prostheses. First generation prostheses preserve motion but do this in a substantially different manner than what has been seen for native disc, giving rise to similar long-term complications as the golden standard ACDF procedure [41], [42]. This raises the question if preserving motion that is not physiological is just as undesirable as blocking the motion with fusion. Several reports have shown that the clinical outcomes between ACDF surgery and total disc replacements were statistically equivalent on the short-to-mid-term [24], [43], [44]. However, in the long-term, more studies have shown improved outcomes for disc replacements [45]–[48]. It is also often argued that this could be the result of a preexisting disease instead of being caused by a postoperative biomechanical alteration [49]. Most likely, the etiology of adjacent segment disease is multifactorial, where both preexisting diseases and biomechanical alterations play a role.

To elucidate how physiological motion preservation implants could reduce the incidence of adjacent segment disease, long-term clinical data is required. Based on current literature, second generation prostheses that contain an elastomer have shown to better reproduce the intact segment behavior compared to metal-on-metal and metal-on-polymer designs [50]. Moreover, a systematic review and meta-analysis also verified that *in vivo* only the Bryan disc, being a monobloc design with elastomer, did not shift the center of rotation while all other metal-on-metal or metal-on-polymer designs did [51]. However, the effect of these biomechanical alterations on the long-term outcome between first-generation and second-generation designs is lacking. One study of Coban et al. (2021) found that metal-on-metal designs resulted in a significant higher incidence of adjacent segment disease compared to metal-on-polymer designs (Bryan and Mobi-C) [52]. This was assumed to be attributed to the

difference in mechanical properties, with the metal-on-metal having higher modulus and stiffness that could have potentially led to increased stresses at the adjacent segments.

For the bioAID, only the initial kinematic behavior in canine spines could be investigated. Although similarities with the intact condition were found, these *ex vivo* experiments cannot provide a full replication of the complex and irregular loading conditions within the spine. As a result, *in vivo* testing remains an essential final step in gaining a better understanding of the performance of the bioAID during long-term repetitive loading under physiological conditions. As planned within the project, assessing the biomechanical behavior after implantation in canines would be very useful to get more insight on how the inclusion of muscle tension, bone ingrowth and complete physiological movements influence the performance of the bioAID. The usage of canine model instead of other large animals, such as sheep and goats, has as a benefit that canines are also a potential patient group that could be targeted. Several canine breeds are known to suffer from disc degeneration and are often treated with (smallest) human fusion cages [53]. Commercialization within the veterinary market could therefore be a promising first step. In the current project, the first two animals have been implanted with the bioAID. Although the aim of this *in vivo* study was not to assess biomechanical performance but to investigate the bone ingrowth on the cranial and caudal surface, unfortunately, one week after implantation failure of the hydrogel became apparent. This emphasizes that besides characterizing the kinematics, other mechanical parameters need to be investigated to ensure clinical safety.

Currently, mainly standardized testing methods using unphysiological loading regimes are reported in the summary of safety and effectiveness reports required by the Food and Drug Administration (FDA) for gaining market approval. As it is hypothesized that preserving physiological motion is more important than preserving motion alone, more physiological testing regimes should be included. As frequently reported in literature, unphysiological motions can often be identified through their COR or facet joint forces. It is therefore suggested to include such parameters in the standardized testing procedures that are currently available. In the current thesis, several mechanical tests have been performed, showing promising results in withstanding physiological (shear)-compressive forces while providing primary stability between the vertebral bodies. Nevertheless, these tests were not sufficient to predict the observed failure of the hydrogel. The failure mechanism is unknown but is hypothesized to be a result of a combination of different stresses applied to the implant which were not replicated in the performed laboratory tests. It is suggested to further investigate the compression-shear failure mechanism of the hydrogel and complete device to identify potential problems under this loading regime, especially since the shear-compression

test set-up in this thesis was limited to test until 100 N. Based on these results, new hydrogel configurations, such as described in the hydrogel paragraph should be explored to avoid this from recurring.

Although several studies have shown close resemblance in biomechanics between canine and humans, most of the experiments were compared with data for human application, while the level of activity and associated stresses might be different within canines [27], [54], [55]. Besides differences in biomechanics, there are also important anatomy related differences. Canines have epiphyseal surfaces that are slightly concave at both cranial and caudal vertebrae, while humans have slightly convex caudal vertebrae and slightly concave cranial vertebrae [56]. However, it is expected that this difference will not have a large effect on the outcome, since the swelling and thus osmotic pressure forces the AID to the vertebrae irrespective of the shape. Finite element simulations might be a promising tool to evaluate the effects of variations in the design while replicating the complex kinematics of the spine and could help to assess potential failure mechanisms. A difficulty in using finite element simulations remains the validation with real life experiments, as well as the amount of detail in the model required to make reliable conclusions. As an alternative method, assessing the kinematic behavior when implanted *in vivo* using imaging modalities, such as CT, could be useful to further elucidate the kinematics.

Although the current design failed after a short period of time, durability and fatigue tests are also recommended. Previous research on the lumbar version of the bioAID reported that fatigue loading seemed to alter the creep response of the bioAID [20]. As a lot of design changes have been made, it is required to reassess the fatigue and durability of the implant and its effects on the functionality of the bioAID.

7.1.4 Trade-off between biomimicry and translational potential

The trade of between complexity and simplicity is an often-reported subject of discussion. On one hand, replicating the native situation as close as possible is beneficial to decrease the risk of altering the loading pattern in the spine and thereby the risk of adjacent segment disease. However, this often goes hand in hand with introducing more and more complexity, which will also result in decreasing the translational potential. By increasing the complexity, the ease of manufacturing, costs and availability will be affected in a negative manner. To be as close as possible to the natural situation, tissue engineering approaches are the most optimal research direction [57]. However, the current state of tissue engineered intervertebral discs is still far from the clinical application [57]. A synthetic biomimetic approach, such as the one presented

in this thesis, is therefore a promising intermediate step to improve the treatment of patients with severely degenerated discs.

7.2 Conclusion

The goal of this thesis was to contribute to the development of a novel biomimetic artificial disc replacement for treating severely degenerated discs of the cervical spine. In the first part of this thesis, the design of the jacket structure and its bioactivity have been optimized to recreate, as close as possible, the native anatomical structure while facilitating osseointegration. In the second part, the biomechanical characteristics of this device have been evaluated, shown to withstand various human physiological loading conditions while providing sufficient stability, and similar kinematics. Altogether, it can be concluded that the biomimetic concept has proven to be a promising alternative disc replacement device that does not only preserve mobility, but also the non-linear and time-dependent properties observed for a natural disc. Whether this novel disc replacement prosthesis will indeed result in lower incidence of adjacent segment disease needs additional research and long-term clinical trials.

References

- [1] M. A. Adams, "Intervertebral Disc Tissues," in *Mechanical properties of aging soft tissues*, Springer International Publishing Switzerland, 2015, pp. 7–35.
- [2] R. Kirschbaum and J. L. J. van Dingenen, "Advances in gel-spinning technology and Dyneema fiber applications," in *Integration of Fundamental Polymer Science and Technology—3*, Springer, Dordrecht, 1989, pp. 178–198.
- [3] K. Kadoya et al., "Biomechanical and Morphologic Evaluation of a Three-Dimensional Fabric Sheep Artificial Intervertebral Disc," *Spine (Phila. Pa. 1976)*, vol. 26, no. 14, pp. 1562–1569, Jul. 2001.
- [4] Y. Kotani et al., "Multidirectional flexibility analysis of cervical artificial disc reconstruction: *in vitro* human cadaveric spine model," *J. Neurosurg. Spine*, vol. 2, no. 2, pp. 188–194, 2005.
- [5] Y. Shikinami, Y. Kotani, B. W. Cunningham, K. Abumi, and K. Kaneda, "A Biomimetic Artificial Disc with Improved Mechanical Properties Compared to Biological Intervertebral Discs," *Adv. Funct. Mater.*, vol. 14, no. 11, pp. 1039–1046, Nov. 2004.
- [6] A. Gloria, R. De Santis, L. Ambrosio, F. Causa, and K. E. Tanner, "A multi-component fiber-reinforced PHEMA-based hydrogel/HAPEXTM device for customized intervertebral disc prosthesis," *J. Biomater. Appl.*, vol. 25, no. 8, pp. 795–810, May 2011.
- [7] A. Gloria, F. Causa, R. De Santis, P. A. Netti, and L. Ambrosio, "Dynamic-mechanical properties of a novel composite intervertebral disc prosthesis," *J. Mater. Sci. Mater. Med.*, vol. 18, no. 11, pp. 2159–2165, Nov. 2007.
- [8] A. H. Chan, P. C. Boughton, A. J. Ruys, and M. L. Oyen, "An interpenetrating network composite for a regenerative spinal disc application," *J. Mech. Behav. Biomed. Mater.*, vol. 65, no. August 2016, pp. 842–848, 2017.
- [9] A. Agrawal, N. Rahbar, and P. D. Calvert, "Strong fiber-reinforced hydrogel," *Acta Biomater.*, vol. 9, no. 2, pp. 5313–5318, Feb. 2013.
- [10] N. Teramoto, O. Shigehiro, Y. Ogawa, Y. Maruyama, T. Shimasaki, and M. Shibata, "Polymer foam-reinforced hydrogels inspired by plant body frameworks as high-performance soft matter," *Polym. J.*, vol. 46, no. 9, pp. 1–6, 2014.
- [11] H. Kienapfel, C. Sprey, A. Wilke, and P. Griss, "Implant fixation by bone ingrowth," *J. Arthroplasty*, vol. 14, no. 3, pp. 355–368, Apr. 1999.
- [12] Y. Shikinami and H. Kawarada, "Potential application of a triaxial three-dimensional fabric (3-DF) as an implant," *Biomaterials*, vol. 19, no. 7–9, pp. 617–635, Apr. 1998.
- [13] G. H. Schuringa, M. Mihajlovic, C. C. van Donkelaar, T. Vermonden, and K. Ito, "Creating a Functional Biomimetic Cartilage Implant Using Hydrogels Based on Methacrylated Chondroitin Sulfate and Hyaluronic Acid," *Gels*, vol. 8, no. 7, 2022.
- [14] FDA, "Summary of Safety and Effectiveness Data - SECURE C," U.S. Food Drug Adm., p. 39, 2007.
- [15] FDA, "Summary of Safety and Effectiveness Data - CoFlex," 2012.
- [16] I. Spinal Kinetics, "Summary of safety and effectiveness data M6-C."
- [17] I. LDR Spine USA, "Summary of Safety and Effectiveness Data Mobi-C," 20013.
- [18] NuVasive, "summary of safety and effectiveness data: PCM," 2012.
- [19] ASTM F2346-05, "Standard Test Methods for Static and Dynamic Characterization of Spinal Artificial," 2012.
- [20] P. R. Van Den Broek, "Development of a biomimetic artificial intervertebral disc," Eindhoven University of Technology, 2012.
- [21] D. Skrzypiec, M. Tarala, P. Pollintine, P. Dolan, and M. A. Adams, "When are intervertebral discs stronger than their adjacent vertebrae?," *Spine (Phila. Pa. 1976)*, vol. 32, no. 22, pp. 2455–2461, 2007.
- [22] N. Bogduk and S. Mercer, "Biomechanics of the Cervical Spine. I: Normal kinematics," *Clin. Biomech.*, vol. 15, pp. 633–648, 2000.

- [23] K. R. Chin, J. R. Lubinski, K. B. Zimmers, B. E. Sands, and F. Pencle, "Clinical experience and two-year follow-up with a one-piece viscoelastic cervical total disc replacement," *J. Spine Surg.*, vol. 3, no. 4, pp. 630–640, Dec. 2017.
- [24] V. M. Lu, R. J. Mobbs, and K. Phan, "Clinical Outcomes of Treating Cervical Adjacent Segment Disease by Anterior Cervical Discectomy and Fusion Versus Total Disc Replacement: A Systematic Review and Meta-Analysis," *Glob. Spine J.*, vol. 9, no. 5, pp. 559–567, Aug. 2019.
- [25] J. A. Youssef et al., "Outcomes of posterior cervical fusion and decompression: a systematic review and meta-analysis," *Spine Journal*, vol. 19, no. 10. *Spine J.*, pp. 1714–1729, 01-Oct-2019.
- [26] G. Hulsart-Billström et al., "A surprisingly poor correlation between *in vitro* and *in vivo* testing of biomaterials for bone regeneration: Results of a multicentre analysis," *Eur. Cells Mater.*, vol. 31, pp. 312–322, Jan. 2016.
- [27] T. H. Smit, "The use of a quadruped as an *in vivo* model for the study of the spine - Biomechanical considerations," *Eur. Spine J.*, vol. 11, no. 2, pp. 137–144, Apr. 2002.
- [28] S. Reitmaier and H. Schmidt, "Review article on spine kinematics of quadrupeds and bipeds during walking," *Journal of Biomechanics*, vol. 102. Elsevier Ltd, p. 109631, 26-Mar-2020.
- [29] J. H. Schimandle and S. D. Boden, "Spine update. The use of animal models to study spinal fusion," *Spine (Phila. Pa. 1976)*, vol. 19, no. 17, pp. 1998–2006, 1994.
- [30] A. A. Dias, N. L. Davison, A. M. Persson, Y. Mengerik, and P. M. De Bueger, "Osteoconductive fibers, Medical Implants comprising such osteoconductive fibers and methods of making US Patent 2021/0299332 A1," 2021.
- [31] M. Kaur and K. Singh, "Review on titanium and titanium based alloys as biomaterials for orthopaedic applications," *Mater. Sci. Eng. C*, vol. 102, pp. 844–862, 2019.
- [32] H. D. Link, P. C. McAfee, and L. Pimenta, "Choosing a cervical disc replacement," *Spine J.*, vol. 4, no. 6, pp. S294--S302, Nov. 2004.
- [33] S.-T. Oh, S.-H. Kim, H.-Y. Jeong, J.-M. Lee, J. W. Cho, and J.-S. Park, "The mechanical properties of polyurethane foam wound dressing hybridized with alginate hydrogel and jute fiber," *Fibers Polym.*, vol. 14, no. 2, pp. 173–181, Feb. 2013.
- [34] J. W. Lee and K. Y. Song, "Evaluation of a polyurethane foam dressing impregnated with 3% povidone-iodine (Betafoam) in a rat wound model," *Ann. Surg. Treat. Res.*, vol. 94, no. 1, pp. 1–7, Jan. 2018.
- [35] C.-D. D. Young, J.-R. R. Wu, and T.-L. L. Tsou, "High-strength, ultra-thin and fiber-reinforced pHEMA artificial skin," *Biomaterials*, vol. 19, no. 19, pp. 1745–1752, Oct. 1998.
- [36] L. Ambrosio, R. De Santis, and L. Nicolais, "Composite hydrogels for implants," *Proc. Inst. Mech. Eng. Part H J. Eng. Med.*, vol. 212, no. 2, pp. 93–99, Feb. 1998.
- [37] J. Maitra and V. K. Shukla, "Cross-linking in Hydrogels - A Review," *Am. J. Polym. Sci.*, vol. 4, no. 2, pp. 25–31, 2014.
- [38] B. H. Park, Y. A. Han, J. H. Choi, and J. O. Lim, "Biocompatibility of Phema and P(Hema-Co-Sma) Hydrogels," *Key Eng. Mater.*, vol. 277–279, pp. 51–55, 2005.
- [39] R. Galante, T. J. A. Pinto, R. Colaço, and A. P. Serro, "Sterilization of hydrogels for biomedical applications: A review," *J. Biomed. Mater. Res. Part B Appl. Biomater.*, vol. 0, no. 0, 2017.
- [40] T. von Woedtke and A. Kramer, "The limits of sterility assurance.," *GMS Krankenhhyg. Interdiszip.*, vol. 3, no. 3, p. Doc19, Sep. 2008.
- [41] A. G. Patwardhan and R. M. Havey, "Prosthesis design influences segmental contribution to total cervical motion after cervical disc arthroplasty," *Eur. Spine J.*, Jul. 2019.
- [42] C. S. Shim et al., "CHARITI versus ProDisc: A comparative study of a minimum 3-year follow-up," *Spine (Phila. Pa. 1976)*, vol. 32, no. 9, pp. 1012–1018, 2007.
- [43] T. K. Wu et al., "Multilevel cervical disc replacement versus multilevel anterior discectomy and fusion: A meta-analysis," *Med. (United States)*, vol. 96, no. 16, pp. 1–9, 2017.
- [44] I. Zechmeister, R. Winkler, and P. Mad, "Artificial total disc replacement versus fusion for the cervical spine: a systematic review," *Eur. Spine J.*, vol. 20, no. 2, pp. 177–184, Feb. 2011.

- [45] G.-L. Li, J.-Z. Hu, H.-B. Lu, J. Qu, L.-Y. Guo, and F.-L. Zai, "Anterior cervical discectomy with arthroplasty versus anterior cervical discectomy and fusion for cervical spondylosis," *J. Clin. Neurosci.*, vol. 22, no. 3, pp. 460–467, Mar. 2015.
- [46] J. G. Heller et al., "Comparison of BRYAN Cervical Disc Arthroplasty With Anterior Cervical Decompression and Fusion," *Spine (Phila. Pa. 1976)*, vol. 34, no. 2, pp. 101–107, Jan. 2009.
- [47] D. Coric et al., "Prospective, randomized, multicenter study of cervical arthroplasty: 269 patients from the Kineflex C artificial disc investigational device exemption study with a minimum 2-year follow-up," *J. Neurosurg. Spine*, vol. 15, no. 4, pp. 348–358, Jun. 2011.
- [48] A. Vaccaro et al., "Long-Term Clinical Experience with Selectively Constrained SECURE-C Cervical Artificial Disc for 1-Level Cervical Disc Disease: Results from Seven-Year Follow-Up of a Prospective, Randomized, Controlled Investigational Device Exemption Clinical Trial," *Int. J. Spine Surg.*, vol. 12, no. 3, pp. 377–387, Jun. 2018.
- [49] D. G. Tobert, V. Antoci, S. P. Patel, E. Saadat, and C. M. Bono, "Adjacent Segment Disease in the Cervical and Lumbar Spine," *Clin. Spine Surg.*, vol. 30, no. 3, pp. 94–101, 2017.
- [50] V. K. Goel, A. Faizan, V. Palepu, and S. Bhattacharya, "Parameters that effect spine biomechanics following cervical disc replacement," *European Spine Journal*, vol. 21, no. SUPPL. 5. Springer, p. 688, 2012.
- [51] H. Sang, W. Cui, D. Sang, Z. Guo, and B. Liu, "How Center of Rotation Changes and What Affects These After Cervical Arthroplasty: A Systematic Review and Meta-analysis," *World Neurosurg.*, vol. 135, pp. e702–e709, Mar. 2020.
- [52] D. Coban et al., "Metal-on-metal versus metal-on-plastic artificial discs in two-level anterior cervical disc replacement: a meta-analysis with follow-up of 5 years or more," *Spine J.*, vol. 21, no. 11, pp. 1830–1838, Nov. 2021.
- [53] N. Bergknut et al., "Spine The Dog as an Animal Model for Intervertebral Disc Degeneration?," *Spine (Phila. Pa. 1976)*, vol. 37, no. 5, pp. 351–358, 2012.
- [54] M. Alizadeh et al., "An EMG-driven biomechanical model of the canine cervical spine," *J. Electromyogr. Kinesiol.*, vol. 32, pp. 101–109, 2017.
- [55] S. P. Moroney, A. B. Schultz, and J. A. A. Miller, "Analysis and measurement of neck loads," *J. Orthop. Res.*, vol. 6, no. 5, pp. 713–720, Sep. 1988.
- [56] A. S. King and R. N. Smith, "A Comparison of the Anatomy of the Intervertebral Disc in Dog and Man," *Br. Vet. J.*, vol. 111, no. 4, pp. 135–149, Apr. 1955.
- [57] I. L. Mohd Isa, S. A. Mokhtar, S. A. Abbah, M. B. Fauzi, A. Devitt, and A. Pandit, "Intervertebral Disc Degeneration: Biomaterials and Tissue Engineering Strategies toward Precision Medicine," *Adv. Healthc. Mater.*, vol. 11, no. 13, 2022.

Curriculum vitae



Celien Antonia Maria Jacobs was born on March 11th, 1994, in Weert, The Netherlands, and she grew up in Stramproy. In 2012 she received her ASO sciences - mathematics diploma at College Heilig Kruis Sint Ursula Maaseik 2 and started the Bachelor Medical Sciences and Technology at Eindhoven University of Technology. She received her bachelor's degree in 2015, with high appreciation, and started the master Biomedical Engineering in the Orthopaedic Biomechanics group of prof. dr. Keita Ito in the same year. As part of her master, she performed her graduation project at LifeTec Group, working on the development of a biomimetic artificial intervertebral disc for the cervical spine. In addition, she performed an internship at the Institute of Health and Biomedical Innovation of the Queensland University of Technology in Brisbane, Australia, working on a hydrogel for tissue engineering cartilage under supervision of Associate Professor Travis Klein. After her graduation in 2018, Cum Laude, she continued to do research as a PhD candidate in the Orthopaedic Biomechanics group under supervision of Prof. Dr. Keita Ito. The work performed in this PhD project is presented in this dissertation.

List of publications

Publications related to this thesis:

C.A.M. Jacobs, C.J. Siepe, K. Ito. Viscoelastic cervical total disc replacement devices: design concepts. *The Spine Journal*, vol. 20, no. 12, p. 1911-1924, Dec. 2020

C.A.M. Jacobs, A.M. Abdelgawad, S. Ghazanfari, S. Jockenhoevel, K. Ito. Warp-knitted fabric structures for a novel biomimetic artificial intervertebral disc for the cervical spine. Submitted to the *Journal of Materials Science*.

C.A.M. Jacobs, E.E.A. Cramer, A.A. Dias, H. Smelt, S. Hofmann, K. Ito. Surface modifications to promote the osteoconductivity of Ultra-High-Molecular-Weight-Polyethylene fabrics for a novel biomimetic artificial disc prosthesis: an *in vitro* study. *Journal of Biomedical Materials Research part B: Applied Biomaterials*, vol. 111, no. 2, p. 442-452, Feb. 2023

C.A.M. Jacobs, R.J.P. Doodkorte, S.A. Kamali, A.M. Abdelgawad, S. Ghazanfari, S. Jockenhoevel, J.J.C. Arts, M.A. Tryfonidou, B.P. Meij, K. Ito. Biomechanical evaluation of a novel biomimetic artificial intervertebral disc in canine cervical cadaveric spines. *JOR Spine*, p. 1-10, Jan. 2023

C.A.M. Jacobs, S.A. Kamali, A. Löwen, S. Ghazanfari, S. Jockenhoevel, K. Ito. Mechanical characterization of a novel biomimetic artificial disc for the cervical spine. *Journal of the Mechanical Behavior of Biomedical Materials*, Apr. 2023.

Conference contributions:

C.A.M. Jacobs, M.W. Wijlaars, M. Harries, K. Ito, L.M. Kock. A novel cervical biomimetic artificial intervertebral disc: a mechanical analysis. 25th Congress of the European Society of Biomechanics, Vienna, Austria, 7-10 July 2019 (Oral)

C.A.M. Jacobs, E.E.A. Cramer, A.A. Dias, H. Smelt, S. Hofmann, K. Ito. Osteoconductivity of UHMWPE fabric for a cervical artificial intervertebral disc: *in vitro* analysis. 28th Annual meeting of the Dutch Society for Biomaterials and Tissue Engineering (NBTE), Lunteren, the Netherlands, 21-22 November 2019 (Poster)

C.A.M. Jacobs, E.E.A. Cramer, A.A. Dias, H. Smelt, S. Hofmann, K. Ito. Osteoconductivity of UHMWPE fabric for a cervical artificial intervertebral disc: *in vitro* analysis. 30th Annual meeting of the Dutch Society for Biomaterials and Tissue Engineering (NBTE), Lunteren, the Netherlands, 4-5 April 2022 (Oral)

C.A.M. Jacobs, E.E.A. Cramer, A.A. Dias, H. Smelt, S. Hofmann, K. Ito. Osteoconductivity of UHMWPE fabric for a cervical artificial intervertebral disc: *in vitro* analysis. 27th Congress of the European Society of Biomechanics, Porto, Portugal, 26-29 June 2022 (Oral)

C.A.M. Jacobs, R.J.P. Doodkorte, A. Kamali, A.M. Abdelgawad, S. Ghazanfari, S. Jockenhoevel, J.J.C. Arts, M.A. Tryfonidou, B.P. Meij, K. Ito. Biomechanical evaluation of a novel biomimetic artificial intervertebral disc in canine cervical cadaveric spines. 27th Congress of the European Society of Biomechanics, Porto, Portugal, 26-29 June 2022 (Oral)

C.A.M. Jacobs, R.J.P. Doodkorte, A. Kamali, A.M. Abdelgawad, S. Ghazanfari, S. Jockenhoevel, J.J.C. Arts, M.A. Tryfonidou, B.P. Meij, K. Ito. Biomechanical evaluation of a novel biomimetic artificial intervertebral disc in canine cervical cadaveric spines. 9th World Congress of Biomechanics, Taipei, Taiwan, 10 – 14 July 2022 (Oral)

Dankwoord (acknowledgements)

Stiekem is de tijd toch snel gegaan en nu ik dit aan het schrijven ben komt het besef dat grootste gedeelte van mijn PhD erop zit. Ik ben dan ook ontzettend blij en kijk met veel plezier terug naar de afgelopen leerzame, en (meestal) leuke jaren als PhD'er bij de TU/e. Dit was natuurlijk niet haalbaar zonder de steun en hulp, direct of indirect, van heel veel collega's, vrienden en familie!

Dear **Keita**, I would like to start by thanking you for the opportunity you gave me already in 2017 to perform my master thesis graduation project with you as my direct supervisor. I enjoyed working with you and I am really happy that I decided to continue to do a PhD with you. I really appreciate your continuous support during the last years, where you were always willing to help me out with even the smallest issues that I came across. Your impressive intelligence and structured way of working made working with you a real pleasure.

I would like to thank the members of my defense committee. I am honored that **dr. Sandra Hofmann, Prof. dr. ir. Olaf van der Sluis, Prof. dr. Ir. Bart Verkerke, Ruth Wilcox, prof. Dr. Björn Meij, and dr. Samaneh Ghazanfari** spent their valuable time on evaluating the thesis manuscript, and grateful for their kind participation in my defense ceremony. **Sandra**, I would like to thank you for your kind support during my cell culture work, I could not have done it without your input and feedback! **Björn Meij and Samaneh Ghazanfari**, as part of the user committee, we had regular contact, and thus you were an important support for me throughout the project. **Björn** thanks for always providing a critical and clinical view on my work! **Samaneh**, thanks for the nice collaboration, although it was not the easiest trajectory to get the jacket design working, we still managed to finish a nice manuscript on this project.

I would also like to thank all the great researchers with whom I have had the pleasure to collaborate with over the past 4 years. **Abdo** and **Amir**, thank you for being such kind and great collaborators on this project, most of the work presented in this thesis would not have been realized without your contributions. **Abdo** although it hasn't been an easy task to get the fiber jackets produced (delivery of the machine, covid etc.), you were really invested and eventually we managed to finalize the design. **Amir**, you joined the project after 2 years, and your enthusiasm and enormous drive came at the perfect moment. I immediately enjoyed working with you, and without you we would have never managed to come up with a novel endplate design. **Marianna Tryfonidou** thank you for being one of the driving forces behind the project, your critical view and concrete suggestions and questions have been extremely valuable. **Stefan Jockenhövel**, thank you for efforts to get the textile machine in place as soon

as possible and your valuable input on the design of the fiber jacket. **Harold Smelt** and **Aylvin Dias** thank you for your continuous and valuable input and feedback during this project.

Mijn twee paranimfen **Michelle** en **Eline**, jullie beide hebben tijdens mijn gehele studententijd en daarna ook tijdens mijn PhD een grote rol in mijn leven gehad. **Michelle**, van introzusjes naar huisgenootjes, naar kantoorgenootjes, OPB-groep collega's en Woensel bewoners, wat hebben wij veel samen meegemaakt! Jij bent iemand waarbij ik altijd terecht kan, voor mentale support, feedback op wetenschappelijk niveau en alle onbenullige vragen waarover ik advies nodig heb. Ik denk dat er maar weinig mensen zijn die mij zo door en door kennen zoals jij, ik ben daarom ook ontzettend dankbaar dat ik zo een goede vriendin als collega heb mogen hebben. **Eline**, ik herinner me nog goed wanneer ik jou voor het eerst leerde kennen, bij de BA van Amoreia. Ik denk dat binnen 5 minuten na de eerste kennismaking we meteen wisten dat hier een hechte vriendschap uit zou groeien. We hebben samen veel gekke, dronken momenten en vakanties meegemaakt die ik nooit zal vergeten. Maar naast veel lol maken, ben je ook iemand waar ik altijd op kan bouwen. Ik ben je dan ook ontzettend dankbaar voor jou altijd eerlijke advies en je luisterende oor gedurende de afgelopen jaren. Lieve Eline en Michelle, ik ben super blij dat jullie tijdens dit laatste onderdeel van mijn universiteitsleven me willen bijstaan!

I am very grateful that I was part of the **Orthopaedic biomechanics research group**. Thanks to all the (former) members of this amazing group, I really enjoyed the nice atmosphere during all sorts of activities that we did, such as the section retreat, self-organized outings, Meerkamp and casual coffees on the hallway. Special thanks to my IVD buddies, **Elias** and **Tara**, with whom I have had nice discussion during our bi-weekly IVD meetings. **Elias**, je bent echt een geweldige collega die altijd (aanstekelijk) enthousiast is, en altijd klaarstaat om te helpen (zoals met mijn ingewikkelde matlab script). **Rienk**, ook jou leerde ik al kennen tijdens een onvergetelijke introductieweek en daarna als collega binnen de OPB-groep. Jij was iemand die ik altijd om hulp kon vragen voor alles in het biolab, maar ook lekker mee kon klagen als dingen niet goed gingen en waarmee ik alle stress eruit sportte tijdens GRIT of spinning. **Bregje**, toen ik begon als PhD'er in kantoor 4.09 was ik blij om jou bekende gezicht te zien. Hoe leuk dat we beide als start van onze PhD ons masterproject mochten presenteren bij ESB in Wenen, en we dit ook weer samen hebben mogen afsluiten bij ESB in Porto. Bedankt voor al jou erg gewaardeerde wetenschappelijk en persoonlijk steun en advies! **Evelien** bedankt voor het plannen en verzetten van alle meetings, regelen van mijn verdediging en de gezellige tijd tijdens ESB in Porto. **Jurgen** bedankt voor al jouw geniale oplossingen, gependeerde uren en open deur waardoor ik me altijd welkom voelde! Jij hebt ontzettend veel bijgedragen aan

Dankwoord (acknowledgements)

alle resultaten die in dit proefschrift zijn opgeschreven, het design van mijn hydrogel mal tot alle mechanische test opstellingen die in dit proefschrift zijn gebruikt.

I would also like to thank all (former) members of **office 4.09**. Thanks for all the coffee's, lunches, and office dinner parties!

Er zijn een aantal mensen die ik al eerder in dit dankwoord had kunnen vermelden, omdat ik het zeldzame privilege heb gehad om samen te mogen werken met een aantal vriendinnen. **Alicia** en **Esther C** wat ben ik ontzettend blij dat jullie ook onderdeel waren van de OPB-groep, hierdoor werd elk groepsuitje of groepsmeeting meteen een momentje om gezellig bij te kletsen of een goed feestje te vieren, of zelfs lekker vakantie te vieren en op het strand te liggen in Porto na een conferentie. Naast alle leuke dingen, kon ik bij jullie ook altijd terecht met alle PhD struggles of om lekker te wijnen op vrijdagavond. **Esther C**, zonder jou was mijn cell culture paper er nooit gekomen, ik ben super dankbaar dat je mij aan de hand hebt genomen in het cellab en ik ben trots dat we samen op een paper staan! Daarnaast wil ik alle andere meiden van de 'BMT chickies' natuurlijk ook benoemen. Lieve **Joni, Sanne, Mylene, Marissa** en **Elcke**, ik wil jullie bedanken voor alle wijn avonden, sinterklaas spelletjes en weekendjes weg. Ook al zien we elkaar niet wekelijks, het is altijd gezellig als we elkaar weer zien en kunnen bijkletsen! Ik kijk nu al uit naar ons volgende uitje!

Lieke en **Esther V** jullie hebben ook een heel speciaal plekje en horen ook zowel bij de BMT-chickies, de bokscheet peeps en de london girls. **Lieke**, wij zaten samen met Michelle en Rienk in hetzelfde introgroepje, en hebben daarna samen met mies 5.5 jaar gewoond in ons superleuke appartementje op de carislaan. **Esther V** werd al snel onderdeel van het meubilair en hebben we vele avondjes geordie shore of planet earth keken, die we afsloten met diepgaande gesprekken tot diep in de nacht op ons balkonnetje. Ondertussen zijn we allemaal volwassen geworden, wonen we op verschillende plekken en is lieks zelfs mama geworden van de lieve Len. Maar toch spreken we elkaar nog geregeld en kan ik altijd bij jullie terecht, en daar ben ik jullie super dankbaar voor.

Ondertussen heb ik al zoveel mensen genoemd uit dezelfde BMT-lichting, en toch is de lijst nog niet compleet. **Bart, Johnick, Willem** en **Vincent** vormen samen met Lieke, Esther en Michelle een vriendengroep genaamd de bokscheet (vernoemd naar de appgroep die een bokscheet emoticon heeft, geen idee hoe we daarop zijn gekomen). We leerden elkaar kennen in het eerste jaar van onze studie doordat een aantal van deze bollebozen calculus moesten herkansen. Samen hebben we talloze herinneringen van onze studententijd, de vele studievereniging- en huisfeestjes, samen studeren in meta, weekendjes naar Antwerpen en

Manchester en dronken kerstdiners die we tot op heden nog elk jaar organiseren. Bart en Johnick waren ook nog promotiebuddies waardoor we elkaar geregeld in het lab of op de gang tegenkwamen en even konden bijkletsen. Dankjewel toppers dat jullie hebben bijgedragen aan fantastische uni tijd, en dat we nog vele kerstdiners en leuke herinneringen mogen maken.

Naast de vele vrienden die ik heb leren kennen via mijn studie, heb ik ook ontzettend veel vrienden gemaakt bij de mooiste studentenvereniging van Eindhoven, SSRE. Ik heb daar het geluk gehad om lid te worden van het fantastische roze dispuut Amoreia. Lieve **Celeste, Martine, Lisa, Annika, Bente, Camilla, Denise, Nora, Kelly** bedankt dat jullie hebben bijgedragen aan een fantastische studententijd. Maar ook de huidige leden wil ik bedanken voor de leuke reünistendagen, toernooien, kerstdiners en lustrumgala's. Ik wil mijn leuke lichter **Eline C, Eline M** en **Lotte** nog even extra benoemen, al sinds 2013 zoveel mooie herinneringen samen en ik ben erg dankbaar dat we nog steeds goed contact weten te houden. Ik kijk altijd uit naar onze leuke jacuzuipen, pubquizen en spelletjes avonden. Naast mijn dispuut heb ik ook samen met **Emma, Felix, Jerry, Annelieke, Puck, Coen** en **Arne** een jaar de eer gehad om aan het roer te staan van de vereniging. Je leert elkaar pas echt goed kennen als je een jaar lang 24/7 op elkaars lip zit. We hebben dan ook zo ontzettend veel herinneringen en ben blij dat we elkaar nog geregeld zien en samen leuke weekendjes weg plannen om nog meer herinneringen te maken. Coen jij besloot, zelfs na mijn 'fantastische' verhalen om ook een PhD te gaan doen bij werktuigbouwkunde. Ik vond het superleuk om af en toe bij jou beneden op kantoor te zitten, waarna je ook verhuisde naar de gezellige 4^e verdieping en we elkaar vaker tegen het lijf liepen op de wandelgang en even een praatje maakten.

Lieve **Rianne** en **Chloé**, we kennen elkaar vanaf de middelbare school en ben ongelooflijk blij dat ondanks dat we niet meer dicht bij elkaar wonen, we deze vriendschap in stand houden. Rianne, wat zijn wij vaak samen op vakantie geweest met de bijbehorende onvergetelijke herinneringen, van Cherso, Albufeira en Sunny beach zuipvakanties tot de jaarlijkse skivakanties waarbij ik mee mocht met jou fantastische familie. Je bent een top vriendin waarbij ik altijd terecht kan. **Chloé** van opstap gaan bij de burens in Sittard, tot in de late uurtjes in de kroeg in Nijmegen naar nu half Nederland doorreizen om onze sushi dates voort te zetten in Didam of Eindhoven. Ik waardeer het enorm dat ondanks dat we onze eigen levens hebben, we nog steeds van elkaars leven op de hoogte blijven en je altijd klaar staat met een luisterend oor en je waardevolle advies.

Dankwoord (acknowledgements)

Sanne, Maja, Yvette en **Jeanet**, oftewel 3 x 2 zusjes, ik ben zo blij dat wij in de veel te grote Jacobs familie zo een goede band hebben. Het is altijd gezellig om bij te kletsen en geniet van onze sinterklaasspelletjes, high-tea's en jaarlijkse weekendjes weg naar Barcelona, Toulouse, Texel etc. Dat we dit komende jaren nog veel vaker mogen doen.

Leonie, ik heb het geluk dat we niet alleen zussen maar ook beste vriendinnen zijn. Zelfs toen je in Oostenrijk en Duisland woonde hielden we contact en kon ik altijd bij je terecht. Wij begrijpen elkaar zonder iets te zeggen, en het lijkt bijna geen toeval meer hoe vaak we exact hetzelfde zeggen op exact hetzelfde moment. Misschien hebben de vele mensen die denken dat we een tweeling zijn toch gelijk haha. Ik ben super trots op jou en je bent echt een voorbeeld voor mij geweest en dat ben je nog steeds, bedankt daarvoor!

Lieve **pap** en **mam**, bedankt voor jullie onvoorwaardelijke liefde, vertrouwen en dat jullie me altijd hebben gesteund bij elke keuze die ik heb gemaakt. Ondanks dat jullie niet altijd alles begrepen waar ik mee bezig was, bleven jullie wel geïnteresseerd en kon ik altijd bij jullie terecht. Jullie hebben me geleerd om met beide voeten op de grond te blijven en iedereen op dezelfde manier te behandelen, en dat heeft me veel gebracht.

Lieve **Jordi**, ondertussen zijn we al 7.5 jaar samen en wonen we ook al 4.5 jaar samen. Jij bent daarom ook degene die alles heeft meegekregen van mijn PhD. Soms kwam ik heel blij thuis en wilde ik enthousiast delen wat ik die dag weer had bereikt, maar soms kwam ik ook chagrijnig thuis en reageerde dat dan weer af op jou. Jij hebt mij leren beter te relativieren, en ik had deze rollercoaster dan ook zeker niet zonder jou kunnen afronden. Ik kijk uit naar onze toekomst samen!

Celien